COOPERATIVE DRUG COMBINATIONS TARGET ONCOGENES AND TUMOR SUPPRESSORS IN CANCER

by

Tyler J. Peat

A Dissertation

Submitted to the Faculty of Purdue University

In Partial Fulfillment of the Requirements for the degree of

Doctor of Philosophy

Department of Comparative Pathobiology

West Lafayette, Indiana

December 2021

THE PURDUE UNIVERSITY GRADUATE SCHOOL
STATEMENT OF COMMITTEE APPROVAL

Dr. Margaret Miller, Co-Chair

Department of Comparative Pathobiology, Purdue University

Dr. Beverly Mock, Co-Chair

Laboratory of Cancer Biology and Genetics, National Cancer Institute, NIH

Dr. Guangjun Zhang

Department of Comparative Pathobiology, Purdue University

Dr. Deborah Knapp

Department of Veterinary Clinical Sciences, Purdue University

Approved by:

Dr. Sanjeev Narayanan

Dedicated to Allison and Siena

ACKNOWLEDGMENTS

Dr. Peat performed doctoral research as a fellow in the NIH Comparative Biomedical Scientist Training Program supported by the NCI in Partnership with Purdue University.

TABLE OF CONTENTS

LIST OF TABLES 8
LIST OF FIGURES 9
CHAPTER 1. INTRODUCTION, RATIONALE, AND HYPOTHESES 11
1.1 Background 11
1.2 Rationale 13
1.3 Hypotheses and Aims 14
1.4 Impact 15
1.5 References 16
CHAPTER 2. HIGH-THROUGHPUT DRUG SCREEN IDENTIFIES THERAPEUTIC COMBINATIONS TARGETING ONCOGENES AND TUMOR SUPPRESSORS IN MULTIPLE MYELOMA 20
2.1 One Sentence Summary 20
2.2 Abstract 20
2.3 Introduction 21
2.4 Results 22
2.4.1 Drug screen reveals combinations cooperatively targeting MYC and p16 that reduce viability of MM cells 22
2.4.2 The top three drug combinations reduce oncogenic MYC activity and increase tumor suppressor activity in MM cell lines, regardless of inherent sensitivity or resistance 26
2.4.3 Evaluation of synergy and microenvironment effects in top drug combinations 28
2.4.4 Comparison of top drug combinations in a novel allograft mouse model of MM 33
2.4.5 Top drug combinations are effective at selectively reducing the viability of human CD138+ MM cells *ex vivo* 33
2.4.6 Genetic pathways commonly affected by the top combinations 37
2.4.7 Overcoming drug resistance in combination therapy by co-targeting the TGFβ pathway 39
2.5 Discussion 40
2.6 Materials and Methods 44

2.6.1 Study design 44
2.6.2 Human MM and other cell lines 44
2.6.3 NCATS MIPE screen 45
2.6.4 *In Silico* analysis 45
2.6.5 Western blot analysis 46
2.6.6 Antibodies (western blot) 46
2.6.7 Cell viability assays in human MM cell lines and primary human MM cells 46
2.6.8 Animal studies 47
2.6.9 *In Vitro* gene response signature of drug treatments 48
2.6.10 Statistical analysis 48
2.6.11 Data processing/normalization 48
2.6.12 Concordant gene response signature 49
2.6.13 GO enrichment analysis 49
2.6.14 Code availability 49
2.7 References and Notes 50
2.8 Supplemental Figures and Tables: 56
CHAPTER 3. EFFICACY AND COOPERATIVE TARGETS OF COMBINED CDK/HDAC INHIBITION IN PRECLINICAL MODELS OF MULTIPLE MYELOMA 64
3.1 One Sentence Summary 64
3.2 Introduction 64
3.3 Results 65
3.3.1 Targeted combined CDK/HDAC inhibition is effective *in vitro* 65
3.3.2 Tolerability of combined CDK/HDAC inhibition in mice 70
3.3.3 *In vivo* target engagement and efficacy of combined CDK/HDAC inhibition in mice 70
3.3.4 Combined CDK/HDAC inhibition cooperatively and selectively reduces MM patient cell viability ex vivo 74
3.3.5 RNA-seq identifies genes differentially expressed by combined CDKi/HDACi 75
3.3.6 GSEA identifies pathways associated with CDKi/HDACi synergy 78
3.3.7 Modified Fisher's exact test identifies function-related gene groups enriched in a synergistic CDKi/HDACi response 82

3.3.8 Master regulators of a combined CDKi/HDACi response 86
3.4 Discussion 90
3.5 Future Directions and Limitations 93
3.6 Materials and Methods 94
3.6.1 Human MM and other cell lines 94
3.6.2 Western blot analysis 95
3.6.3 Cell viability assays in human MM cell lines and primary human MM cells 95
3.6.4 Flow cytometry assay for apoptosis in human MM cell lines 96
3.6.5 *In vivo* experiments 96
3.6.6 RNA-seq and differential gene expression analysis of combined CDK-HDAC inhibition 97
3.6.7 Gene set enrichment analysis 98
3.6.8 DAVID enrichment analysis of GO data set 99
3.7 References and Notes 99
3.8 Supplemental Figures and Tables: 106
APPENDIX A 120
APPENDIX B. 127
APPENDIX C 128
PUBLICATIONS 133

LIST OF TABLES

Table 2.1. Top Drug Combinations Against Multiple Myeloma Cells Based on Robust Regression 24

Table 2.2. Combinations That Reduced MYC Protein Expression in L363 MM Cells 25

Table 2.3. Forty-seven Multiple Myeloma Cell Lines Ranked by Mean AC50 27

Table 3.1. Upstream master regulators of a combined CDKi/HDACi response..... 87

Table S.2.1. Effect of top 3 drug combination on viability of parental and drug-resistant multiple myeloma cell lines..... 63

Table S.3.1. Tolerability of combined CDKi/HDACi in naïve NSG mice 119

Table S.3.2. Tolerability of combined CDKi/HDACi in naïve Bcl-xL mice 119

LIST OF FIGURES

Figure 1.1. Current treatment strategies for MM.. 11

Figure 1.2. Genetic pathways dysregulated in human myeloma and susceptibility genes in mouse plasma cell tumors identify druggable MM targets..... 12

Figure 2.1. Prediction workflow used to find top drug combinations against MM. 23

Figure 2.2. High-throughput drug screen reveals combinations that cooperatively target MYC and p16 and reduce viability of MM cells.. 29

Figure 2.3. Evaluation of synergy in top drug combinations. 32

Figure 2.4. Evaluating the top drug combinations in a novel allograft mouse model of MM and human myeloma cells *ex vivo*..... 35

Figure 2.5. Pathways most commonly affected by the top 3 combinations 38

Figure 2.6. Co-targeting the TGFβ pathway with combination therapy 40

Figure 3.1. *In vitro* evaluation of combined targeted CDK/HDAC inhibition in MM. 68

Figure 3.2. *In vivo* evaluation of combined targeted CDK/HDAC inhibition. 72

Figure 3.3. Selective efficacy of combined CDK/HDAC inhibition in smoldering multiple myeloma (SMM) patient cells ex vivo. 74

Figure 3.4. RNA-seq identified genes synergistically changed compared to single agent treatment. L363 MM cells were treated for 48h with dinaciclib (4 nM), entinostat (250 nM) or the..... 76

Figure 3.5. GSEA reveals enriched pathways associated with cooperative CDKi/HDACi response 80

Figure 3.6. DAVID pathway analysis reveals enriched function-related gene groups in a synergistic CDKi/HDACi response 84

Figure 3.7. Ingenuity upstream regulator analysis identifies predicted master transcriptional regulators of combined CDK/HDAC inhibition 88

Figure S.2.1. Robust regression analysis of active compounds revealed potentially effective combinations against MM..... 56

Figure S.2.2. Evaluating synergy and efficacy in various sensitive and resistant cell lines and tolerability in normal human fibroblasts 57

Figure S.2.3. Efficacy of the top 3 combinations in a novel mouse model of myeloma 59

Figure S.2.4. Common genetic pathways similarly affected by the top drug combinations..... 61

Figure S.2.5. L363 MM cell viability upon single agent or combined treatment with dinaciclib and mocetinostat..... 62

Figure S.3.1. Evaluation of on- and off-target CDK and HDAC effects by dinaciclib and/or entinostat treatment 106

Figure S.3.2. Evaluation of targeted CDKi/HDACi in LP-1 parental and PI-resistant MM cells 107

Figure S.3.3. Efficacy of combined CDK/HDAC inhibition in mouse models of MM 109

Figure S.3.4. GSEA reveals enriched pathways associated with cooperative CDKi/HDACi response 110

CHAPTER 1. INTRODUCTION, RATIONALE, AND HYPOTHESES

1.1 Background

Multiple myeloma (MM), a neoplastic clonal proliferation of plasma cells affecting mostly older individuals, is one of the most common hematologic malignancies [1, 2], with an estimated 34,920 new cases and 12,410 deaths in the United States in 2019 alone [3]. Development of new therapeutics such as proteasome inhibitors (PI), immunomodulatory drugs, monoclonal antibodies, and autologous stem cell transplantation, used in varying combinations, has resulted in prolonged survival of MM patients [1, 2, 4, 5 – Fig. 1.1]. However, no therapy thus far is curative, and relapsed and/or refractory multiple myeloma (RRMM) eventually develops, particularly as a result of PI therapy [1, 2]. Thus, combining targeted agents has become important in treating RRMM and oncology in general [6]. Combining drugs circumvents tumor resistance by utilizing synergy, in which the total effect of two or more drugs is greater than the sum of individual drugs. Furthermore, identifying the mechanisms of molecular synergy provides a biologic rationale for proposed combinations and is essential for predicting clinical responses [7].

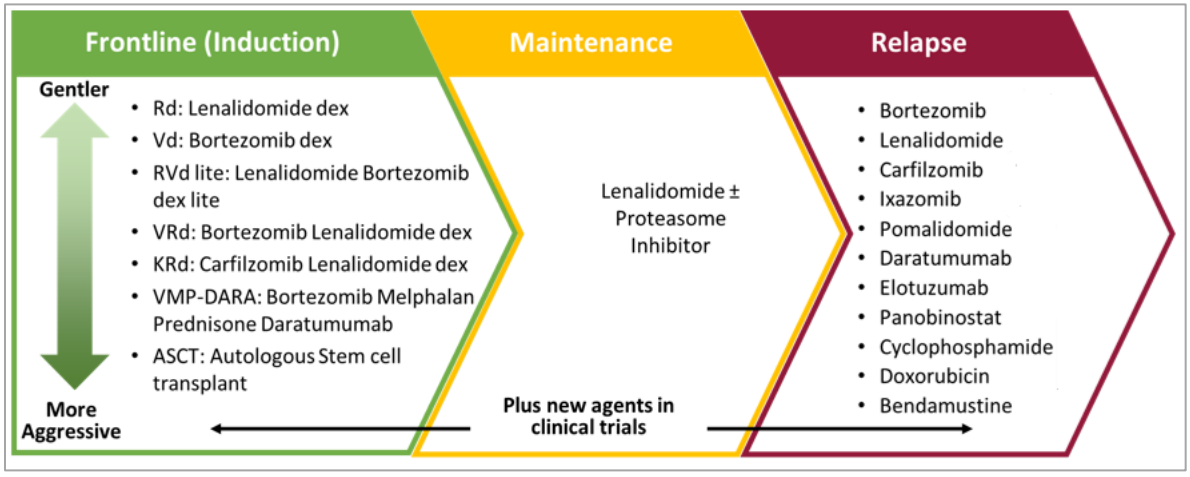

Figure 1.1. Current treatment strategies for MM. Newly diagnosed MM is treated with combinations of thalidomide derivatives, proteasome inhibitors, and corticosteroids, followed by maintenance therapy [1, 2, 4, 5]. Monoclonal antibodies, anthracyclines and alkylating agents are reserved typically for relapsed myeloma [2, 5].

Sensitivity and drug synergy for the combination of mTOR inhibitors (mTORi) and histone deacetylase inhibitors (HDACi) have been shown in human MM cell lines, a diverse set of cancer cell types, and MM cells isolated from patients [7, 8]. Importantly, a proposed mechanism of action of synergy in the combination – degradation of the transcription factor MYC – was elucidated via a biologically integrated, network-based approach using MM cell lines and patient datasets [7] – [Figure 1.2]. MYC activation (most commonly through locus rearrangements and gains, mRNA overexpression, and deregulation) is found in approximately 67% of MM and is associated with disease progression [9-11]. Additionally, NRAS and KRAS genes are frequently mutated in MM, associated with disease progression, and increase the stabilization of MYC via phosphorylation of Serine 62 [7, 8, 12]. Targeting MYC directly, however, has remained a key challenge in oncology due to large protein-protein interaction interfaces, lack of deep protein pockets, and nuclear localization [13, 14]. Instead, finding drug combinations that indirectly target MYC, while acting upon their own respective direct targets, serves as a useful alternative strategy and may provide additional opportunities for synergy in treating MM.

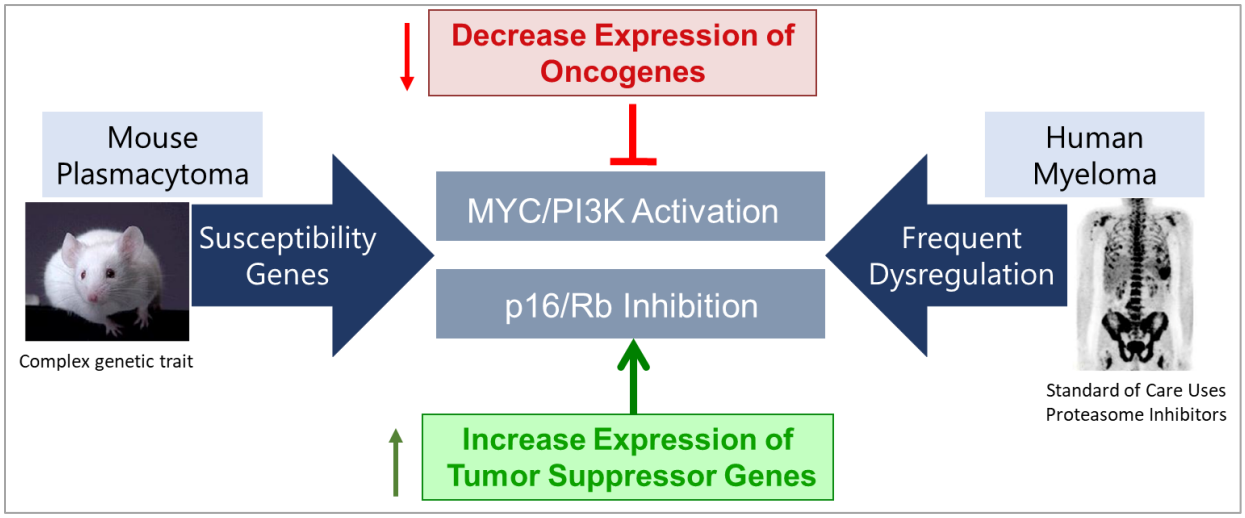

Figure 1.2.Genetic pathways dysregulated in human myeloma and susceptibility genes in mouse plasma cell tumors identify activated oncogenes and simultaneously downregulated tumor suppressor genes as druggable MM targets.

1.2 Rationale

A useful strategy in addressing the issue of acquired drug resistance in cancer, particularly MM, is combining targeted therapies. Given the large number of small molecules used to treat cancer and the even larger number of possible combinations, predictive computational methods are essential for identifying the most effective potential treatments [15-17]. Although there are several competing methods for predicting drug combinations from pharmacologic studies [16-18], we chose to utilize robust regression analysis of the AC50 concentrations, defined as the concentration at half-maximal activity, of active drugs [19]. This strategy overcomes the limitations of other regression models, such as ordinary least squares, in that it's not overly affected by extreme outliers [20]. As previously mentioned, the oncogene MYC is a known driver in the progression of premalignant monoclonal gammopathy of undetermined significance to MM [7, 9, 10], has been found to be overexpressed in MM compared to healthy donor $CD138^+$ cells, and importantly has been implicated as a master regulator of mTORi/HDACi cooperation [7]. Also, dysregulation of tumor suppressors such as RB, p16, p21, and p27 via downregulating expression or hindering activity is a common feature in B cell neoplasia, including MM [7, 8, 21, 22], and other cancers [23]. Therefore, a useful strategy for discovering new effective treatments in MM is to screen for active combinations that reduce oncogenic MYC expression, while also increasing activity of tumor suppressors. Finally, although the use of immunomodulatory drugs and proteasome inhibitors (PI) such as carfilzomib or oprozomib have significantly prolonged the survival of patients with MM [1, 2, 24], most patients eventually relapse [25]. Therefore, it is imperative to test potential combinations in not only cell lines sensitive to common therapies like PI but those that have acquired resistance because any combinations identified from preclinical studies would be evaluated in RRMM patients clinically. Therefore, we propose the ability of candidate combinations to maintain efficacy in PI resistant cells as our final criterion for selection.

The use and outcome of validated and predictive animal models is pivotal in translating preclinical findings to the clinic. Further, evaluating the proposed combination(s) *in vivo* will provide insight into target engagement, efficacy, and safety endpoints. Additionally, we aim to evaluate efficacy of CDKi/HDACi in three separate models, each fulfilling a specific purpose. First, naïve athymic NCr-nu/nu (nude) mice are useful for testing dose tolerance of the combination, and nude mice bearing subcutaneous MM xenografts can be assessed for drug-

induced changes in tumor burden via examining tumor volume over the course of treatment [8]. Second, the Bcl-xL transgenic mouse model allows the study of combination effects in an immunocompetent model of plasma cell tumors, with features similar to human MM and Burkitt lymphoma [7, 26]. Lastly, the transplantable tumor model of sublethally irradiated C57BL/6 mice injected with MM cells from Vk*MYC; $Nras^{LSL\ Q61R/+}$; IgG1-Cre donor mice (VQ cells), which home to the bone of recipient mice, aids in evaluating the combination's efficacy in a model that closely recapitulates features of human MM [10, 27, 28].

Understanding the molecular mechanism(s) of synergy for a combination is imperative in its preclinical development. Importantly as well, a strong biologic rationale for a proposed combination, along with an understanding of on- and off-target effects and validated biomarkers of a molecular response, are critical in proposing a novel drug combination for clinical development [29]. The top candidate combination determined from the drug screen described above is the CDK/HDAC inhibitor combination of dinaciclib and entinostat, respectively. Dinaciclib (Merck & Co.) inhibits CDK1,2,5,9, and entinostat (Syndax) inhibits HDAC1 and 3 [30-33]. Both drugs are currently under study in clinical trials (NCT01711528, NCT02115282). Understanding how this combination affects the proposed targets will provide insight into on- and off-target effects, mechanism of action, and circumvention of certain toxicities in the individual drugs in treating MM by using lower doses of each drug. Finally, mechanisms of synergy can be elucidated by investigating how the combination affects apoptosis, the MM cell cycle, the activity of RB, and the transcription, protein stability, or degradation of MYC.

1.3 Hypotheses and Aims

We hypothesized that a novel agnostic drug combination discovery approach would reveal potentially synergistic combinations for treating MM. Further, we hypothesized that effective combinations would reduce expression of oncogenic MYC, and increase activity of tumor suppressors, while cooperatively reducing cell viability *in vitro* and prolonging survival *in vivo* in sublethally irradiated C57BL/6 recipient mice injected with MM cells from Vk*MYC; $Nras^{LSL\ Q61R/+}$; IgG1-Cre genetically engineered donor mice [27]. Finally, we aimed to identify mechanisms of a cooperative drug response for the top candidate combination and evaluate its efficacy in several mouse models of MM.

We aimed to develop an agnostic discovery approach for identifying drug combinations to target MM utilizing a high-throughput drug screen of a compound library of over 1900 small molecules in 47 MM cell lines and *in silico* regression analysis to identify drug combinations predicted to reduce MM viability. Additionally, considering the importance of MYC in MM progression, our study aimed to identify candidate tool combinations that cooperatively reduce MYC protein expression and increase tumor suppressor (p16, RB) activity, while synergistically reducing the viability of MM cell lines, regardless of inherent or induced resistance to chemotherapeutics, *in vitro*.

Additionally, we aimed to evaluate efficacy of CDKi/HDACi in three separate models, each fulfilling a specific purpose. First, the transplantable tumor model of sublethally irradiated C57BL/6 mice injected with MM cells from Vk*MYC; $Nras^{LSL\ Q61R/+}$; IgG1-Cre donor mice (VQ cells), which home to the bone of recipient mice, facilitated evaluating the efficacy of our top combinations in a model that closely recapitulates features of human MM [9, 26, 27]. Second, naïve athymic NCr-nu/nu (nude) mice bearing subcutaneous MM xenografts were assessed for drug-induced changes in tumor burden via examining tumor volume, survival and intravital imaging [8]. Third, the Bcl-xL transgenic mouse model allowed the study of combination effects in an immunocompetent model of plasma cell tumors, with features similar to human MM and Burkitt lymphoma [7, 25].

Additionally, we aimed to 1) identify mechanisms of molecular synergy for the candidate combination, which will be useful in evaluating preclinical and clinical efficacy, and 2) assess the mechanism of action of drug synergy and identify biomarkers for cooperative activity by generating a transcriptional response network (RNA Sequencing, gene set enrichment analysis (GSEA)) in proteasome inhibitor sensitive and resistant MM cell lines.

1.4 Impact

Together, these data provide evidence for a new multilayered drug combination prediction workflow to identify novel drug combinations for treating MM and may reveal mechanisms of combined drug sensitivity and resistance. Further, this research provides first evidence for combining a CDK inhibitor with an HDAC inhibitor in treating multiple myeloma, along with biomarkers of a molecular response. Additionally, utilizing sublethally irradiated mice injected

with MM cells from genetically engineered Vk*MYC; $Nras^{LSL\ Q61R/+}$; IgG1-Cre donor mice, provides pathologic characterization of, and evidence for using this model to evaluate therapeutic efficacy of novel drug combinations in a transplantable mouse model of highly malignant MM that more closely recapitulates human MM.

1.5 References

[1] Gulla A, Anderson KC. Multiple myeloma: the (r)evolution of current therapy and a glance into future. *Haematologica*. 2020 Oct 1;105(10):2358-2367.

[2] Kumar SK, Rajkumar S. The multiple myelomas - current concepts in cytogenetic classification and therapy. *Nat Rev Clin Oncol.* 2018 Jul;15(7):409-21.

[3] Howlader N, Noone AM, Krapcho M, Miller D, Brest A, Yu M, Ruhl J, Tatalovich Z, Mariotto A, Lewis DR, Chen HS, Feuer EJ, Cronin KA (eds). SEER cancer statistics review, 1975-2017, NCI. Bethesda, MD, https://seer.cancer.gov/csr/1975_2017/, based on November 2019 SEER data submission, posted to the SEER web site, April 2020.

[4] Castella M, Fernández de Larrea C, Martín-Antonio B. Immunotherapy: A novel era of promising treatments for multiple myeloma. *Int J Mol Sci*. 2018 Nov;19(11):3613.

[5] Rajkumar SV, Kumar S. Multiple myeloma current treatment algorithms. *Blood Cancer J*. 10, 94 (2020).

[6] Dancey J, Chen H. Strategies for optimizing combinations of molecularly targeted anticancer agents. *Nat Rev Drug Discov*. 2006 Aug;5(8):649-59.

[7] Simmons JK, Michalowski AM, Gamache BJ, DuBois W, Patel J, Zhang K, Gary J, Zhang S, Gaikwad SM, Connors D, Watson N, Leon E, Chen JQ, Kuehl WM, Lee MP, Zingone A, Landgren O, Ordentlich P, Huang J, Mock BA. Cooperative targets of combined mTOR/HDAC inhibition promote MYC degradation. *Mol Cancer Ther*. 2017 Sep;16(9):2008-21.

[8] Simmons JK, Patel J, Michalowski AM, Zhang S, Wei BR, Sullivan P, Gamache B, Felsenstein K, Kuehl WM, Simpson RM, Zingone A, Landgren O, Mock BA. TORC1 and class I HDAC inhibitors synergize to suppress mature B cell neoplasms. *Mol Oncol*. 2014 Mar;8(2):261-72.

[9] Jovanović KK, Roche-Lestienne C, Ghobrial IM, Facon T, Quesnel B, Manier S. Targeting MYC in multiple myeloma. *Leukemia*. 2018 Jun;32(6):1295-306.

[10] Chesi M, Robbiani DF, Sebag M, Chng WJ, Affer M, Tiedemann R, Valdez R, Palmer SE, Haas SS, Stewart AK, Fonseca R, Kremer R, Cattoretti G, Bergsagal PL. AID-dependent activation of a MYC transgene induces multiple myeloma in a conditional mouse model of postgerminal center malignancies. *Cancer Cell*. 2008 Feb;13:167–80.

[11] Chng WJ, Huang GF, Chung TH, Ng SB, Gonzalez-Paz N, Troska-Price T, Mulligan G, Chesi M, Bergsagel PL, Fonseca R. Clinical and biological implications of MYC activation: a common difference between MGUS and newly diagnosed multiple myeloma. *Leukemia*. 2011 Jun;25(6):1026–35.

[12] Sears R, Nuckolls F, Haura E, Taya Y, Tamai K, Nevins JR. Multiple Ras-dependent phosphorylation pathways regulate Myc protein stability. *Genes Dev*. 2000 Oct 1;14(19):2501–14.

[13] Whitfield JR, Beaulieu ME, Soucek L. Strategies to inhibit Myc and their clinical applicability. *Front Cell Dev Biol*. 2017 Feb 23;5:10.

[14] Dang CV, Reddy EP, Shokat KM, Soucek L. Drugging the 'undruggable' cancer targets. *Nat Rev Cancer*. 2017 Aug;17(8):502-08.

[15] Weinstein ZB, Bender A, Cokol M. Prediction of synergistic drug combinations. *Curr Opin Syst Biol*. 2017 May 11;4(1):24–28.

[16] Gayvert KM, Aly O, Platt J, Bosenberg MW, Stern DF, Elemento O. A computational approach for identifying synergistic drug combinations. *PLoS Comput Biol*. 2017 Jan 13;13(1):e1005308.

[17] Madani Tonekaboni SA, Soltan Ghoraie L, Manem VSK, Haibe-Kains B. Predictive approaches for drug combination discovery in cancer. *Brief Bioinform*. 2018 Mar 1;19(2):263-276.

[18] Jeon M, Kim S, Park S. In silico drug combination discovery for personalized cancer therapy. *BMC Syst Biol*. 2018 Mar 19:12(Suppl 2):16.

[19] Shockley KR. Estimating Potency in High-Throughput Screening Experiments by Maximizing the Rate of Change in Weighted Shannon Entropy. *Sci Rep*. 2016 Jun 15;6:27897.

[20] Sliwoski G, Kothiwale S, Meiler J, Lowe WE Jr. Computational methods in drug discovery. *Pharmacol Rev*. 2014 Jan; 66(1):334–95.

[21] Dyson NJ. *RB1*: a prototype tumor suppressor and an enigma. *Genes Dev*. 2016 Jul 1; 30(13): 1492–1502

[22] Fernandez V, Hartmann E, Ott G, Campo E, Rosenwald A. Pathogenesis of mantle-cell lymphoma: all oncogenic roads lead to dysregulation of cell cycle and DNA damage response pathways. *J Clin Oncol*. 2005. Sep 10;23(26):6364-69.

[23] Kumari R, Silic MR, Jones-Hall YL, Nin-Velez A, Yang JY, Mittal SK, Zhang G. Identification of *RECK* as an evolutionarily conserved tumor suppressor gene for zebrafish malignant peripheral nerve sheath tumors. *Oncotarget*. 2018 May 4;9(34):23494-504.

[24] Riz I, Hawley RG. Increased expression of the tight junction protein TJP1/ZO-1 is associated with upregulation of TAZ-TEAD activity and an adult tissue stem cell signature in carfilzomib-resistant multiple myeloma cells and high-risk multiple myeloma patients. *Oncoscience*. 2017 Aug 1;4(7-8):79-94.

[25] Robak P, Drozdz I, Szemraj J, Robak T. Drug resistance in multiple myeloma. *Cancer Treat Rev*. 2018 Nov;70:199-208.

[26] Kovalchuk AL, duBois W, Mushinski E, McNeil NE, Hirt C, Qi CF, Li Z, Janz S, Honjo T, Muramatsu M, Ried T, Behrens T, Potter M. AID-deficient Bcl-xL transgenic mice develop delayed atypical plasma cell tumors with unusual Ig/Myc chromosomal rearrangements. *J Exp Med*. 2007 Nov 26;204(12):2989–3001.

[27] Wen Z, Rajagopalan A, Flietner ED, Yun G, Chesi M, Furumo Q, Burns RT, Papadas A, Ranheim EA, Pagenkopf AC, Morrow ZT, Finn R, Zhou Y, Li S, You X, Jensen J, Yu M, Cicala A, Menting J, Mitsiades CS, Callander NS, Bergsagel PL, Wang D, Asimakopoulos F, Zhang J. Expression of NrasQ61R and MYC transgene in germinal center B cells induces a highly malignant multiple myeloma in mice. *Blood*. 2021 Jan 7;137(1):61-74.

[28] Kong G, Chang YI, You X, Ranheim EA, Zhou Y, Burd CE, Zhang J. The ability of endogenous Nras oncogenes to initiate leukemia is codon-dependent. *Leukemia*. 2016 Sep;30(9):1935-38.

[29] LoRusso PM, Canetta R, Wagner JA Balogh EP, Nass SJ, Boerner SA, Hohneker J. Accelerating cancer therapy development: the importance of combination strategies and collaboration. Summary of an Institute of Medicine workshop. *Clin Cancer Res*. 2012 Nov 15;18(22):6101–09.

[30] Kumar SK, LaPlant B, Chng WJ Zonder J, Callander N, Fonseca R, Fruth B, Roy V, Erlichman C, Stewart AK. Dinaciclib, a novel CDK inhibitor, demonstrates encouraging single-agent activity in patients with relapsed multiple myeloma. *Blood*. 2015 Jan 15;125(3):443-48.

[31] Parry D, Guzi T, Shanahan F, Davis N, Prabhavalkar D, Wiswell D, Seghezzi W, Paruch K, Dwyer MP, Doll R, Nomeir A, Windsor W, Fischmann T, Wang Y, Oft M, Chen T, Kirschmeier P, Lees EM. Dinaciclib (SCH 727965), a novel and potent cyclin-dependent kinase inhibitor. *Mol Cancer Ther*. 2010 Aug;9(8):2344-53.

[32] Kumar SK, Rajkumar V, Kyle RA, van Duin M, Sonneveld P, Mateos MV, Gay F, Anderson KC. Multiple myeloma. *Nat Rev Dis Primers*. 2017 Jul 20;3:17046.

[33] De Souza C, Chatterji BP. HDAC Inhibitors as novel anti-cancer therapeutics. *Recent Pat Anticancer Drug Discov*. 2015;10(2):145-62.

CHAPTER 2. HIGH-THROUGHPUT DRUG SCREEN IDENTIFIES THERAPEUTIC COMBINATIONS TARGETING ONCOGENES AND TUMOR SUPPRESSORS IN MULTIPLE MYELOMA

2.1 One Sentence Summary

A single agent drug screen identified combinations against multiple myeloma (MM) effective in MM cell lines, a novel animal model, and patient cells.

2.2 Abstract

Multiple myeloma (MM) is a neoplasm involving plasma cells in the bone marrow. Drug resistance and progression are common, underscoring the need for new drug combinations. We utilized a high-throughput screen of tool compounds to limit growth of 47 human MM cell lines. *In silico* robust regression analysis of drug responses revealed 43 potential synergistic combinations. We hypothesized that effective combinations would reduce oncogene expression and/or enhance tumor suppressor gene activity based on earlier genetic and drug studies that identified p16, Myc and mTOR as appropriate targets in myeloma. Thus, candidate combinations were evaluated for cooperative reductions in MYC protein expression in MM cells. Ten combinations cooperatively reduced MYC expression, which is frequently over-expressed in MM. Cooperative reductions in viability were observed with top combinations in proteasome inhibitor-resistant and sensitive MM cell lines but did not limit normal fibroblast viability. The combinations cooperatively increased p16 activity, while also enhancing cleaved caspase 3, leading to increased apoptosis. Combination-associated survival was evaluated in a transplantable Ras-driven allograft model of advanced MM that closely recapitulates myeloma in humans. Three combinations significantly prolonged survival in sublethally-irradiated C57BL/6 mice injected intracardiac with donor MM cells compared to control mice. Furthermore, the top three combinations reduced viability of *ex vivo* treated patient cells. Common genetic pathways similarly affected by the top drug combinations were those implicated in promoting cell cycle transition and pathways most upregulated by all combinations were involved in TGFB and SMAD3 signaling. These data identify potentially useful drug combinations for preclinical evaluation in drug-resistant MM and may ultimately reveal novel mechanisms of combined drug sensitivity.

2.3 Introduction

Multiple myeloma (MM), a neoplastic clonal proliferation of plasma cells affecting mostly older individuals, is one of the most common hematologic malignancies [1, 2], with an estimated 34,920 new cases and 12,410 deaths in the United States in 2019 alone [3]. Development of new therapeutics such as proteasome inhibitors (PI), immunomodulatory drugs, monoclonal antibodies, and autologous stem cell transplantation has resulted in prolonged survival of MM patients [1, 2, 4]. However, no therapy thus far is curative, and relapsed and/or refractory multiple myeloma (RRMM) eventually develops; particularly as a result of PI therapy [1, 2]. Thus, combining targeted agents has become important in treating RRMM and oncology in general [5]. Combining drugs circumvents tumor resistance by utilizing synergy, wherein the total effect of two or more drugs is greater than the sum of individual drug effects. Furthermore, identifying the mechanisms of molecular synergy provides a biologic rationale for proposed combinations and is essential for predicting clinical responses [6].

Previous research has provided evidence of efficacy and drug synergy for the combination of mTOR inhibitors (mTORi) and histone deacetylase inhibitors (HDACi) in human MM cell lines, a diverse set of cancer cell types, and MM cells isolated from patients [6, 7]. Importantly, a proposed mechanism of action of synergy in the combination – degradation of the transcription factor MYC – was elucidated via a biologically integrated, network-based approach using MM cell lines and patient datasets [6]. MYC activation (most commonly through locus rearrangements and gains, mRNA overexpression, and deregulation) is found in approximately 67% of MM and is associated with disease progression [8-10]. Additionally, NRAS and KRAS are frequently mutated in MM, associated with disease progression, and increase the stabilization of MYC via phosphorylation of serine 62 [6, 8, 11]. Furthermore, retroviral constructs overexpressing MYC alone or RAS alone were not very effective in inducing mouse plasma cell tumors compared with constructs that overexpressed both MYC and RAS under an IgM promoter and produced aggressive tumors in less than 30 days [12, 13]. Targeting MYC directly, unfortunately, has remained a key challenge in oncology due to large protein-protein interaction interfaces, lack of deep protein pockets, and nuclear localization [14, 15]. However, finding drug combinations that indirectly target MYC, while acting upon their own respective direct targets, serves as a useful alternative strategy and may provide additional opportunities for synergy in treating MM. Also,

loss of function of cell cycle transition checkpoint control gene p16 may result in uncontrolled cell proliferation, invasion, and metastasis of MM and other cancers, and inactivation may contribute to progression of disease [16].

We employed an agnostic discovery approach for identifying drug combinations to target MM utilizing a high-throughput drug screen of a compound library of over 1900 small molecules in 47 MM cell lines and *in silico* regression analysis to identify drug combinations predicted to reduce MM viability. Additionally, considering the importance of MYC in MM progression, we identified candidate tool combinations that cooperatively reduce MYC protein expression and increase tumor suppressor activity, while synergistically reducing the viability of both PI resistant and PI sensitive MM cell lines *in vitro*. We then evaluated the efficacy of our top drug combinations in prolonging viability in a transplantable Ras-driven allograft model of advanced MM that closely recapitulates myeloma in humans. The ability of the top three combinations to reduce the viability of patient cells *ex vivo* was evaluated via dose-response assays. Finally, gene set enrichment analysis of MM cells treated with the combinations revealed commonly affected pathways. Through expansion of the *in vitro* findings, extension to unique *in vivo* models, and investigation into the mechanisms of synergistic drug responses, this study provides strong preclinical rationale for further evaluation of novel drug combinations in treating MM.

2.4 Results

2.4.1 Drug screen reveals combinations cooperatively targeting MYC and p16 that reduce viability of MM cells

As part of our drug development approach, we screened ~1900 small molecules in 47 different MM lines with the NCATS Mechanism of Interrogation Platform E (MIPE) screen, normalized dose responses with positive (bortezomib) and negative (DMSO) controls and evaluated the results *in silico* using Palantir's foundry platform (Fig. 2.1). Drugs were selected for activity based on the following criteria: single agent dose-response curve class of -1.1 (complete response), AC50 < 2.0 μM, and activity in at least 25 of the 47 MM cell lines tested. In addition, drugs paired for regression analysis were selected as having different mechanisms of action, i.e., not targeting the same pathway. Robust regression analysis (Fig. S2.1A) of each drug versus every

other drug was utilized to generate a Pearson correlation coefficient (r^2) for each drug pair. Forty-three combinations were noted with r^2 values of at least 0.5 (indicating correlation) - (Table 2.1).

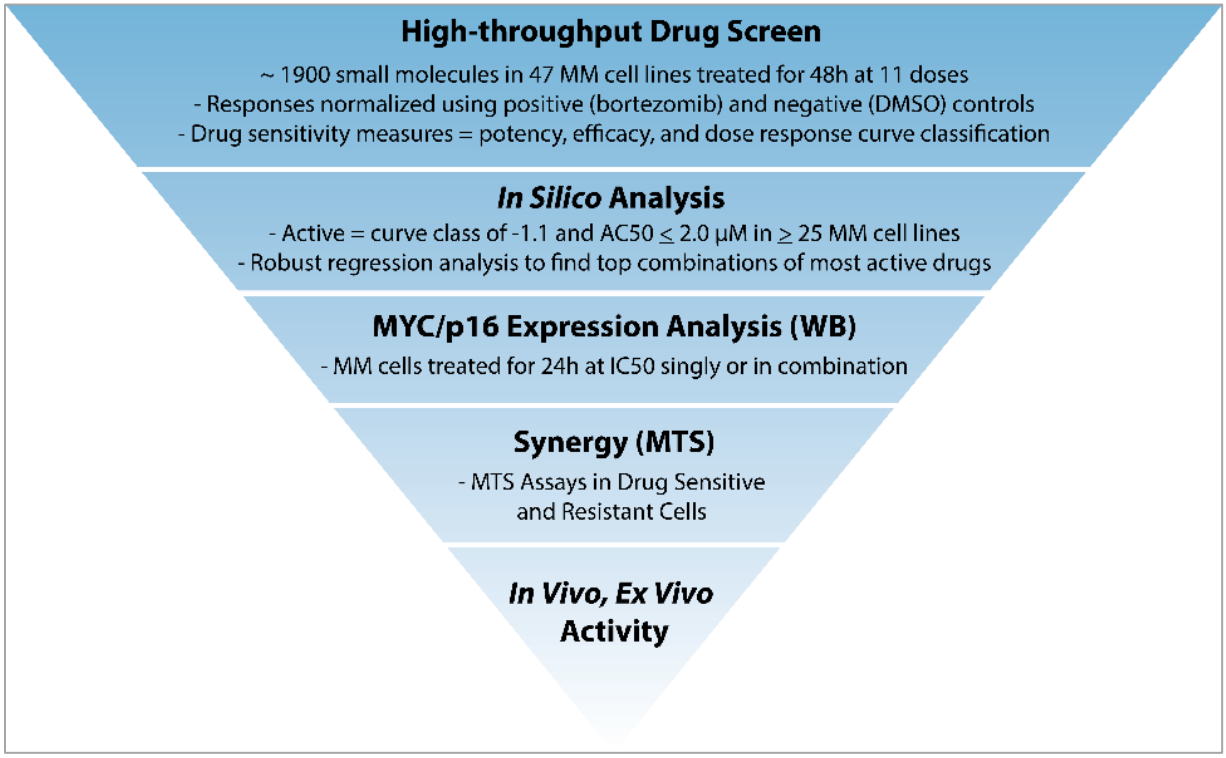

Figure 2.1. Prediction workflow used to find top drug combinations against MM. AC50 = half maximal activity concentration, WB = western blot, MTS = tetrazolium-based cell proliferation assay.

Table 2.1. Top Drug Combinations Against MM Cells Based on Robust Regression

r2	Compound 1 Target Gene	Compound 1 Name	Compound 2 Name	Compound 2 Target Gene	Cmpd 1 count	Cmpd 2 count
0.804	**HSP90AB1**	SNX-5422	NCGC00344999-01 = ITK(1)	**ITK**	35	39
0.836	**ITK**	NCGC00344999-01 = ITK(1)	VER-82576	**HSP90AB1**	39	33
0.822	**HSP90AB1**	Ganetespib	BS-194	**CDK1**	35	46
0.765	**HSP90AB1**	SNX-5422	NCGC00188382-01 = ITK(2)	**ITK**	35	45
0.732	**HDAC1**	Romidepsin	SR-3306	**MAPK8**	45	46
0.714	**TUBB**	XRP-44X	BMS-3	**LIMK1**	28	37
0.702	**HSP90AB1**	SNX-5422	NCGC00344990-01= ITK(3)	**ITK**	35	38
0.678	**TUBB**	XRP-44X	ON-01910	**PLK1**	28	37
0.671	**IKBKB**	IMD-0354	Niclosamide	**STAT3**	45	41
0.658	**HSP90AB1**	Ganetespib	Dacinostat	**HDAC1**	35	44
0.655	**AURKA**	Alisertib	Doxorubicin	**TOP2A**	29	46
0.645	**PIM3**	GDC-0349	PP242	**MTOR**	34	34
0.644	**TLR7**	CPG-52364	Sepantronium bromide	**BIRC5**	44	36
0.643	**ITK**	NCGC00344990-01 = ITK(3)	VER-82576	**HSP90AB1**	38	33
0.634	**HSP90AB1**	AT-13387AU	NCGC00344990-01= ITK(3)	**ITK**	39	38
0.634	**CDK1**	BS-194	Dacinostat	**HDAC1**	46	44
0.626	**MAPK8**	TCS JNK 5a	Indibulin	**TUBB**	33	28
0.616	**CDK1**	7-Hydroxystaurosporine	PIK-75	**PIK3CA**	37	33
0.614	**ITK**	NCGC00188382-01 = ITK(2)	Methylrosaniline chloride	**TNFRSF1A**	45	36
0.611	**PIK3CA**	PIK-75	Flavopiridol	**CDK1**	33	44
0.606	**TUBB**	XRP-44X	IVX-214	**PLK1**	28	30
0.602	**TUBB**	4-Demethylepipodophyllotoxin	Picropodophyllin	**IGF1R**	40	38
0.602	**MET**	Tivantinib	4-Demethylepipodophyllotoxin	**TUBB**	28	40
0.597	**TUBB**	XRP-44X	Picropodophyllin	**IGF1R**	28	38
0.594	**MAPK8**	SR-3306	Pracinostat	**HDAC1**	46	34
0.583	**PLK1**	IVX-214	Noscapine	**TUBB**	30	36
0.571	**CDK1**	BS-194	VER-82576	**HSP90AB1**	46	33
0.563	**TUBB**	Lexibulin hydrochloride	ON-01910	**PLK1**	27	37
0.557	**HSP90AB1**	SNX-5422	Methylrosaniline chloride	**TNFRSF1A**	35	36
0.556	**TUBB**	XRP-44X	AST-1306	**ERBB2**	28	28
0.540	**HSP90AB1**	Geldanamycin	Idarubicin hydrochloride	**TOP2A**	34	41
0.540	**HSP90AB1**	CNF-2024	Idarubicin hydrochloride	**TOP2A**	35	41
0.536	**TUBB**	XRP-44X	Tivantinib	**MET**	28	28
0.535	**MCL1**	VU0482089-2	AV-412	**EGFR**	29	33
0.534	**HSP90AB1**	CNF-2024	Doxorubicin	**TOP2A**	35	45
0.531	**MCL1**	VU0482089-2	1-alpha-Hydroxyergocalciferol	**VDR**	29	28
0.524	**PIM3**	GDC-0349	GNE-493	**PIK3CA**	34	40
0.524	**IGF1R**	Picropodophyllin	Noscapine	**TUBB**	38	36
0.521	**CDK1**	R-547	PIK-75	**PIK3CA**	29	33
0.516	**HDAC1**	Abexinostat	3-Methyladenine	**PIK3CA**	43	47
0.515	**MAPK8**	TCS JNK 5a	Noscapine	**TUBB**	33	36
0.508	**SRC**	KX-01	Indibulin	**TUBB**	38	28
0.504	**TUBB**	Lexibulin hydrochloride	Merck-22-6	**AKT1**	27	25

As shown in Table 2.1, the top 43 combinations selected for *in vitro* analysis were selected based on a Pearson correlation coefficient (r^2) of ≥ 0.5. Listed are each compound's target gene and name, as well as the number of cell lines in which each compound (cmpd) is active (dose-response curve class -1.1 [complete response], AC50 <2.0 μM).

The top 43 combinations of tool compounds with r^2 values of at least 0.5 were then evaluated for cooperative reduction of MYC protein expression in L363 MM cells via western blot (WB) assay when treated at the AC50 dose for 24 hours. Ten of the 43 combinations cooperatively reduced expression of MYC (Table 2.2) and six of the ten combinations also increased tumor suppressor activity as indicated by increased p16 protein (Table 2.2, Fig. S2.1B-G, WB).

Table 2.2. Combinations That Reduced MYC Protein Expression in L363 MM Cells

Reduced MYC Protein Expression vs. Single Agent/Control in L363 MM Cells					
Drug 1	**Primary Target 1**	**Drug 2**	**Primary Target 2**	**r^2 (Robust Regr.)**	**↑p16 vs. ctrl**
BS-194	**CDK1**	Dacinostat	**HDAC1**	0.64	✓
Alisertib	**AURKA**	Doxorubicin	**TOP2A**	0.66	✓
Geldanamycin	**HSP90**	Idarubicin Hcl	**TOP2A**	0.54	✓
Noscapine	**TUBB**	IVX-214	**PLK1**	0.58	✓
XRP-44X	**TUBB**	IVX-214	**PLK1**	0.61	✓
BS-194	**CDK1**	VER-82576	**HSP90**	0.57	✓
AT13387AU	**HSP90**	ITKi (4990)	**ITK**	0.63	
SNX-5422	**HSP90**	ITKi (4990)	**ITK**	0.70	
VER-82576	**HSP90**	ITKi (4990)	**ITK**	0.84	
VU-482089	**MCL1**	AV-412	**EGFR**	0.54	

As shown in Table 2.1, the top 43 combinations selected for *in vitro* analysis were selected based on a Pearson correlation coefficient (r^2) of ≥ 0.5. Listed are each compound's target gene and name.

In the next step, compounds that were selected for further testing of the six combinations included drugs already approved to treat MM or other hematologic malignancies and/or drugs currently in clinical trials to treat MM, as well as novel combinations not yet investigated in treating MM. Out of the six combinations that simultaneously reduced MYC and increased p16 protein expression, three combinations were found to be synergistic in their ability to inhibit myeloma growth (Fig. 2.2D-F). The three combinations were the cyclin dependent kinase inhibitor (CDKi) dinaciclib + the histone deacetylase inhibitor (HDACi) entinostat and a topoisomerase II inhibitor (doxorubicin – TOP2Ai) combined with either the aurora kinase A inhibitor (AURKAi) alisertib or heat shock protein 90 inhibitor (HSP90i) SNX-2112.

2.4.2 The top three drug combinations reduce oncogenic MYC activity and increase tumor suppressor activity in MM cell lines, regardless of inherent sensitivity or resistance

The 47 cell lines were ranked for their overall sensitivity/resistance based on the mean AC50 for all 1900 compounds in the initial screen (Table 2.3). The ability of the top three drug combinations (CDKi/HDACi, TOP2Ai/AURKAi, and TOP2Ai/HSP90i) to reduce MYC protein while increasing p16 was evaluated in three cell lines inherently more sensitive to the compounds from the high-throughput drug screen, as well as three cell lines inherently more resistant. Of the three top combinations, CDKi/HDACi was the most effective overall at reducing MYC protein, increasing p16, and inducing apoptosis (as indicated by cleavage of caspase 3) in all three (L363, JIM1, INA6) inherently more sensitive cell lines (Fig. 2.2A) and in two (Karpas-417, LP1) of the three more resistant cell lines (Fig. 2.2C).

Table 2.3. Forty-seven Multiple Myeloma Cell Lines Ranked by Mean AC50

Cell Line	mean AC50 for drugs (Robust Regression)	
KMS21BM_JCRB	10.123	
Karpas417_ECACC	**4.309**	R
MMM1_PLB	3.449	
RPMI8226_ATCC	**2.866**	
OCIMY1_PLB	2.675	
JJN3_DSMZ	2.583	
KMS26_JCRB	2.566	
OPM2_DSMZ	2.526	
EJM_DSMZ	2.363	
SKMM1_PLB	2.357	
U266_ATCC	2.218	
LP1_DSMZ	**2.132**	
MOLP8_DSMZ	1.766	
KMS28PE_JCRB	1.690	
MM1R_ATCC	1.683	
NCIH929_DSMZ	1.659	
MM1S_ATCC	1.481	
KMS34_JCRB	1.365	
FR4_PLB	1.252	
Karpas620_DSMZ	1.140	
H1112_PLB	1.094	
ARP1_JJKsccF8	1.074	
OCIMY7_PLB	1.024	
PE2_PLB	1.018	
KMS12BM_JCRB	0.949	
PCM6_Riken	0.877	
KMS12PE_JCRB	0.835	
KHM11_PLB	0.825	
ARD_JJKsccE7	0.758	
JIM3_ECACC	0.736	
KMM1_JCRB	0.687	
KMS28BM_JCRB	0.680	
AMO1_DSMZ	0.639	
XG6_PLB	0.605	
OCIMY5_PLB	0.598	
OPM1_PLB	0.573	
KMS20_JCRB	0.547	
Delta47_JCRB	0.537	
KMS27_JCRB	0.522	
UTMC2_PLB	0.503	
L363_DSMZ	**0.482**	
Karpas25_ECACC	0.464	
JIM1_ECACC	**0.447**	
INA6_PLB	**0.391**	
XG1_PLB	0.332	
VP6_DJ	0.318	S
KMS11_JCRBsus	0.294	

In Table 2.3, the 47 different MM cell lines were stratified based on their overall sensitivity (S) or resistance (R) to all 1900 compounds in the NCATS MIPE screen. Bolded cell lines were used to test top combination efficacy in inherently sensitive (L363, JIM1, and INA6) and resistant (LP-1, RPMI-8226, Karpas417) MM lines.

2.4.3 Evaluation of synergy and microenvironment effects in top drug combinations.

Dose-response curves were generated via MTS assay for the top 3 drug combinations in L363 MM cells, treated for 48 hours with each drug singly or in combination at a 1:1 molar ratio (Fig. 2.2C-E). All three combinations synergistically reduced the viability of L363 MM cells, as determined by Chou-Talalay combination indices (CI) less than 1.0 [17]. An 8x8 dose matrix combination response screen of each of the top three combinations at 7 different concentrations, all combinations thereof, was performed in L363 MM cells to ascertain the activity and synergy across a spectrum of doses. Heatmaps (Fig. 2.2F-H) indicate the percent inhibition of treated cells vs. vehicle control after 48 hours of exposure to drugs. For each of the top three combinations, synergy was achieved at a lower concentration of each drug than the half maximal inhibitory concentration (IC50) of each individual agent, indicating lower concentrations of each drug may be used in combination to generate a pharmacologically achievable reduction in MM viability. Surface plots of the excess inhibition of highest single agent (EOSHA) are shown in supplemental figure S2.2A-C, with the CDKi/HDACi combination achieving an HSA score of 15.

Figure 2.2. High-throughput drug screen reveals combinations that cooperatively target MYC and p16 and reduce viability of MM cells. A-B) Representative WB analysis of MM cell lines resistant (1A) or sensitive (1B) to all drugs used in screen treated for 24 hours with the top 3 drug combinations at the AC50 concentration (the concentration at half-maximal activity; equal to IC50) for each line (C1 = dinaciclib (CDKi) + entinostat (HDACi), C2 = Doxorubicin (TOP2Ai) + Alisertib (AURKAi), C3 = Doxorubicin + SNX-2112 (HSP90i). Lysates of treated cells were probed for MYC, p16, total and cleaved caspase 3 (Casp3 and CC3, respectively), and β-actin. C-E) Dose-response curves for top 3 drug combinations in L363 MM cells. Cell viability was assessed with MTS assay 48h after treatment with escalated dose concentrations of either drug individually or in combination at a 1:1 molar ratio. Each data point represents mean of 4 wells and error bars indicate replicate standard deviation. IC50 (in nM) for individual drugs and combination in each table. Chou-Talalay computation of combination indices (CI) for treated cells are shown for 50% affected fraction 48 hours post-exposure. Synergy is interpreted as CI<1.0. F-H) Graphical depiction of dose-matrix analyses for the top drug combinations in L363 MM cells. Percent inhibition of cell growth is shown for each different combination of doses and colorized in red. Cells were treated for 48 hours with different concentrations of each drug (indicated by X- and Y-axes) singly or in combination. Arrows indicate individual drug IC50 (half-maximal inhibitory concentration) as determined by MTS dose-response assay, ovals surround optimal dose for combinations, as determined by synergy scoring.

Figure 2.2 continued

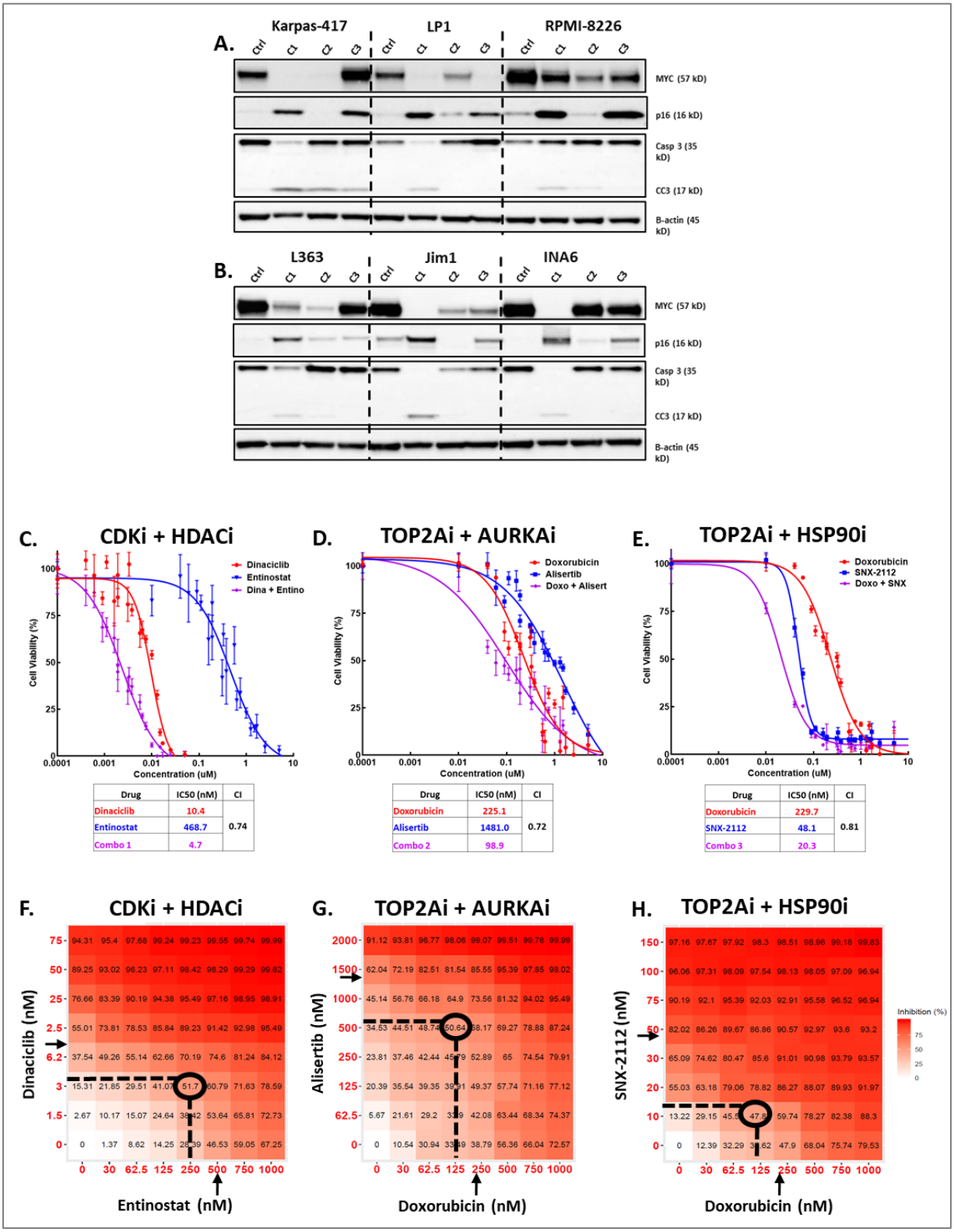

The ability of the top combinations to reduce the viability of MM cells under *in vitro* conditions that more closely recapitulate the bone marrow microenvironment was evaluated by co-culturing L363 MM cells with a feeder layer of immortalized HS-5 bone marrow stromal cells (BMSCs). HS-5 BMSCs treated alone with the drugs, singly or in combination, for 48 hours were more resistant to inhibition compared to L363 cells alone (Fig. 2.3A-C). Two of the combinations (CDKi/HDACi and TOP2Ai/AURKAi) were still effective at reducing the IC50 compared to single agent, while the combination of TOP2Ai/HSP90i did not (Fig. 2.3A-C). These results indicate that the drug combinations are somewhat selective for MM cells and, in two of the combinations, are still effective at reducing MM viability in the context of co-culture. Additionally, the top combinations were largely non-toxic in non-neoplastic human H1634 fibroblasts, treated for 48 hours with drugs from each of the top combinations (Fig. S2.2D-F) compared to L363 MM cells. The large difference between the cytotoxic effects of the combinations in MM tumor cells compared to that in non-neoplastic H1634 fibroblasts at achievable drug concentrations indicates a favorable safety margin for each combination.

Each combination was also evaluated in the context of drug-resistance via *in vitro* dose response assays in cell lines selected for resistance to some of the most common first-line therapeutics against MM (Fig. 2.3D): LP1, MM1, and RPMI-8226 parental MM cell lines, and cell lines with resistance-induced by treatment with a proteasome inhibitor (LP1-OpzR, oprozomib), a corticosteroid (MM1.R, dexamethasone), or a topoisomerase inhibitor (RPMI-8226 Dox40, doxorubicin), respectively, for repeated passages. Resistance to respective drugs compared to parental cell line (or sensitive line in the case of MM1.S cells) was confirmed via 48-hour dose response assay (Fig. S2.2G-I). Parental and resistant cell lines were treated for 48 hours in dose-response assays with the top three drug combinations, either singly or in combination. IC50 for each combination in each of the parental and resistant (or sensitive and resistant in the case of MM1 cells) is shown in Supplemental Table 2.1. As shown in the heatmap (Fig. 2.3D), the Chou-Talalay combination index (CI) scores were all below 1, indicating synergy. Further, the CI scores were largely similar for each combination, regardless of induced drug-sensitivity/resistance, with the exception of the doxorubicin/alisertib combination in MM1 parental and dexamethasone-resistant MM cells. The CDKi/HDACi combination of dinaciclib/entinostat performed best overall at synergistically reducing viability of the diverse set of parental and drug-resistant MM cells.

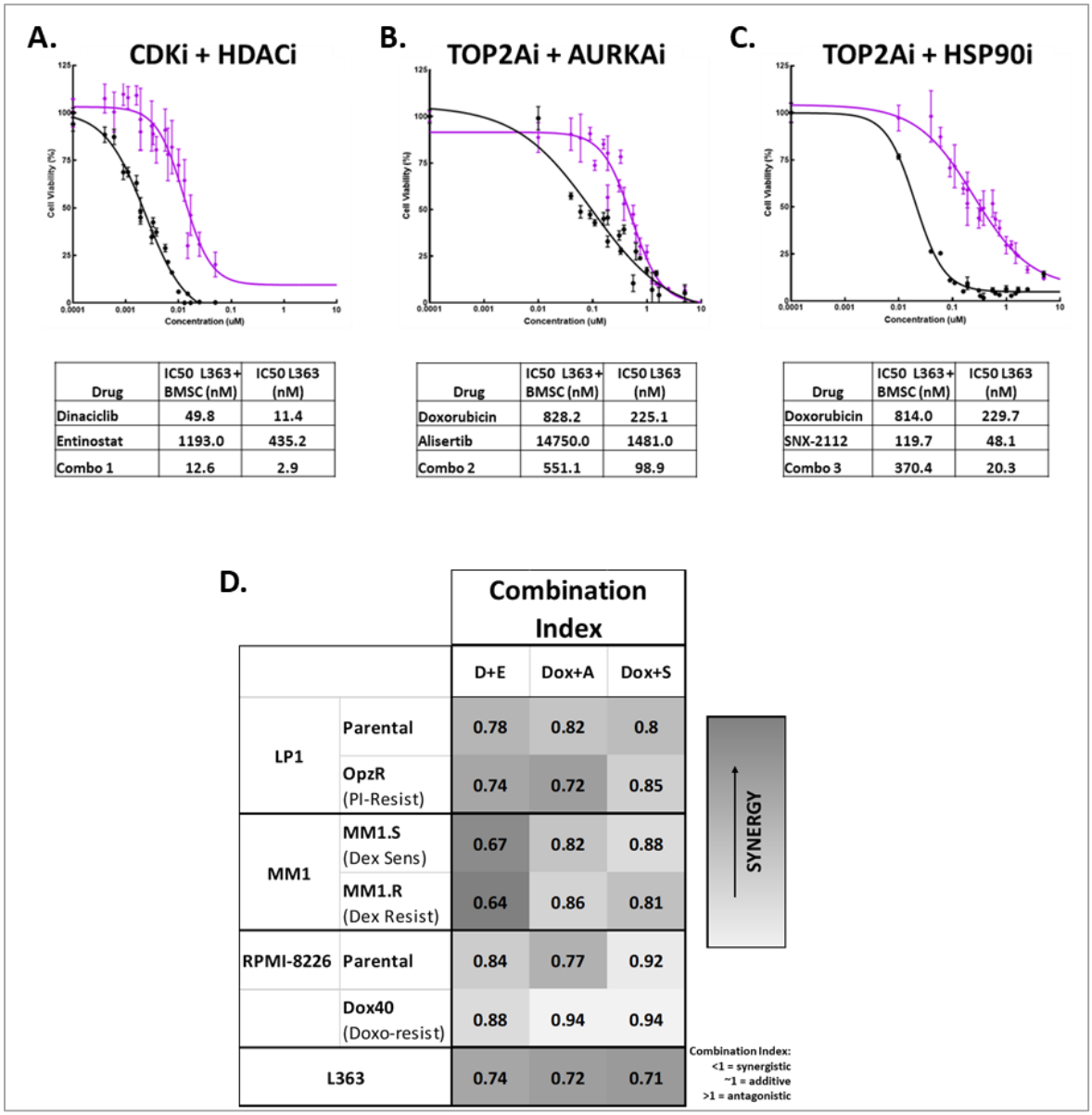

Drug	IC50 L363+ BMSC (nM)	IC50 L363 (nM)
Dinaciclib	49.8	11.4
Entinostat	1193.0	435.2
Combo 1	12.6	2.9

Drug	IC50 L363+ BMSC (nM)	IC50 L363 (nM)
Doxorubicin	828.2	225.1
Alisertib	14750.0	1481.0
Combo 2	551.1	98.9

Drug	IC50 L363+ BMSC (nM)	IC50 L363 (nM)
Doxorubicin	814.0	229.7
SNX-2112	119.7	48.1
Combo 3	370.4	20.3

D.

		Combination Index		
		D+E	Dox+A	Dox+S
LP1	Parental	0.78	0.82	0.8
	OpzR (PI-Resist)	0.74	0.72	0.85
MM1	MM1.S (Dex Sens)	0.67	0.82	0.88
	MM1.R (Dex Resist)	0.64	0.86	0.81
RPMI-8226	Parental	0.84	0.77	0.92
	Dox40 (Doxo-resist)	0.88	0.94	0.94
L363		0.74	0.72	0.71

SYNERGY

Combination Index:
<1 = synergistic
~1 = additive
>1 = antagonistic

Figure 2.3. Evaluation of synergy in top drug combinations. A-C) Dose-response curves, along with tables listing IC50 in nM, for L363 MM cells in monoculture and L363 MM cells cocultured with HS-5 BMSCs treated for 48 hours with increasing concentrations of the top 3 drug combinations (A = CDKi/HDACi, B = TOP2Ai/AURKAi, C = TOP2Ai/HSP90i). Black curves represent percent viability, relative to DMSO-treated control, in L363 cells cultured alone, purple curves show dose responses for L363 cocultured with human HS-5 bone marrow derived stromal cells (BMSC). D) Heat map depicting Chou-Talalay combination index scores for the following parental MM cell lines and their drug-resistant counterparts: LP1-Parental and LP1-OpzR (resistance induced via prolonged incubation with the proteasome inhibitor (PI) oprozomib (Opz)), Dexamethasone (Dex)-sensitive MM1.S and Dex-resistant MM1.R cells, RPMI-8226-Parental and RPMI-8226-Dox40 (treatment-induced resistance to the topoisomerase inhibitor doxorubicin), all compared to CI scores of L363. D+E = dinaciclib (CDKi) + entinostat (HDACi), Dox + A = doxorubicin (TOP2Ai) + alisertib (AURKAi), Dox + S = doxorubicin + SNX-2112 (HSHP90i). Darker gray = more synergy.

2.4.4 Comparison of top drug combinations in a novel allograft mouse model of MM

In an initial assessment of the *in vivo* activity of the top drug combinations elucidated from the high-throughput drug screen, a 16-week *in vivo* efficacy study was performed in C57BL/6J mice first sublethally irradiated then injected intravenously with murine Vk*MYC; $Nras^{LSL\ Q61R/+}$; IgG1-Cre (VQ) cells harvested from bone marrow of donor mice (Fig. 2.4A). After 6-8 weeks, serum M-spikes, as evidenced by Igγ band on serum protein electrophoresis, are evident (Fig. 2.4A; Fig. S2.3A). As shown in the representative sternal bone marrow photomicrographs of a C57BL/6J mouse 12 weeks after being sublethally irradiated and intravenously injected with saline (Fig. 3B) versus sternal bone marrow of a sublethally irradiated C57BL/6J mouse injected intravenously with $5x10^6$ VQ cells (Fig. 3C), the VQ cells completely obliterate normal hematopoietic cells within the marrow and even induce bony lysis of the cortex (Fig. S3 B, bony lesion); similar to what is observed in the bone and marrow of humans affected by MM. Treatment with the top drug combinations commenced when M-spikes were first detected in mice (Fig. 3D). Treatments were as follows: CDKi/HDACi (dinaciclib and entinostat), TOP2Ai (doxorubicin) and AURKAi (alisertib) or HSP90i (SNX-2112), and mTORi/HDACi (rapamycin and entinostat); n=5 (doses and regimens described in methods section 2.6.7). Survival of C57BL6/J mice injected with $5x10^6$ VQ cells IC, treated with the top drug combinations was significantly prolonged compared to control mice and was also slightly longer compared to a previously investigated combination of rapamycin (mTORi) and entinostat (HDACi). Further, as depicted in the graphical representation of M-spikes determined from electrophoretograms, the mean M-spike percentage in treated mice remained lower than that of control until the final weeks of treatment (Fig. 3E), when animals became moribund necessitating humane euthanasia.

2.4.5 Top drug combinations are effective at selectively reducing the viability of human CD138+ MM cells *ex vivo*

The capability of the top combinations to selectively reduce the viability of MM cells was evaluated in bone marrow biopsy samples obtained from patients with confirmed smoldering multiple myeloma (SMM). Cells were selected for CD138 status using magnetic-activated cell sorting (MACS) (Fig. 2.4F). CD138 positive and negative cells were treated with the top 3 combinations of dinaciclib (10 nM) and Entinostat (500 nM), doxorubicin (225 nM) and Alisertib

(2 uM), or doxorubicin (225 nM) and SNX-2112 (50 nM) for 48 hours; viability was compared to that of control CD138 positive or CD138 negative cells treated with DMSO) (n = 3). Overall, all three combinations effectively reduced the viability of CD138 positive MM cells compared to DMSO alone. However, the CDKi/HDACi and TOP2Ai/AURKAi combinations were more selective in reducing MM viability compared to the TOP2Ai/HSP90i.

Figure 2.4. Evaluating the top drug combinations in a novel allograft mouse model of MM and human myeloma cells *ex vivo*. A) Illustration of VQ inoculation scheme. 6–8-week-old C57BL/6J mice were sublethally irradiated then injected intracardiac with 5x10^6 Vk*MYC; $Nras^{LSL\ Q61R/+}$; IgG1-Cre (VQ) cells harvested from bone marrow of donor mice. After 6-8 weeks, serum M-spikes, as evidenced by the γ immunoglobulin band on serum protein electrophoresis, are evident. Once M-spikes were detected in mice, treatment with the top drug combinations commenced. B-C) Photomicrographs (bar = 100 µm; inset bar = 250 µm; H&E stain) of C57BL/6J mouse sternum 12 weeks post-IC injection with either saline (B, normal bone marrow) or VQ cells (C, marrow replaced by neoplastic plasma cells). D) Survival plots of C57BL6/J mice injected with 5x10^6 VQ cell IC, treated with the top drug combinations vs a previously investigated combination of rapamycin (mTORi) and entinostat (HDACi), all compared to DMSO-treated control mice. CDKi (dinaciclib, 20 mg/kg, IP, 3x/week + HDACi (entinostat, 20 mg/kg, PO 5x/week; TOP2Ai, (doxorubicin,4 mg/kg IV 1x/week) + AURKAi (alisertib,30 mg/kg PO 5x/week); or HSP90i (SNX-2112, 20 mg/kg, PO, 3x/week), n= 5. * indicates significantly prolonged survival vs. DMSO-treated control mice ($p < 0.01$, Log-Rank test). E) Graphical representation of mean M-spike percentage for each treatment group of mice administered one of the top drug combinations, combined mTORi-HDACi, or DMSO control. Each data point represents mean M-spike percentage of all mice for a given time point, error bars indicate standard deviation amongst group mice. F) Viability of human CD138 positive (MM) and 138 negative cells extracted from bone marrow of smoldering multiple myeloma patients (n=3). Cells were selected for CD138 status using magnetic-activated cell sorting (MACS). CD138 positive and negative cells were treated with the top 3 combinations of dinaciclib (10 nM) and entinostat (500 nM), doxorubicin (225 nM) and alisertib (2 uM), or doxorubicin (225 nM) and SNX-2112 (50 nM) for 48 hours. Solid bars indicate average viability for each combination in CD138 positive cells, hash-marked bars indicate the average viability for CD138 negative cells. Error bars = standard deviation. ∗ =$p < 0.001$; NS = no significance $p > 0.05$ by unpaired two-tailed Student's t test.

Figure 2.4 continued

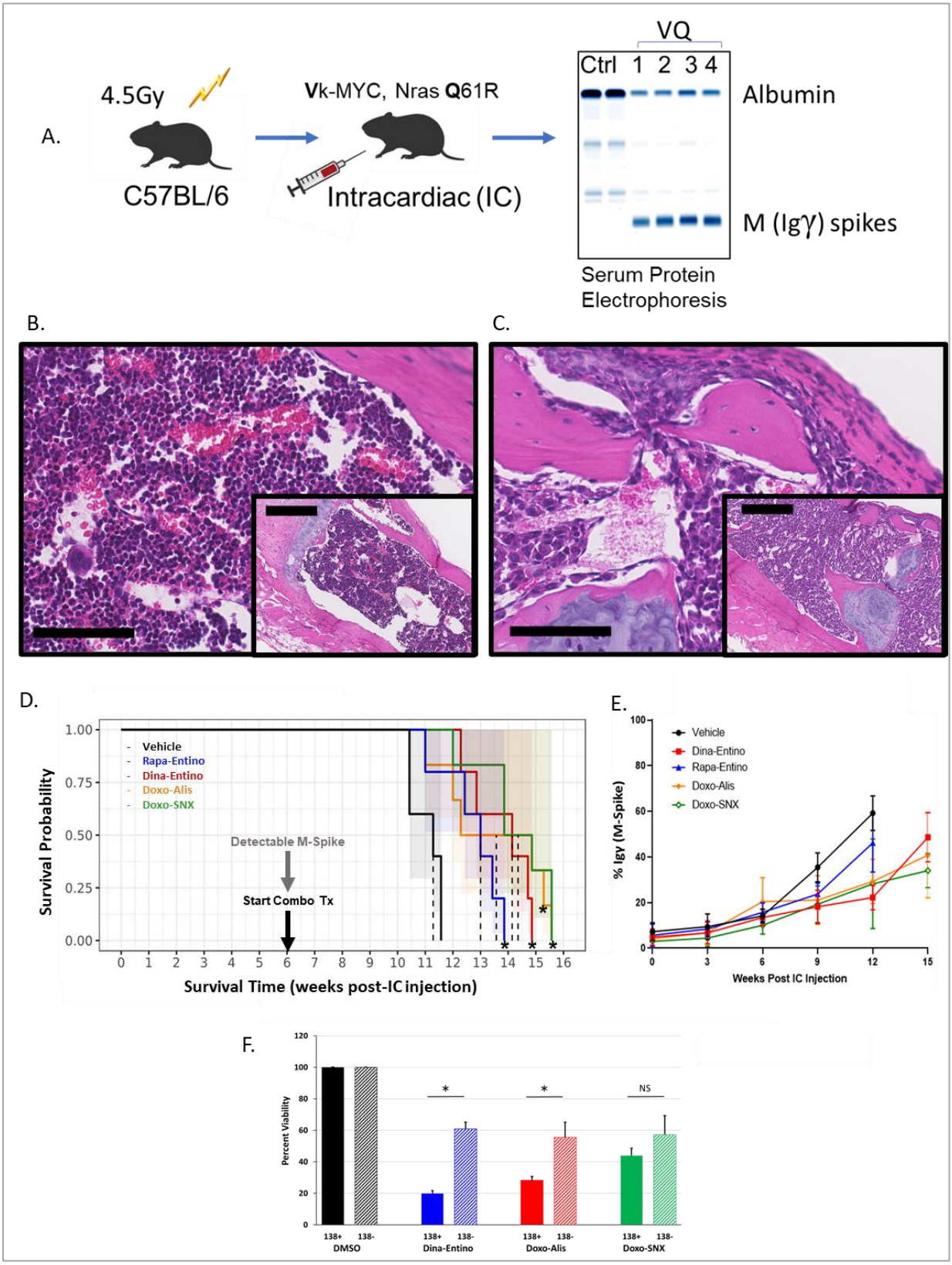

2.4.6 Genetic pathways commonly affected by the top combinations

To determine if common genetic pathways are similarly affected by the top drug combinations, L363 MM cells were treated for 48 hours with single agent IC50 concentrations of the top three drug combinations (CDKi/HDACi, TOP2Ai/AURKAi, and TOP2Ai/HSP90i). Two separate CDKi/HDACi combinations (dinaciclib/entinostat and dinaciclib/mocetinostat) were included to provide more robust results for the most promising combination. 48-hour dose response results for dinaciclib and mocetinostat in L363 cells are shown in supplemental figure S2.5. Purified RNAs from each treatment were analyzed via the Nanostring nCounter® digital gene expression codeset system, and counts were normalized to mRNA of five housekeeping genes (ZNF384, MRPS5, CNOT4, NUBP1, and SF3A3). Of the 143 genes significantly changed by the top drug combinations versus control (Fig. S2.4A-B), a total of 125 genes were significantly upregulated simultaneously, or downregulated simultaneously, by all combination treatments (Fig. S2.4C). Forty-nine genes were concordantly upregulated and 76 were concordantly downregulated. Next, 78 of the concordantly upregulated or downregulated genes were found to induce a two-fold change in the average profile calculated across all the combination treatments (38 up-regulated and 40 down-regulated genes). We then utilized DAVID pathway analysis and Fisher's exact test to determine the overrepresented Gene Ontology (GO) function in the concordant response signature of the 78 genes (Fig. 2.5A), and enriched GO terms were selected with nominal p-values less than 0.05. For each over-represented GO term a z-score was computed based on the number of up-regulated and down-regulated genes according to the formula (up or down)/sqrt(total) proposed by Walter et al. [18] and visualized with bubble-plots. The pathways most downregulated by all combinations (GO:0005654, GO:0044770, GO:0044772) were those implicated in promoting cell cycle transition (Fig. 2.5, Appendix A), indicating a common beneficial effect in preventing MM cell growth. The genes most downregulated by the combinations included HISTH1H3B, MNAT1, CDK4, CCND2, CHEK1, E2F1, CASP3 and BCL2. The pathways most upregulated by all combinations (GO:0007178 and GO:0007179) were involved in TGFB and SMAD3 signaling. Among these pathways, genes most downregulated included ID1, ID2, HSPB1, HSPA1A, SMAD3, UBB, FUT8 and TGFB1. Increasing TGFB and SMAD3 signaling may be an undesired effect and a potential resistance mechanism against these combinations.

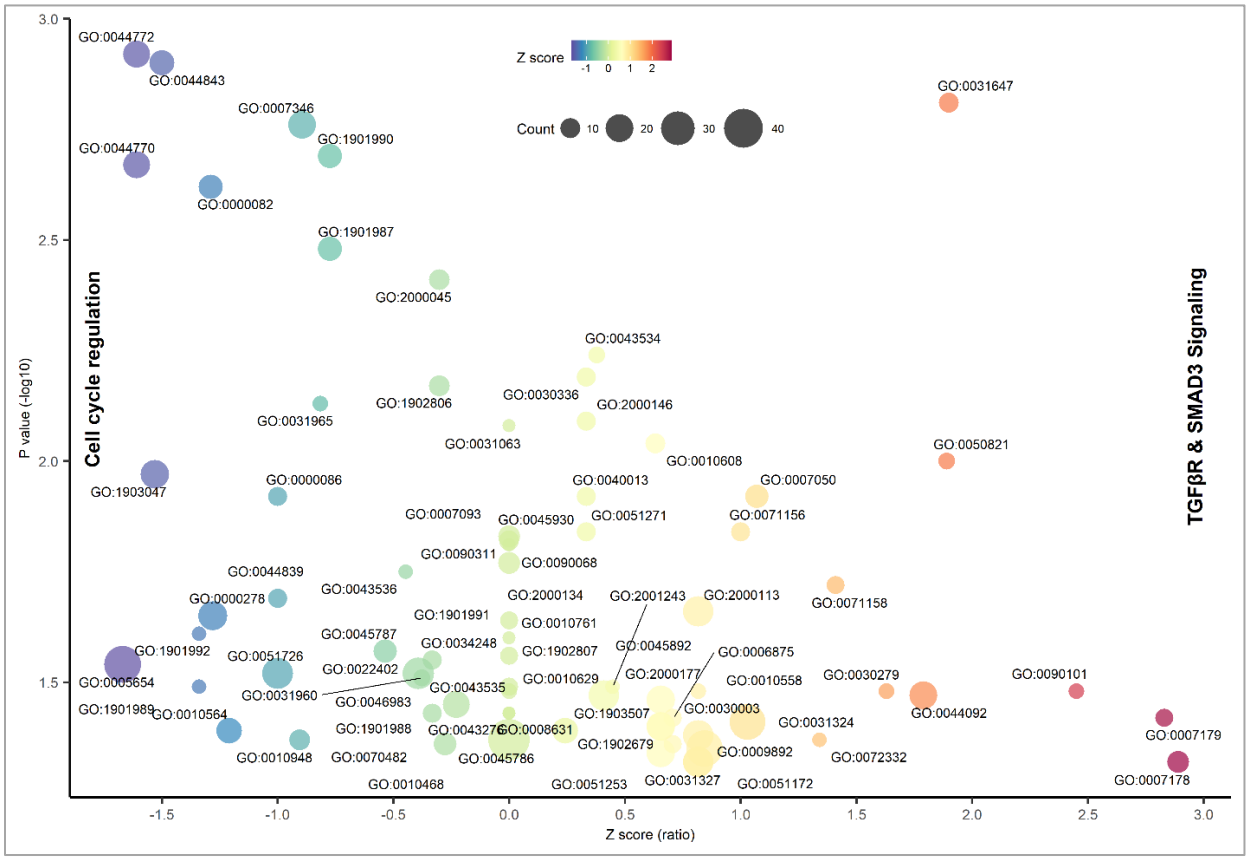

Figure 2.5. Pathways most commonly affected by the top 3 combinations (CDKi/HDACi, TOP2Ai/AURKAi, and TOP2Ai/HSP90i) using single agent IC50 concentrations of each drug. Purified RNA from each sample was analyzed using the nanoString nCounter® system. Raw counts were normalized to mRNA of five housekeeping genes (ZNF384, MRPS5, CNOT4, NUBP1, and SF3A3). Statistical significance based on false discovery rate of 5%. The concordant response signature includes genes significantly changed in the same direction by each combination treatment (Total=125, 49 up-regulated and 76 down-regulated genes), and that reached 2-fold change in the average fold-change profile calculated across all the combination treatments (Total=78, 38 up-regulated and 40 down-regulated genes). Fisher's exact test was used to determine overrepresented Gene Ontology (GO) functions in the concordant response signature of 78 genes. Enriched GO terms were selected with nominal p-value less than 0.05. For each over-represented GO term a z-score was computed based on the number of up-regulated and down-regulated genes according to the formula (up-down)/sqrt(total) proposed by Walter et al. [18] and visualized with bubble-plots. The pathways most downregulated by all combinations include those involved in cell cycle regulation. All top combinations also commonly increase TGFB and SMAD3 signaling, which may be an undesired effect, potentially identifying a resistance mechanism for these combinations.

2.4.7 Overcoming drug resistance in combination therapy by co-targeting the TGFβ pathway.

Upregulating the transforming growth factor β (TGFβ) signaling pathway is a common, potentially deleterious, effect of the top three combinations based on the gene set enrichment analysis and Fisher's exact test results (Fig. 2.5). With this knowledge we set out to determine if the addition of a drug targeting the TGFβ pathway would be effective in further reducing the viability of L363 MM cells co-cultured with HS-5 BMSCs (Fig. 2.6A). Indeed, the addition of the TGFβ-receptor inhibitor SB505124 was effective at cooperatively reducing L363 MM cell viability in co-culture with HS5 cells. The IC50 value for triple therapy (CDKi /HDACi + TGFβi) was 4.6 times lower than that of the CDKi/HDACi combination alone. Additionally, in a 48-hour viability assay of human SMM patient bone marrow biopsy sample cells, the addition of SB505124 to the CDKi/HDACi combination selectively and effectively reduced the viability of CD138 positive cells by almost 40%; while relatively sparing CD138 negative cells (n = 3) – (Fig. 2.6B).

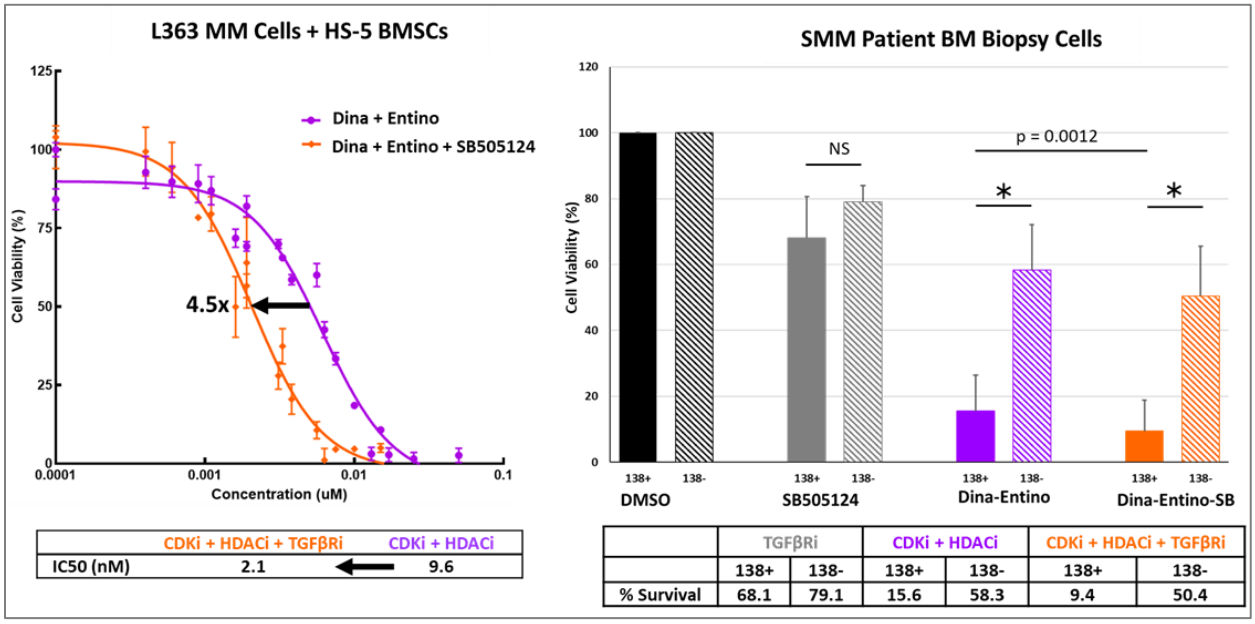

Figure 2.6. Co-targeting the TGFβ pathway with combination therapy. A) Dose-response curves for L363 MM cells, cocultured with HS-5 BMSCs for 48 hours with escalated doses of either combined CDKi/HDACi of dinaciclib and Entinostat (purple curve) or combined CDKi/HDACi + TGFβRi (orange curve; dinaciclib + entinostat + SB505124) at a 1:1 or 1:1:1 molar ratio (in nM), respectively. Arrow = IC50 shift. B) Viability of human CD138 positive (MM) and 138 negative cells extracted from bone marrow of SMM patients (n=3). Cells were selected for CD138 status using MACS. CD138 positive and negative cells were treated with the SB505124 (TGFβRi – 5 uM), dinaciclib (CDKi – 10 nM) and entinostat (HDACi – 500 nM), or CDKi + HDACi + TGFβRi for 48 hours. Solid bars indicate the average viability of CD138 positive cells and hash-marked bars represent the average viability for CD138 negative cells. Error bars = standard deviation. ∗ =p <0.001; NS = no significance p > 0.05 by unpaired two-tailed Student's t test. p = 0.0012 indicates p-value for significance in comparison of CD138 positive cells treated with CDKi + HDACi versus CDKi + HDACi + TGFβRi.

2.5 Discussion

To find potentially cooperative drug combinations for treating MM, we used a multilayered drug combination prediction workflow based on a high-throughput drug screen to identify effective single agents in most of the tested MM cell lines, followed by *in silico* robust regression analysis of all active drugs, and selection for combinations that reduced oncogenic MYC protein expression while increasing p16 tumor suppressor activity. These selection methods were then followed by several *in vitro* methods of evaluating synergy of our top combinations. The efficacy of the top three drug combinations (CDKi/HDACi, TOP2Ai/AURKAi, and TOP2Ai/HSP90i) was further investigated in cell lines with varying degrees of inherent sensitivity or resistance to the

drugs. The combinations were generally non-toxic in non-neoplastic human fibroblasts based on the 48-hour viability assay and the large difference in the cytotoxicity on myeloma cells versus fibroblasts; this suggests favorable safety margins for the combinations. Together, these data provide a relatively agnostic approach to identify novel drug combinations for further preclinical development in treating multiple myeloma, especially in cases resistant to first-line treatments.

Robust regression analysis was employed to identify potentially cooperative combinations based on individual drug activity across most of the MM cell lines tested. This strategy overcomes the limitations of other regression models, such as ordinary least squares, in that it's not overly affected by extreme outliers [19]. Additionally, robust regression analysis enabled the prediction of potential combinations, regardless of drug target, to treat a wide variety of MM subtypes without the cumbersome and time-consuming step of individually testing each of the approximately 5 million potential drug combinations/cell lines *in vitro* [19-23]. Many of the target classes for the 43 drug combinations selected based on the robust regression analysis (Table 2.1) are proposed targets for chemotherapeutics in MM and/or other cancers [24]; providing further evidence that our combination discovery approach was appropriate.

The combination of a CDK inhibitor and an HDAC inhibitor, based on these results, was most effective overall in treating multiple myeloma. This combination was the most effective of the top three combinations at simultaneously reducing MYC protein expression while increasing p16 tumor suppressor activity and inducing apoptosis in a variety of MM cell lines with inherent sensitivity or resistance to most drugs in the MIPE screen (Figs. 2.2A and 2.2B). Further, combined CDK and HDAC inhibition was the most synergistic combination overall in MM cell lines with induced resistance to common first-line chemotherapeutics (Fig. 1D). Dinaciclib (Merck & Co.) inhibits CDK1,2,5,9 [25-28]. Entinostat (Syndax), a class I HDAC inhibitor, inhibits HDAC 1 and 3 [29, 30]. Both drugs are being actively pursued in clinical trials for cancer. Dinaciclib has been studied in combination with the proteasome inhibitor bortezomib and the corticosteroid dexamethasone for treating patients with relapsed MM (NCT01711528) in a phase I clinical trial. Additionally, dinaciclib has been or is currently being investigated in phase I-III clinical trials in combination with other agents aimed at treating different hematologic malignancies (NCT0348520, NCT01650727, NCT01580228), solid tumors (NCT01434316), metastatic triple negative breast cancer (NCT01624441), and pancreatic cancer (NCT01783171). Entinostat has

been studied in phase III clinical trial in combination with hormone therapy in treating patients with recurrent hormone receptor-positive breast cancer (NCT02115282) and has been investigated as a combined agent with immune checkpoint inhibitors (PD-1/PD-L1 antagonists in particular) in clinical trials treating patients with various solid tumors (NCT02437136) [30, 31]. Further understanding of how this combination affects the proposed targets and determining a cooperative response signature for the combination will provide insight into on- and off-target effects, mechanism(s) of action, and biomarkers of a combined response, and may facilitate circumvention of certain side-effects of treating MM by using lower doses.

Additionally, utilizing sublethally irradiated mice injected with MM cells from genetically engineered Vk*MYC; $Nras^{LSL\ Q61R/+}$; IgG1-Cre (VQ) donor mice, enabled evaluation of therapeutic efficacy in a transplantable mouse model of highly malignant MM that more closely recapitulates human MM [30] in an immunocompetent animal. In this model, sublethally irradiated C57BL mice implanted with VQ donor mouse bone marrow cells developed M-spikes (signifying Igγ band on serum protein electrophoresis) at approximately 6 weeks. The appearance of an M-spike is also observed within human MM patients and serves as a means of tracking progression of disease and response to treatment [33, 34]. Additionally, the histologic appearance of myeloma within the bone marrow of mice in this model closely resembles that of myeloma in human patients, with neoplastic plasma cells disrupting marrow architecture and lysing bone [35]. In the present study, all 3 combinations extended survival and were superior to treatment with one of our previously identified mTORi/HDACi combinations [6, 7].

The combinations were assessed in freshly isolated myeloma cells from human patients to ensure that their efficacy was not limited to cultured cell lines and engineered mouse cells. The data suggest that all three of the top combinations effectively reduced the viability of human CD138+ myeloma cells, and that the CDKi/HDACi and TOP2Ai/AURKAi combinations were more selective than the TOP2A/HSP90i combination when comparing CD138+ MM cell viability to that of non-MM CD138-negative cells. The difference in combination-induced toxicity between neoplastic and non-neoplastic bone marrow cells may suggest that these treatments would impart less off-target bone marrow depletion. More investigation into the effects of combination therapy on human myeloma cells *ex vivo* is necessary, particularly because the samples were obtained from

smoldering (asymptomatic) myeloma patients rather than from symptomatic patients or those refractory to first-line therapies.

Fisher's exact testing of the genes affected by the top 3 drug combinations identified cell cycle pathways as the most downregulated and TGFβ pathways as the most upregulated. Of the seven genes most downregulated by each of the combinations, low levels of expression of four genes (HIST1H3B, EIF4EBP1, CASP3, CDK4) have been linked to better overall survival ($p < 0.005$) amongst a series of survival cohorts. Expression of the two genes (ID2 and HSPB1) consistently upregulated by all 3 combinations was not consistently associated with survival (p values > 0.1). ID2, the most upregulated gene by all 3 drug combinations, heterodimerizes with bHLH proteins and functions as a dominant negative inhibitor of them [36]. ID2 has been implicated as either an oncogene or a tumor suppressor depending on the cellular context, and recently has been shown to act as a tumor suppressor in multiple myeloma [37]; thus, increased expression of ID2 may be a benefit associated with these drugs. However, increased signaling of the TGFβ pathway may be considered a negative consequence associated with these drug treatments, due predominantly to effects on the tumor microenvironment [38].]. Treating co-cultures of myeloma cells and HS5 stromal cells with a TGFβR1 inhibitor (SB505124) as well as ex vivo patient samples, suggests that combining this agent with dinaciclib and entinostat could help to prevent potentially deleterious effects of TGFβ receptor signaling and lead to even further decreases in myeloma cell proliferation.

The primary limitation of this study was the restriction in potential combinations imposed by our approach. For example, selecting only drugs with a dose-response curve class of -1.1 (complete response), although pragmatic, may eliminate certain drugs from the screen that may still be potent against myeloma. Similarly, targeting genes vertically in the same pathway with similar mechanisms of action may also be beneficial. Nevertheless, our study identified new drug combinations to evaluate in the treatment of plasma cell neoplasia and potential resistance mechanisms associated with these treatments.

2.6 Materials and Methods

2.6.1 Study design

A high-throughput drug screen was employed to identify single agents from a pool of 1900 compounds that were effective, at a concentration of 2 μM or less, in reducing the viability of at least 25 of the 47 multiple myeloma (MM) cell lines tested. Drugs that were both effective and had different mechanisms of action were paired for robust regression analysis. The 43 selected combinations were highly correlated in their responses (r^2 value ≥ 0.5). These combinations were tested (Western blot) for their ability to cooperatively reduce MYC protein expression relative to single agent and/or control and increase protein expression of tumor suppressor p16. Of the six combinations that reduced MYC protein and increased p16 protein expression, three (CDKi/HDACi, TOP2Ai/ AURKAi, TOP2Ai/HSP90i) were selected for further efficacy evaluation via testing for their ability to reduce MYC protein and increase p16 protein expression in 3 cell lines with inherent resistance to oncology drugs and three cell lines with inherent sensitivity to oncology drugs, as well as their ability to cooperatively reduce viability of L363 MM cells in monoculture or co-cultured with human bone marrow fibroblasts. Further, efficacy of the top 3 drug combinations was evaluated *in vivo* in sublethally irradiated C57BL/6J mice injected intravenously with murine Vk*MYC; $Nras^{LSL\ Q61R/+}$; IgG1-Cre (VQ) cells harvested from bone marrow of donor mice, and *ex vivo* in CD138+ and CD138- MM cells obtained fresh from bone marrow biopsies of human MM patients. Finally, gene set enrichment analysis was used to find common genetic pathways similarly affected in L363 MM cells treated with the top three drug combinations.

2.6.2 Human MM and other cell lines

L363 human MM cells were obtained in 2014, cultured, and authenticated as described previously [6]. LP-1 oprozomib-resistant and RPMI-8226 doxorubicin-resistant MM cell lines were generated from parental MM cell lines (obtained from M. Kuehl, NCI and Leif Bergsagel, Mayo Clinic Scottsdale, AZ, respectively) by exposure to increasing concentrations of oprozomib (up to 400 nM) or doxorubicin (up to 5 μM), respectively, over a period of up to 18 weeks [39]. MM1.S and MM1.R cells were obtained from Leif Bergsagel (Mayo Clinic Scottsdale, AZ). Cells

were cultured in RPMI 1640 with GlutaMAX L-glutamine (Life Technologies) supplemented with 10% fetal bovine serum (Cambrex BioScience), 100 U/ml penicillin and 100 μg/ml streptomycin (life technologies). HS-5 human bone marrow stromal cells (purchased from American Type Culture Collection) and H1634 human foreskin fibroblasts (obtained from Douglas Lowy, NCI) were maintained in DMEM with GlutaMAX L-glutamine (Life Technologies) supplemented with 10% fetal bovine serum, 100 U/ml penicillin and 100 μg/ml streptomycin.

2.6.3 NCATS MIPE screen

The National Center for Advancing Translational Sciences MIPE (Mechanism Interrogation PlatE) compound library of approximately 1900 small molecules was screened in 47 multiple myeloma cell lines (Table 3; https://ncats.nih.gov/pubs/features/screening-platform). Cell lines were treated in 1,536-well plates and the response was measured after 48-hour drug exposure with CellTiter-Glo® (Promega) luminescent cell viability assay at 11 doses (a serial of 3-fold dilutions) [40]. Viability was defined as percent viable cells relative to the trimmed median of positive control (bortezomib, a proteasome inhibitor) wells in a plate and the trimmed median of negative control (DMSO, dimethyl sulfoxide) wells in a plate DMSO-treated controls, as determined from the luminescence-based readout as follows: Viability (%) = (100 x ((Cells – Negative) / (Negative – Positive))) + 100. Following normalization, drug sensitivity measures (potency, efficacy, and dose-response curves) were obtained with an automated grid algorithm for large-scale curve fitting and curve classification [41].

2.6.4 *In Silico* analysis

Palantir's Foundry® platform was used to identify potentially cooperative drug combinations from the NCATS MIPE screen. Drugs were selected for robust regression analysis with the following criteria: single agent dose-response curve class of -1.1 (complete response), AC50 > 2.0 μM, and activity in at least 25 of the 47 MM cell lines tested. Next, robust regression analysis of each drug versus every other drug was utilized to generate a Pearson correlation coefficient (r^2) for each drug pair. 43 combinations had r^2 values of at least 0.5 (indicating correlation).

2.6.5 Western blot analysis

Immunoblot analyses were performed on cells lysed with RIPA buffer (Thermo Fisher Scientific), electrophoresed on 4-20% Tris-Glycine SDSPAGE gels (Novex), and blotted on to nitrocellulose using iBlot (Invitrogen). Each experiment was repeated at least three times, and a representative blot is shown in the figure. Antibodies for β-actin were obtained from Cell Signaling and used at 1:1000 dilutions.

2.6.6 Antibodies (western blot)

All antibodies were diluted in 1 M phosphate buffered saline containing 5% bovine serum albumin.

- Rabbit monoclonal antibody against MYC (Abcam, #32072)

    -dilution ratio: 1:10,000

-Mouse monoclonal antibody against β-actin (CST, #3700)

    -Dilution ratio: 1:4,000

-Mouse monoclonal antibody against CDKN2A/p16INK4a (p16) (Santa Cruz, #1661)

    -Dilution ratio: 1:500

-Rabbit monoclonal antibody against cleaved caspase 3 (CST, #9662)

    -Dilution ratio: 1:1,000

2.6.7 Cell viability assays in human MM cell lines and primary human MM cells

MM cell lines (L363, LP1, LP1-OpzR) were treated with increasing doses of a single agent or a combination of two drugs (1:1 molar ratio). Cells were seeded in 96-well plates at 50,000 cells per well in 200 ml media and treated for 48 hours and MTS assay using CellTiter96® Aqueous One Solution Cell Proliferation Assay (Promega) was performed to determine cell titers. Ratios of inhibitor-treated to untreated control cell titers were calculated. Activity and synergy analyses were performed on a dose matrix comprised of eight single agent concentrations for each compound, and the 64 combinations thereof. MM cells were seeded in 96-well plates at 50,000 cells per well in 200m media with four replicates per dose. Viability was assessed after 48 h of treatment with CellTiter96® Aqueous One MTS reagent (Promega).

For *ex vivo* viability assays, bone marrow aspirates were collected from patients with confirmed smoldering multiple myeloma (SMM) enrolled in clinical trials at the NCI/NIH. Informed consent forms were reviewed and signed by all patients prior to admission. Ficoll-Paque PLUS density gradient sedimentation (Cytiva) was utilized to isolate bone marrow mononuclear cells and primary SMM cells as per the manufacturer's protocol. CD138 positive cells were further separated from bone marrow samples by antibody-mediated positive selection using anti-CD138 magnetic-activated cell separation microbeads (Miltenyi Biotech). The percentage of CD138 positive cells in the positive fraction was quantified by flow cytometric analysis using FlowJo software and found to be greater than 98%. Ex vivo patient cell viability was determined in CD138 positive and CD138 negative cells maintained in DMEM supplemented with 5% human serum and treated with the three top combinations (at IC50 doses of each drug) compared to DMSO-treated control cells.

2.6.8 Animal studies

All animal experiments were conducted in accordance with the Guide for the Care and Use of Laboratory Animals and institutionally approved (LCBG-009, ACUC, NCI) in a facility approved by the Association for Assessment and Accreditation of Laboratory Animal Care. Sublethally irradiated (4.5 GY) C57BL/6J (Jackson Labs) were administered 5 x 10^6 Vk*MYC; $Nras^{LSL\ Q61R/+}$; IgG1-Cre (VQ) cells obtained from the bone marrows of donor mice generously provided by Jing Zhang at the McArdle Research Labs, University of Wisconsin; Madison, WI. Recipient mice were monitored for serum M-spikes via retroorbital bleeds and serum protein electrophoresis as previously described [10, 30]. Upon detectable M-spikes, treatment with the top drug combinations commenced. Treatments were as follows: CDKi (dinaciclib, 20 mg/kg, IP, 3x/week) + HDACi (entinostat, 20 mg/kg, PO 5x/week); TOP2Ai (doxorubicin,4 mg/kg IV 1x/week) + AURKAi (alisertib, 30 mg/kg PO, 5x/week) or HSP90i (SNX-2112, 20 mg/lg, PO, 3x/week); or mTORi (rapamycin, 2.5 mg/kg, IP, 5x/week) + HDACi (entinostat, 20 mg/kg, PO 5x/week) n = 5. Animals were monitored for M-spikes via SPEP every 2 weeks for the remainder of the study, as well as for progression of clinical signs (prolonged hunched posture, hindlimb paralysis). Animals were humanely euthanized when moribund.

2.6.9 *In Vitro* gene response signature of drug treatments

L363 MM cells were treated for 48 hours with the one of the top 3 combinations (10 nM dinaciclib and 500 nM entinostat, 225 nM doxorubicin and 1500 nM alisertib, or 225 nM doxorubicin and 50 nM SNX-2112), as well as the combined CDKi/HDACi of dinaciclib (10 nM) and mocetinostat (175nM). Total RNA was extracted using TRIzol® (Invitrogen). 100 ng of RNA was added to Nanostring reagents and analyzed using the NanoString nCounter® system as per the protocol proved by the manufacturer (Nanostring Technologies). Data processing/normalization, concordant gene response signature, GO enrichment methods, and code enrichment availability are described in the supplemental methods section.

2.6.10 Statistical analysis

For cell viability dose response studies, mean and standard deviation were calculated and plotted from four technical replicates using Graphpad Prism 8® software. For dose matrix experiments, four technical replicates of each dose combination were used to determine mean and standard deviation. Combination Index (CI) derived by Chou and Talalay [15] from the mass-action law principle allows quantifying drug interactions in terms of synergy (CI < 1), antagonism (CI > 1) and additivity (CI = 1) based on the median effect equation. CI computations for the dose response experiments were performed using CompuSyn software (http:// www.combosyn.com/). Excess over Highest Single Agent (EOHSA) was calculated as the difference of the effect produced by the drug combination and the greatest effect produced by each of the combination's single agents at the same concentrations as when combined [42]. Ex vivo MM cell viability among CD138 positive and CD138 negative cells within each treatment, as well as between the CDKi/HDACi combination and CDKi/HDACi/TGFβR1 inhibitor, were compared via unpaired two-tailed Student's t test

2.6.11 Data processing/normalization

Raw counts generated by the NanoString nCounter® system (RCC files) were imported into the nanoString nSolver™ Analysis Software 4.0 for QC screen and selection of optimal housekeeping genes with geNorm algorithm [43]. Subsequently, the raw counts were normalized

to mRNA of five housekeeping genes (ZNF384, MRPS5, CNOT4, NUBP1, and SF3A3) with DESeq2's [44] median of ratios method and variance-stabilizing transformation (VST) [45].

2.6.12 Concordant gene response signature

For each combination treatment and DMSO control the responsive genes were identified using DESeq2 negative binomial modeling and Wald statistic p-values [44]. False discovery rates (FDR) were estimated with Benjamini and Hochberg method [46] and an FDR of 5% was chosen as the level of statistical significance. The concordant response signature includes genes significantly changed in the same direction by each combination treatment (Total=125, 49 up-regulated and 76 down-regulated genes), and that reached 2-fold change in the average fold-change profile calculated across all the combination treatments (Total=78, 38 up-regulated and 40 down-regulated genes).

2.6.13 GO enrichment analysis

Database for Annotation, Visualization, and Integrated Discovery (DAVID) [48, 49] was used to determine overrepresented Gene Ontology (GO) functions in the lists of significant genes. Enriched GO terms were selected with nominal p-value less than 0.05 with the Nanostring data and the false discovery rate [46] less than 5%. For each over-represented GO term a z-score was computed based on the number of up-regulated and down-regulated genes according to the formula (up-down)/sqrt(total) proposed by Walter et.al [18] and visualized with bubble-plots.

2.6.14 Code availability

R programming language version 3.6.3 [50], R Studio version 1.2.5033, and NIH Integrated Data Analysis platform (NIDAP) were used for performing the analyses. R scripts are available upon request.

2.7 References and Notes

[1] Goldschmidt H, Ashcroft J, Szabo Z, Garderet L. Navigating the treatment landscape in multiple myeloma: which combinations to use and when? *Ann Hematol.* 2018 Nov;23(1)1-18.

[2] Kumar SK, Rajkumar S. The multiple myelomas - current concepts in cytogenetic classification and therapy. *Nat Rev Clin Oncol*. 2018 Jul;15(7):409-21.

[3] Howlader N, Noone AM, Krapcho M, Miller D, Brest A, Yu M, Ruhl J, Tatalovich Z, Mariotto A, Lewis DR, Chen HS, Feuer EJ, Cronin KA (eds). SEER cancer statistics review, 1975-2017, NCI, Bethesda, MD, https://seer.cancer.gov/csr/1975_2017/, based on November 2019 SEER data submission, posted to the SEER web site, April 2020.

[4] Castella M, Fernández de Larrea C, Martín-Antonio B. Immunotherapy: a novel era of promising treatments for multiple myeloma. *Int J Mol Sci*. 2018 Nov;19(11):3613.

[5] Dancey J, Chen H. Strategies for optimizing combinations of molecularly targeted anticancer agents. *Nat Rev Drug Discov*. 2006 Aug;5(8):649-59.

[6] Simmons JK, Michalowski AM, Gamache BJ, DuBois W, Patel J, Zhang K, Gary J, Zhang S, Gaikwad SM, Connors D, Watson N, Leon E, Chen JQ, Kuehl WM, Lee MP, Zingone A, Landgren O, Ordentlich P, Huang J, Mock BA. Cooperative targets of combined mTOR/HDAC inhibition promote MYC degradation. *Mol Cancer Ther*. 2017 Sep;16(9):2008-21.

[7] Simmons JK, Patel J, Michalowski AM, Zhang S, Wei BR, Sullivan P, Gamache B, Felsenstein K, Kuehl WM, Simpson RM, Zingone A, Landgren O, Mock BA. TORC1 and class I HDAC inhibitors synergize to suppress mature B cell neoplasms. *Mol Oncol*. 2014 Mar;8(2):261-72.

[8] Jovanović KK, Roche-Lestienne C, Ghobrial IM, Facon T, Quesnel B, Manier S. Targeting MYC in multiple myeloma. *Leukemia*. 2018 Jun;32(6):1295-306.

[9] Chesi M, Robbiani DF, Sebag M, Chng WJ, Affer M, Tiedemann R, Valdez R, Palmer SE, Haas SS, Stewart AK, Fonseca R, Kremer R, Cattoretti G, Bergsagal PL. AID-dependent activation of a MYC transgene induces multiple myeloma in a conditional mouse model of postgerminal center malignancies. *Cancer Cell.* 2008 Feb;13:167–80.

[10] Chng WJ, Huang GF, Chung TH, Ng SB, Gonzalez-Paz N, Troska-Price T, Mulligan G, Chesi M, Bergsagel PL, Fonseca R. Clinical and biological implications of MYC activation: a common difference between MGUS and newly diagnosed multiple myeloma. *Leukemia.* 2011 Jun;25(6):1026–35.

[11] Sears R, Nuckolls F, Haura E, Taya Y, Tamai K, Nevins JR. Multiple Ras-dependent phosphorylation pathways regulate Myc protein stability. *Genes Dev*. 2000 Oct 1;14(19):2501–14.

[12] Mock B, Wax J, Clynes R, Marcu KB, Potter M. The genetics of susceptibility to RIM-induced plasmacytomagenesis. *Curr Top Microbiol Immunol*. 1988;141:125-7.

[13] Clynes R, Stanton LW, Wax J, Smith-Gill S, Potter M, Marcu KB. Synergy of an IgH promoter-enhancer-driven c-myc/v-Ha-ras retrovirus and pristane in the induction of murine plasmacytomas. *Curr Top Microbiol Immunol*. 1988;141:115-24.

[14] Whitfield JR, Beaulieu ME, Soucek L. Strategies to Inhibit Myc and Their Clinical Applicability. *Front Cell Dev Biol*. 2017 Feb 23;5:10.

[15] Dang CV, Reddy EP, Shokat KM, Soucek L. Drugging the 'undruggable' cancer targets. *Nat Rev Cancer*. 2017 Aug;17(8):502-08.

[16] Gonzalez-Paz N, Chng WJ, McClure RF, Blood E, Oken MM, Van Ness B, James CD, Kurtin PJ, Henderson K, Ahmann GJ, Gertz M, Lacy M, Dispenzieri A, Greipp PR, Fonseca R. Tumor suppressor p16 methylation in multiple myeloma: biological and clinical implications. *Blood*. 2007 Feb 1;109(3):1228-32.

[17] Chou TC. Drug combination studies and their synergy quantification using the Chou-Talalay method. *Cancer Res*. 2010 Jan 15;70(2):440-46.

[18] Walter, Wencke, Fatima Sanchez-Cabo, and Mercedes Ricote. GOplot: An R package for visually combining expression data with functional analysis. *Bioinformatics* (2015): btv300.

[19] Sliwoski G, Kothiwale S, Meiler J, Lowe WE Jr. Computational methods in drug discovery. *Pharmacol Rev*. 2014 Jan; 66(1):334–95.

[20] Weinstein ZB, Bender A, Cokol M. Prediction of synergistic drug combinations. *Curr Opin Syst Biol*. 2017 May 11;4(1):24–28.

[21] Gayvert KM, Aly O, Platt J, Bosenberg MW, Stern DF, Elemento O. A computational approach for identifying synergistic drug combinations. *PLoS Comput Biol*. 2017 Jan 13;13(1):e1005308.

[22] Jeon M, Kim S, Park S. In silico drug combination discovery for personalized cancer therapy. *BMC Syst Biol*. 2018 Mar 19:12(Suppl 2):16.

[23] Zhan F, Huang Y, Colla S, Stewart JP, Hanamura I, Gupta S, et al. The molecular classification of multiple myeloma. *Blood*. 2006; 108(6):2020–8.

[24] Ovejero S, Moreaux J. Multi-omics tumor profiling technologies to develop precision medicine in multiple myeloma. *Explor Target Antitumor Ther*. 2021;2:65-106.

[25] Kumar SK, LaPlant B, Chng WJ, Zonder J, Callander N, Fonseca R, Fruth B, Roy V, Erlichman C, Stewart AK; Mayo Phase 2 Consortium. Dinaciclib, a novel CDK inhibitor, demonstrates encouraging single-agent activity in patients with relapsed multiple myeloma. *Blood*. 2015 Jan 15;125(3):443-48.

[26] Parry D, Guzi T, Shanahan F, Davis N, Prabhavalkar D, Wiswell D, Seghezzi W, Paruch K, Dwyer MP, Doll R, Nomeir A, Windsor W, Fischmann T, Wang Y, Oft M, Chen T, Kirschmeier P, Lees EM. Dinaciclib (SCH 727965), a novel and potent cyclin-dependent kinase inhibitor. *Mol Cancer Ther*. 2010 Aug;9(8):2344-53.

[27] Kumar SK, Rajkumar V, Kyle RA, van Duin M, Sonneveld P, Mateos MV, Gay F, Anderson K. Multiple myeloma. *Nat Rev Dis Primers*. 2017 Jul 20;3:17046.

[28] De Souza C, Chatterji BP. HDAC inhibitors as novel anti-cancer therapeutics. *Recent Pat Anticancer Drug Discov*. 2015;10(2):145-62.

[29] Connolly RM, Rudek MA, Piekarz R. Entinostat: a promising treatment option for patients with advanced breast cancer. *Future Oncol*. 2017 Jun;13(13):1137-1148.

[30] Connolly RM, Zhao F, Miller KD, Lee MJ, Pikarz RL, Smith KL, Brown-Glaberman UA, Winn JS, Faller BA, Adedayo AO, Burkard ME, Budd GT, Levine EG, Royce ME, Kaufman PA, Thomas A, Trepel JB, Wolff AC, Sparano JA. E2112: Randomized phase III trial of endocrine therapy plus entinostat or placebo in hormone receptor–positive advanced breast cancer. A trial of the ECOG-ACRIN cancer research group. *Journal of Clinical Oncology* 2021 39:28, 3171-3181.

[31] Hellmann MD, Jänne PA, Opyrchal M, Hafez N, Raez LE, Gabrilovich DI, Wang F, Trepel JB, Lee MJ, Yuno A, Lee S, Brouwer S, Sankoh S, Wang L, Tamang D, Schmidt EV, Meyers ML, Ramalingam SS, Shum E, Ordentlich P. Entinostat plus pembrolizumab in patients with metastatic NSCLC previously treated with anti-PD-(L)1 therapy. *Clin Cancer Res*. 2021 Feb 15;27(4):1019-1028.

[32] Wen Z, Rajagopalan A, Flietner ED, Yun G, Chesi M, Furumo Q, Burns RT, Papadas A, Ranheim EA, Pagenkopf AC, Morrow ZT, Finn R, Zhou Y, Li S, You X, Jensen J, Yu M, Cicala A, Menting J, Mitsiades CS, Callander NS, Bergsagel PL, Wang D, Asimakopoulos F, Zhang J. Expression of NrasQ61R and MYC transgene in germinal center B cells induces a highly malignant multiple myeloma in mice. *Blood*. 2021 Jan 7;137(1):61-74.

[33] Rajkumar SV, Kyle RA, Therneau TM, Melton LJ 3rd, Bradwell AR, Clark RJ, Larson DR, Plevak MF, Dispenzieri A, Katzmann JA. Serum free light chain ratio is an independent risk factor for progression in monoclonal gammopathy of undetermined significance. *Blood*. 2005 Aug 1;106(3):812-7.

[34] Dejoie T, Corre J, Caillon H, Hulin C, Perrot A, Caillot D, Boyle E, Chretien ML, Fontan J, Belhadj K, Brechignac S, Decaux O, Voillat L, Rodon P, Fitoussi O, Araujo C, Benboubker L, Fontan C, Tiab M, Godmer P, Luycx O, Allangba O, Pignon JM, Fuzibet JG, Legros L, Stoppa AM, Dib M, Pegourie B, Orsini-Piocelle F, Karlin L, Arnulf B, Roussel M, Garderet L, Mohty M, Meuleman N, Doyen C, Lenain P, Macro M, Leleu X, Facon T, Moreau P, Attal M, Avet-Loiseau H. Serum free light chains, not urine specimens, should be used to evaluate response in light-chain multiple myeloma. *Blood*. 2016 Dec 22;128(25):2941-2948.

[35] Fujino M. The histopathology of myeloma in the bone marrow. *J Clin Exp Hematop*. 2018;58(2):61-67.

[36] Benezra R, Davis RL, Lockshon D, Turner DL, Weintraub H. The protein Id: a negative regulator of helix-loop-helix DNA binding proteins. *Cell*. 1990 Apr 6;61(1):49-59.

[37] Perini T, Szalat R, Samur MK, Fulciniti M, Lopez MA, Lawlor M, Ott CJ, Li N, Xu Y, Wen K, Amodio N, Morelli E, Anderson K, Ciceri F, Munshi N. Inhibitor of DNA binding 2 (ID2) plays a key tumor suppressor role in promoting oncogenic transformation in multiple myeloma. *Blood* 2018; 132 (Supplement 1): 60.

[38] Dong M, Blobe GC. Role of transforming growth factor-beta in hematologic malignancies. *Blood*. 2006 Jun 15;107(12):4589-96.

[39] Riz I, Hawley RG. Increased expression of the tight junction protein TJP1/ZO-1 is associated with upregulation of TAZ-TEAD activity and an adult tissue stem cell signature in carfilzomib-resistant multiple myeloma cells and high-risk multiple myeloma patients. *Oncoscience*. 2017 Aug 1;4(7-8):79-94.

[40] Mathews Griner LA, Guha R, Shinn P, Young RM, Keller JM, Liu D, Goldlust IS, Yasgar A, McKnight C, Boxer MB, Duveau DY, Jiang JK, Michael S, Mierzwa T, Huang W, Walsh MJ, Mott BT, Patel P, Leister W, Maloney DJ, Leclair CA, Rai G, Jadhav A, Peyser BD, Austin CP, Martin SE, Simeonov A, Ferrer M, Staudt LM, Thomas CJ. High-throughput combinatorial screening identifies drugs that cooperate with ibrutinib to kill activated B-cell-like diffuse large B-cell lymphoma cells. *Proc Natl Acad Sci U S A*. Feb 11;111(6):2349-54 (2014).

[41] Wang Y, Jadhav A, Southal N, Huang R, Nguyen DT. A grid algorithm for high throughput fitting of dose-response curve data. *Curr Chem Genomics*. 2010 Oct 21;4:57-66.

[42] Borisy AA, Elliott PJ, Hurst NW, Lee MS, Lehar J, Price ER, Serbedzja G, Zimmermann GR, Foley MA, Stockwell Br, Keith CT. 2003. Systematic discovery of multicomponent therapeutics. *Proc Natl Acad Sci USA*. 100;14982-14987.

[43] Vandesompele J, De Preter K, Pattyn F, Poppe B, Van Roy N, De Paepe A, Speleman F. Accurate normalization of real-time quantitative RT-PCR data by geometric averaging of multiple internal control genes. *Genome Biol Research* (2002).

[44] Love MI, Huber W, Anders S (2014). Moderated estimation of fold change and dispersion for RNA-seq data with DESeq2. *Genome Biology*, 15, 550. 8.

[45] Anders S, Huber W. Differential expression analysis for sequence count data. *Genome Biology 2010*, 11:106.

[46] Benjamini Y, Hochberg, Y. Controlling the false discovery rate: a practical and powerful approach to multiple testing. *J R Stat Soc Series B*. 1995 57(1), 289–300.

[47] Finney R. (2020). l2p: l2p. R package version 0.1-9.

[48] Huang DW, Sherman BT, Lempicki RA. Systematic and integrative analysis of large gene lists using DAVID Bioinformatics Resources. *Nature Protoc*. 2009;4(1):44-57.

[49] Huang DW, Sherman BT, Lempicki RA. Bioinformatics enrichment tools: paths toward the comprehensive functional analysis of large gene lists. *Nucleic Acids Res*. 2009;37(1):1-13.

[50] R Core Team R: A language and environment for statistical computing. R Foundation for Statistical Computing, Vienna, Austria. (2020). URL https://www.R-project.org/.

2.8 Supplemental Figures and Tables:

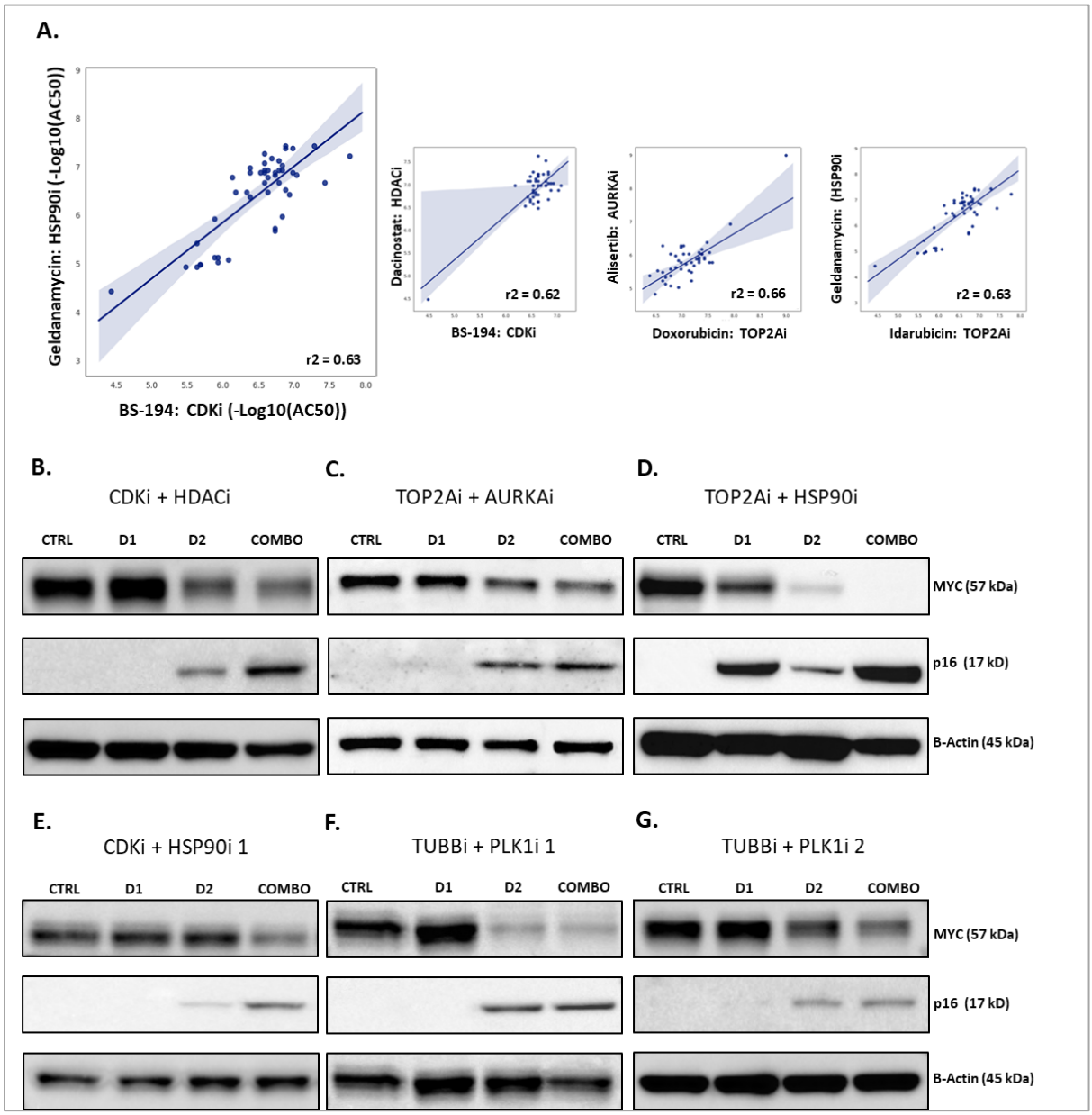

Figure S. 2.1. Robust regression analysis of active compounds revealed potentially effective combinations against MM. 1A) Example robust regression plots of all AC50 doses for a particular single agent (x-axis) plotted against those of the corresponding partner single agent (y-axis). r2 = Pearson correlation coefficient. 1B-E) Representative western blots of combinations from robust regression analysis that reduced MYC protein and simultaneously increased p16 expression vs. control or single agent in L363 MM cells treated for 24 hours with IC50 concentrations of drugs. CDKi (D1) + HDACi (D2) = BS194 + Dacinostat, 1C – TOP2Ai (D1) + AURKAi (D2) = Doxorubicin + Alisertib,1D – HSP90i (D1) + TOP2Ai (D2) = Geldanamycin + Idarubicin HCl, 1E – CDKi + HSP90i = BS-194 + VER-82576, 1F –TUBBi + PLK1 1 = Noscapine +IVX-214, 1G – TUBBi + PLK1i 2 = XRP-44X + IVX-214.

Figure S. 2.2. Evaluating synergy and efficacy in various sensitive and resistant cell lines and tolerability in normal human fibroblasts. A-C) Matrix dose response testing for activity and synergy with representative heat maps and topographical graphs of excess of highest single agent (EOSHA) showing the amount of additional activity achieved each combination over the highest single agent dose in each respective row. L363 MM cells were treated with the top 3 combinations for 48 hours at 8 different doses (64 total dose combination). HSA Score = highest single agent synergy score (>10 indicates synergy). D-F) Dose response cell viability plots for H1634 non-neoplastic human fibroblasts and L363 MM cells treated at escalating doses of each combination. Orange = combination dose response curve in H1634 cells, black = combination dose response curve in L363 MM cells. Each table shows the IC50 for single agent or combination in H1634 and L363 cells. G-I) Representative cell viability dose response curves for sensitive (blue curve) vs. resistant (red curve) MM cell lines at 48 hours validating resistance to respective drugs. G – LP-1-Parental vs. LP-1-OpzR treated with escalating doses of oprozomib, H – MM1.S vs. MM1.R treated at escalating doses of dexamethasone, I – RPMI-8226-Parental vs. RPMI-8226-Dox40 treated at escalating doses of doxorubicin.

Figure S. 2.2 continued

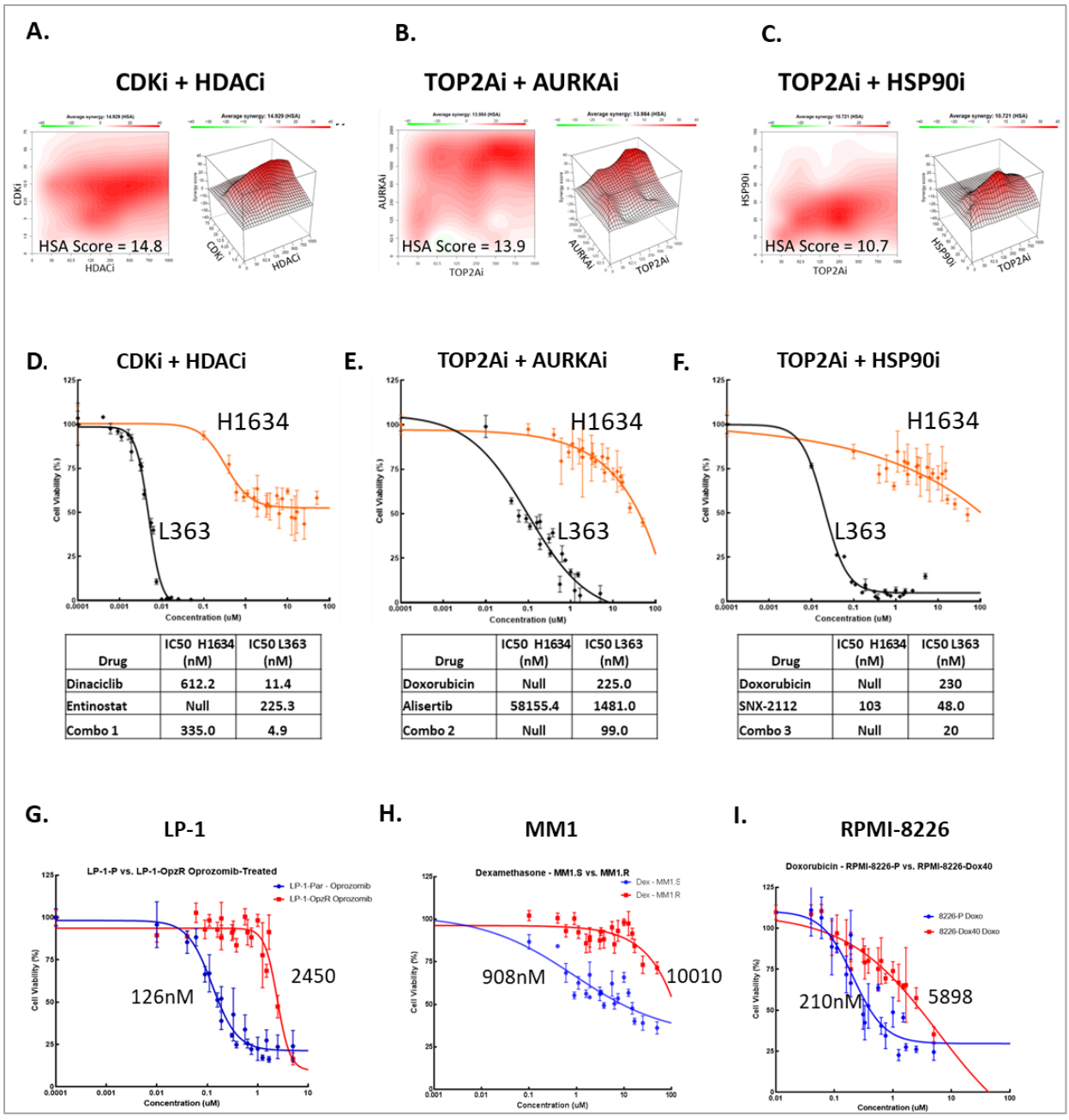

Drug	IC50 H1634 (nM)	IC50 L363 (nM)
Dinaciclib	612.2	11.4
Entinostat	Null	225.3
Combo 1	335.0	4.9

Drug	IC50 H1634 (nM)	IC50 L363 (nM)
Doxorubicin	Null	225.0
Alisertib	58155.4	1481.0
Combo 2	Null	99.0

Drug	IC50 H1634 (nM)	IC50 L363 (nM)
Doxorubicin	Null	230
SNX-2112	103	48.0
Combo 3	Null	20

Figure S. 2.3. Efficacy of the top 3 combinations in a novel mouse model of myeloma. A) Electrophoreograms from sublethally irradiated C57BL/6 mice administered 5x10^6 VQ cells. Top electrophoreograms are from an individual mouse on day 1 of treatment (42 days since administration of VQ cells via intracardiac injection) and bottom electrophoreograms are from the same animal after 21 days of treatment with either DMSO (vehicle control - black box), CDKi/HDACi (dinaciclib and entinostat – blue box), TOP2Ai/AURKAi (doxorubicin and alisertib – red box) or TOP2Ai/HSP90i (doxorubicin and SNX-2112 – green box). Tx = treatment B) Representative radiograph of left hind limb from a sublethally irradiated C57BL/6 mice administered 5x10^6 VQ cells 11 weeks after intracardiac injection. Circles and yellow arrows indicate radiolucent foci of osteolysis caused by VQ cells.

Figure S. 2.3 continued

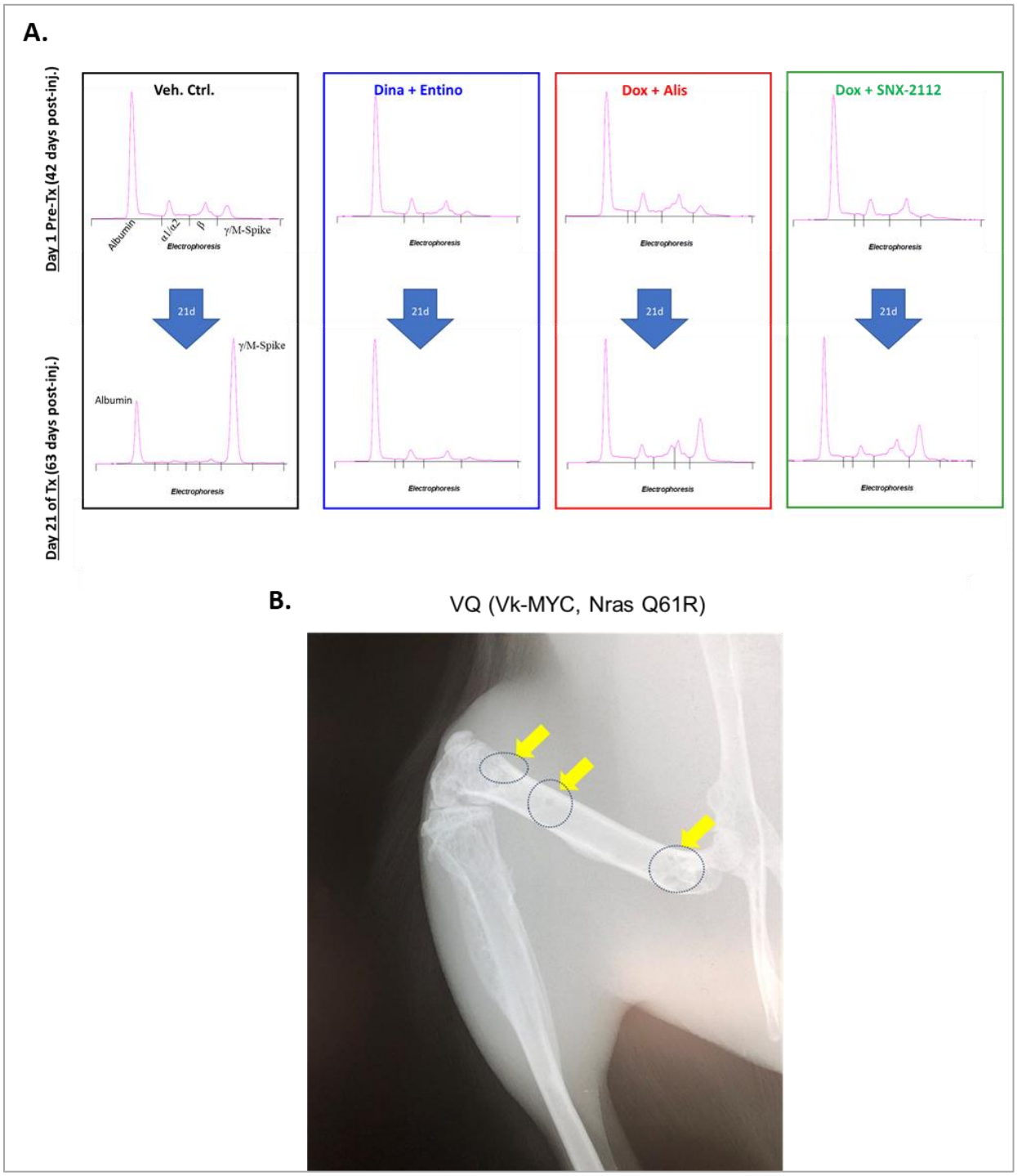

Figure S. 2.4. Common genetic pathways are similarly affected by the top drug combinations. A) The number of significant genes shared (bar chart = total number significant genes for each single combination treatment or shared between different combination treatments; Venn diagram = percent of total genes (out of 501) common between different combinations). Gene selection; 125 based on FDR < 5% in each of the 4 combos; 78 genes based on 2-fold change for the mean Treatment vs DMSO-treated across the 4 combos. Of the 143 genes in common, 125 were concordant in increased or decreased expression by all 4 combos. Of these 125 genes, 78 were increased or decreased at least 2-fold in the mean treatment effect. B) Heatmap of the significantly changed genes concordantly changed by all combinations (upregulated = red, downregulated = blue). C-D) Enriched pathways based on a modified Fisher's exact test (EASE score) using DAVID [48, 49] and GO_FAT pathways for the list of differentially expressed genes common between all combination treatments. Upregulation and downregulation of the enriched pathways was determined with a pathway z-score as described by Walter et al. [18]. C = commonly upregulated pathways with z-score greater than 1, D = commonly downregulated pathways with z-score less than -1.

Figure S.2.4 continued

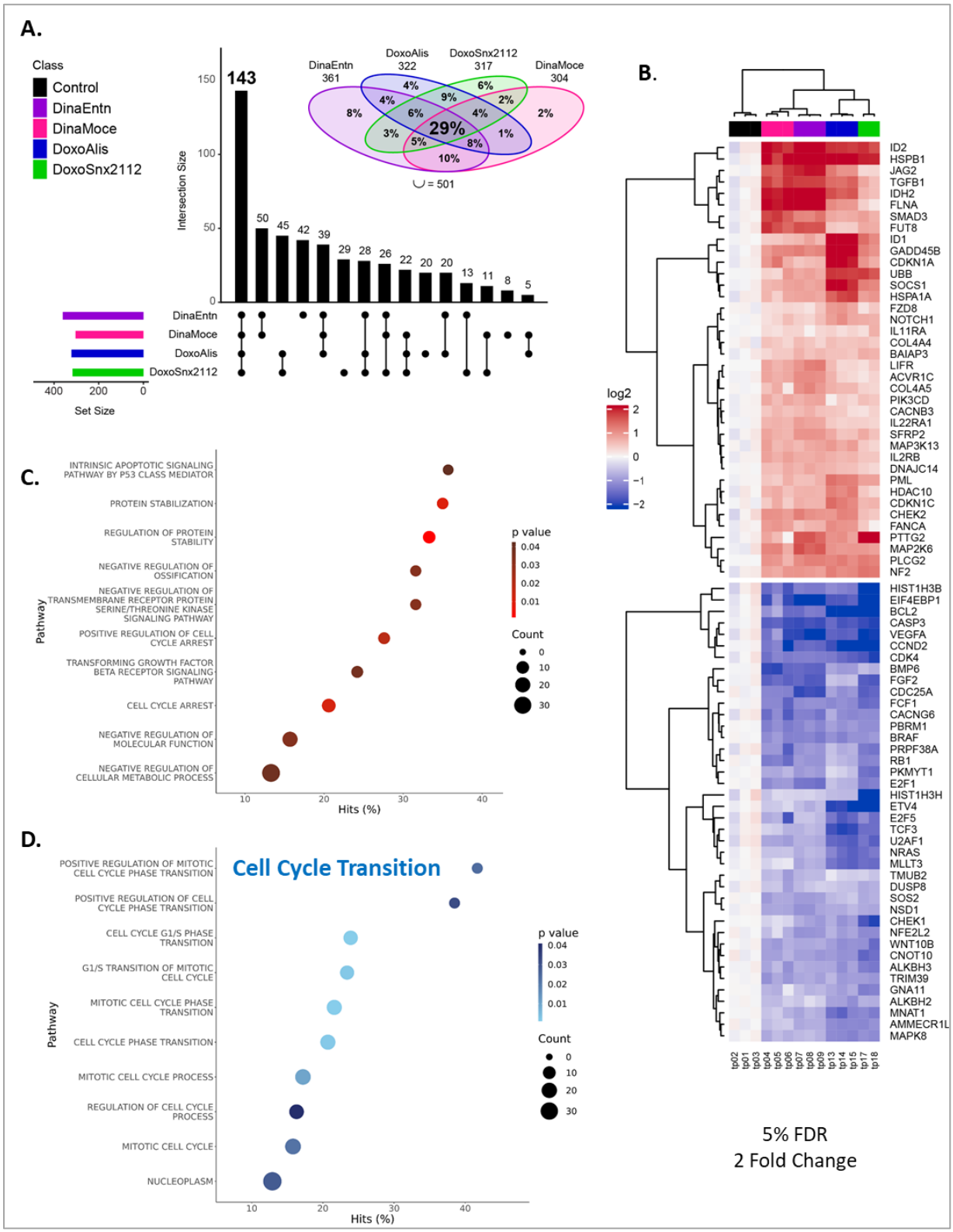

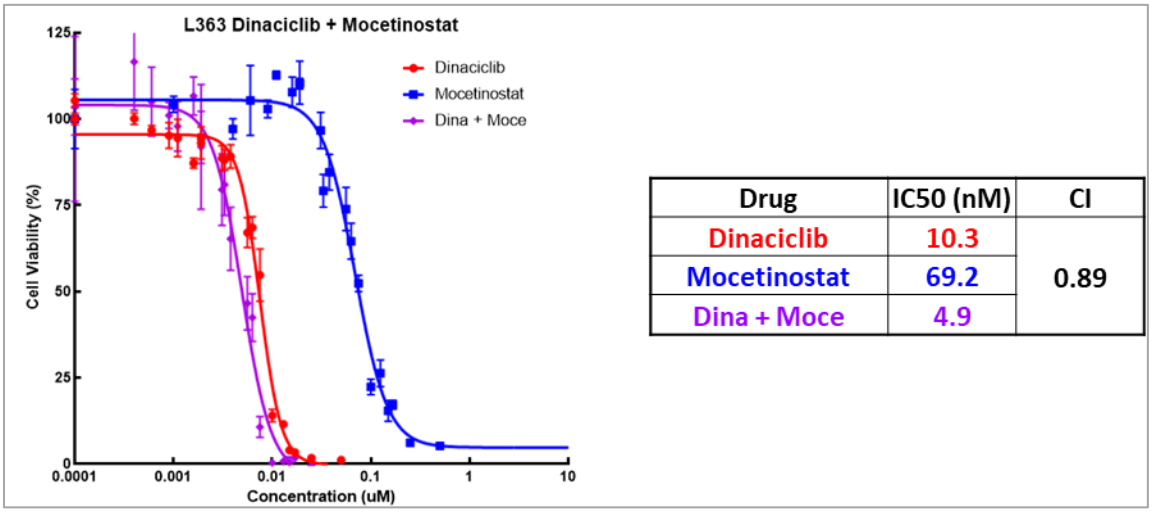

Drug	IC50 (nM)	CI
Dinaciclib	10.3	0.89
Mocetinostat	69.2	
Dina + Moce	4.9	

Figure S. 2.5. L363 MM cell viability upon single agent or combined treatment with dinaciclib and mocetinostat. Cell viability was assessed with MTS assay 48h after treatment with escalated dose concentrations of either drug individually or in combination at a 1:1 molar ratio. Each data point represents mean of 4 wells and error bars indicate replicate standard deviation. IC50 (in nM) for individual drugs and combination in each table. Chou-Talalay computation of combination indices (CI) for treated cells are shown for 50% affected fraction 48 hours post-exposure. Synergy is interpreted as CI<1.0.

Table S. 2.1. Effect of Top 3 Drug Combinations on Viability of Parental and Drug-Resistant Multiple Myeloma Cell Lines

Cell Line		**Combination IC50 (nM)**		
		CDKi / HDACi	TOP2Ai / ARUKAi	TOP2Ai / HSP90i
LP-1	LP-1 Parental	10.2	335.1	204.0
	LP-1-OpzR (oprozomib-resistant)	4.2	99.0	24.0
MM1	MM1.S	4.9	225.5	55.6
	MM1.R (dexamethasone-resistant)	4.8	276.3	129.9
RPMI-8226	RPMI-8226-Parental	5.6	67.0	42.0
	RPMI-8226-Dox40 (doxorubicin-resistant)	8.8	918.0	546.0

CHAPTER 3. EFFICACY AND COOPERATIVE TARGETS OF COMBINED CDK/HDAC INHIBITION IN PRECLINICAL MODELS OF MULTIPLE MYELOMA

3.1 One Sentence Summary

Combined targeted CDK/HDAC inhibition is effective in human multiple myeloma (MM) cell lines, MM patient cells, and mouse models of MM, and RNA sequencing identified the top pathways affected by the combination.

3.2 Introduction

In recent years advances in several novel agents have improved the survival of patients suffering from multiple myeloma (MM), a neoplastic clonal proliferation of plasma cells in the bone marrow and other organs [1, 2]. However, MM is still an incurable cancer and patients often develop relapsed and/or refractory multiple myeloma (RRMM), with particular resistance to the common first-line treatment proteasome inhibitors [1, 3]. Previous research identified the transcription factor MYC as a master regulator of the cooperative response to combined targeting of mTOR (mammalian target of rapamycin) and HDAC (histone deacetylase) [4, 5]. MYC activation (commonly through locus rearrangements and gains, mRNA overexpression, and deregulation) is found in approximately 67% of MM and is associated with cancer progression [6-8]. Unfortunately, direct pharmacologic targeting of MYC has remained a key challenge in oncology [9, 10]. However, finding drug combinations that indirectly target MYC, while acting upon their own respective direct targets, serves as a useful alternative strategy and may provide additional opportunities for synergy in treating MM.

A multilayered drug combination prediction workflow was employed to discover novel combinations for treating MM comprised of a high-throughput single agent drug screen and *in silico* robust regression analysis to determine potentially cooperative drug combinations. Potential combinations were then selected for the ability to simultaneously reduce oncogenic MYC protein expression and increase p16 tumor suppressor activity. These combinations were further evaluated with several *in vitro* methods to measure synergy in MM cell line models, *ex vivo* responses in myeloma patient samples, and *in vivo* responses in a novel mouse model of MM [chapter 2, 11].

From these data, three drug combinations, consisting of a cyclin dependent kinase (CDK) inhibitor combined with an HDAC inhibitor and a topoisomerase II inhibitor combined with either an aurora kinase A inhibitor or a heat shock protein 90 inhibitor, were found to reduce MYC protein while simultaneously increasing p16 activity in MM cells, all while cooperatively decreasing MM cell viability compared to single agent therapy. Moreover, the CDKi + HDACi combination of dinaciclib and entinostat emerged as the top candidate combination for further investigation and preclinical development.

Dinaciclib (Merck & Co.) inhibits CDK1,2,5, and 9 [12-15]. Entinostat (Syndax), a class I HDAC inhibitor, inhibits HDAC 1 and 3 [16, 17]. Both drugs have proven utility in various therapies and are in clinical trials to treat myeloma and/or other cancers [17-20], but have not been combined previously, thus representing a new combination strategy for myeloma therapy. Further understanding of which known and potential targets are affected by this combination *in vitro* and *in vivo* and determining a cooperative response signature for combination therapy will provide insight into on- and off-target effects, mechanism(s) of action, and biomarkers of a combined response, and may provide rationale for further preclinical development and clinical trials. Evaluating the proposed CDKi/HDACi combination *in vivo* provides insight into target engagement, efficacy, and safety endpoints. Although the safety of both drugs has been independently investigated [14, 21, 22], it has yet to be seen if combining dinaciclib and entinostat results in toxicities that would preclude further preclinical development.

Herein, targets, mechanism of action, and efficacy of combined CDK/HDAC inhibition were investigated both *in vitro* and *in vivo*. Freshly obtained smoldering myeloma patient bone marrow biopsy cells were utilized to evaluate efficacy of the combination compared to single agent treatment. Finally, attempts to elucidate a genetic signature of combined CDK/HDAC inhibition were made in MM cells through RNA sequencing.

3.3 Results

3.3.1 Targeted combined CDK/HDAC inhibition is effective *in vitro*

Effects on oncogenic MYC protein expression, tumor suppressor p16 activity, apoptosis, and downstream effector molecules from CDK/HDAC inhibition with dinaciclib and/or entinostat

(targets outlined in Fig. 3.1A) were evaluated in L363 multiple myeloma cells treated at IC50 concentrations of each drug as determined previously [Chapter 2] – (dinaciclib = 10 nM, entinostat 500 nM) for 24 or 48 hours via western blot (WB) – (Fig. 3.1B). Experiments were repeated at least 3 times. The CDK/HDAC inhibitor combination reduced MYC protein expression, with a greater reduction in total MYC protein noted at 48 hours. Additionally, the combination effectively increased p16 tumor suppressor protein, indicating an increase in p16 activity in L363 MM cells, at both 24 and 48 hours. Further, single agent treatment with dinaciclib or entinostat induced cleavage of caspase 3 protein (at 24 and 48 hours with dinaciclib, and 48 hours with entinostat), indicating induction of apoptosis; however, caspase 3 cleavage was greater with combined CDK/HDAC inhibition at 24 hours. Protein expression of phosphorylated RNA polymerase II at Serine 2 (Pol II^{ser2}), a target of MYC and CDK9 [23, 24], was decreased at 48 hours by dinaciclib alone but was cooperatively reduced by combined dinaciclib/entinostat treatment at 24 hours and undetectable at 48 hours. Acetylation of histone H3, an indicator of HDAC inhibition [25], was evident at 24 and 48 hours after treatment with entinostat, but not increased with combination treatment.

Selective targeting of CDKs and HDACs by dinaciclib and entinostat was assessed via WB in L363 MM cells treated with IC50 doses of each drug singly, or in combination (Fig. S3.1A-B) for 24 and 48 hours. Dinaciclib alone reduced protein expression of known targets total CDK1, CDK2, and CDK5 at 24- and 48-hours post-treatment. Dinaciclib also reduced protein expression of phosphorylated CDK9 at threonine 186 ($pCDK9^{Thr186}$), a key indicator CDK9 kinase activity and, in turn, an indicator of dinaciclib activity [26], at 48-hours post treatment. As expected, dinaciclib did not reduce expression of CDK6. Administration of entinostat reduced protein levels of targets HDAC1 and HDAC3 at 24- and 48-hours post-treatment; while HDAC2, HDAC4, HDAC7, and HDAC11 were either unchanged or increased at 24-hours post-treatment, and HDAC7 was decreased at 48 hours. Combined CDK/HDAC inhibition with dinaciclib and entinostat was more effective at reducing expression of total CDK1, 2, and 5 and cooperatively reduced expression of $pCDK9^{Thr186}$ at 24 and 48 hours. Combined CDK/HDAC inhibition also resulted in reduced HDAC1, 3 and to a small degree HDAC7 by 48 hours.

Combined CDK/HDAC efficacy, targeting, and synergy were also evaluated in the context of drug-resistance in a cell line selected for proteasome inhibitor resistance (PIR), one of the most

common causes for failure of first-line therapeutics against MM. Oprozomib resistance was induced in LP1 parental MM cells via prolonged treatment with a proteasome inhibitor for repeated passages. LP1 parental (LP1-P) and oprozomib-resistant (LP1-PIR) cells, were then treated with the CDK/HDAC inhibitor combination for 24, 48, or 72 hours and lysates were evaluated via WB (Fig S3.2A). MYC protein was reduced relative to DMSO-treated control cells at 48- and 72-hours post-treatment with the combination and was undetectable post-treatment in PIR cells. Additionally, p16 protein expression was increased in both parental and PIR cells. As noted in L363 MM cells, HDAC1 and HDAC3, as well as CDK1, 2, and 5, total proteins were reduced upon combined CDK/HDAC inhibition in LP1-P cells at 24-, 48- and 72-hours post-treatment. Target HDAC and CDK total proteins were reduced by the combination in LP1-PIR cells at all time points other than CDK2 at 24-hours post-treatment.

CDKi/HDACi treated L363, LP1-P and LP1-PIR cells were evaluated via flow cytometry for evidence of enhanced apoptosis (FITC/Annexin) with combined treatment (Fig 3.1C-F). Combined dinaciclib and entinostat treatment enhanced the percentage of apoptotic cells relative to total cells counted after 24, 48 and 72 hours of treatment compared to single agents. Combined CDK/HDAC inhibition effects on viability were evaluated in LP1 parental and oprozomib-resistant myeloma lines (Fig. 3.1G-H; Fig S3.2B-C). Combined CDK/HDAC inhibition reduced cell viability relative to single agent treatment, regardless of proteasome inhibitor sensitivity or resistance. An 8x8 dose matrix combination response screen of dinaciclib and entinostat at 7 different concentrations, and all combinations thereof, was performed in LP1-P and LP1-PIR MM cells to ascertain the activity and synergy across a spectrum of doses. Heatmaps (Fig. 3.1G-H) indicate the percent inhibition of treated cells vs. vehicle control after 48 hours of exposure to drugs. Synergy was achieved at a lower concentration of each drug than the IC50 of each individual agent, indicating lower concentrations of each drug may be used in combination to generate a pharmacologically achievable reduction in MM viability, regardless of proteasome inhibitor sensitivity or resistance. Surface plots of the excess inhibition of highest single agent (EOSHA) are shown in supplemental figure S3.2D-E, with the combined CDK/HDAC inhibition achieving a highest single agent (HSA) score of 20.3 in LP1-P cells and 17.3 in LP1-PIR cells; indicating synergy.

Figure 3.1 *In vitro* evaluation of combined targeted CDK/HDAC inhibition in MM. A) Summary of CDK and HDAC targets of dinaciclib and entinostat, respectively, as well as drug target effects. B) Representative WB analysis of L363 MM cells treated for 24 or 48 hours with dinaciclib (10 nM), entinostat (500 nM) or both. CTRL = DMSO control. Cell lysates were probed for MYC, p16, total and cleaved caspase 3 (Casp3 and CC3, respectively), phosphorylated RNA polymerase II (pPol II^{Ser2}), acetylated histone 3 (acetyl-H3), and β-actin. C-F Flow cytometric evaluation of apoptosis in L363, LP1-P and LP-OpzR cell lines at 24, 48, and 72 hours after single agent or combined CDK/HDAC inhibitor treatments. C = Representative flow cytometric dot plots of LP1-OpzR (proteasome inhibitor-resistant) cells at 48 hours treated with single agent or combined dinaciclib-entinostat versus control. X-axis = number of Annexin V positive cells; Y-axis = number of PI positive cells D-F). Bar charts representing percent apoptosis (as determined by Annexin V high and PI low (early apoptosis)+ Annexin V high and PI high (late apoptosis) cell counts). Green bar = DMSO control, red bar = dinaciclib (10 nM), yellow bar = entinostat (500 nM), black bar = combination (10 nM dinaciclib + 500 nM entinostat). G-H) Graphical depiction of dose-matrix analyses for the combined CDK/HDAC inhibition in LP-1-P and LP-1-PIR MM cells. Percent inhibition of cell growth is shown for each different combination of doses and colorized in red. Cells were treated for 48 hours with different concentrations of each drug (indicated by X- and Y-axes) singly or in combination. IC50 concentrations for each drug in parental and oprozomib-resistant cell lines as determined by MTS dose-response assay, are shown in adjacent tables; ovals and dotted lines indicate optimal dose for dinaciclib and entinostat in each cell line, determined by synergy scoring.

Figure 3.1 continued

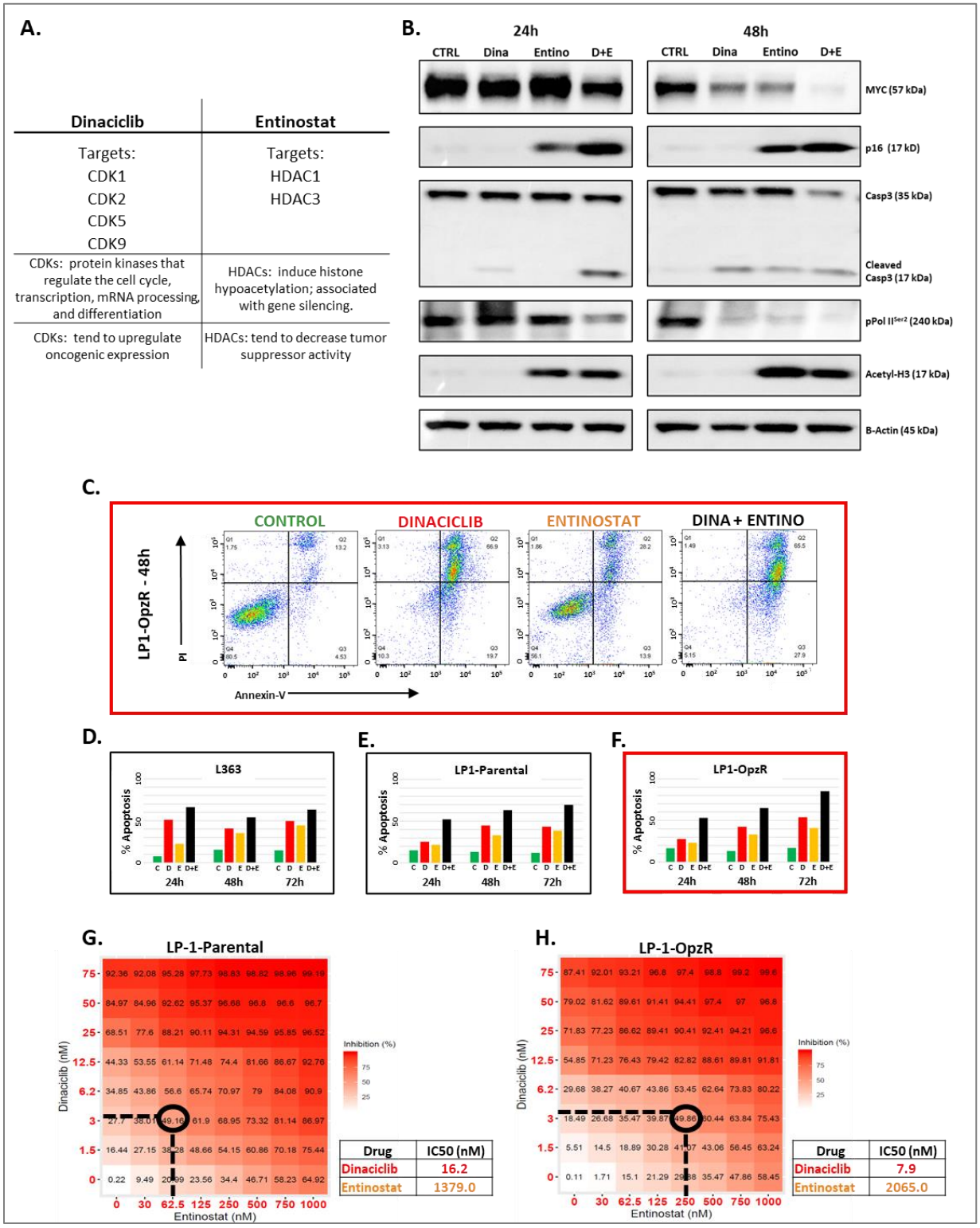

3.3.2 Tolerability of combined CDK/HDAC inhibition in mice

Tolerability of combined CDKi/HDACi in 8-week-old NSG mice treated with dinaciclib (intraperitoneal [IP], in 20% β-Cyclodextrin) and entinostat (via oral gavage [PO] or IP, in 20% β-Cyclodextrin). Drug doses were chosen based on previously published animal data [14, 21]. Mice were treated with either drug once every other day with dinaciclib, and every day with entinostat, for 5 days. (Table S.3.1). None of the chosen dose groups elicited overt clinical signs of toxicity (such as diarrhea, hunched posture, etc.) during treatment, and there was no evidence of severe decreases in body weight (as defined by a ≥20% decrease in body weight [27]) in any of the combination groups after 5 days of treatment. Microscopically, minimally to slightly decreased sternal bone marrow cellularity, characterized by loss of myeloid and erythroid precursors, was noted in both groups of mice administered 20 mg/kg dinaciclib. Based on these results, a dose regimen of 15 mg/kg dinaciclib IP two times per week and 15 mg/kg entinostat PO five times per week was chosen for NSG mouse studies. In a five-day tolerability study of the combination in naïve male and female BALB/c-Bcl-xL (Bcl-xL) transgenic mice, liquid feces, hunched posture, and an average weight loss of 15.03% were observed in mice administered 15 mg/kg dinaciclib IP iand15 mg/kg entinostat PO (Table S.3.2). Liquid feces was also observed in Bcl-xL mice administered 10 mg/kg dinaciclib IP and 15 mg/kg entinostat PO but not in mice administered 7.5 mg/kg dinaciclib IP and entinostat PO. Based on these results, a dose regimen of 7.5 mg/kg dinaciclib IP two times per week and 15 mg/kg entinostat PO two times per week was utilized for the long-term Bcl-xL mouse model survival study.

3.3.3 *In vivo* target engagement and efficacy of combined CDK/HDAC inhibition in mice

Cooperative CDKi/HDACi target engagement was assessed *in vivo* in NSG mice bearing L363 MM xenografts. 6–8-week-old NSG mice were inoculated with $5x10^6$ L363 MM cells subcutaneously into each flank, and tumors allowed to grow for 13 days before randomization into four treatment groups: vehicle control, dinaciclib (D) (15 mg/kg, IP, 3x/week), entinostat (E) (15 mg/kg, PO, 5x/week), or the D+E combination. For the target engagement experiment, xenografts from euthanized tumor-bearing mice (n = 3) were collected on day 5 for WB analysis (Fig. 3.2A). Combined CDK/HDAC inhibition was more effective at reducing MYC protein expression and increasing p16 expression overall in L363 xenografts compared to dinaciclib alone, and both

dinaciclib and the combination reduced total caspase 3 protein, indicating apoptosis; however, cleaved caspase protein was not detected via western blotting of tumor lysates.

Combination efficacy versus single agent or control was evaluated in NSG mice bearing L363 MM xenografts. For visualization, L363 cells were transfected with the pSicoLV-luciferase-green fluorescent protein fusion gene (luc/GFP+) [7, 35]. NSG female Mice (n = 10) were treated with the same dose regimen as in the NSG efficacy study until tumors grew large enough to necessitate humane euthanasia. Tumor volumes were measured twice per week and growth of luc/GFP+ L363 MM xenografts was measured every two weeks by bioluminescence imaging. While single agent treatment with dinaciclib or entinostat significantly improved survival (Log Rank test $p < 0.05$), combined treatment with dinaciclib and entinostat significantly improved survival versus control or single agent ($p < 0.01$) (Fig. 3.2B). Additionally, an increase in mean tumor volume, measured via calipers, was delayed in the mice administered the combination of dinaciclib and entinostat compared to those administered single agent only (Fig. S3.3A). The overall increase in luc/GFP+ L363 MM xenograft mean radiance (p/s/cm^2/sr), as detected via bioluminescent imaging, was slower to increase throughout the course of the efficacy study in NSG mice (Fig. S3.3B). However, mean tumor radiance increases over time were similar to those observed in tumor bearing NSG mice administered dinaciclib alone.

In vivo efficacy of CDK/HDAC inhibition was assessed in an immunocompetent model of plasma cell tumors bearing similar features as human MM and Burkitt lymphoma [22]. Adult Bcl-xL transgenic mice administered pristane oil via IP injection develop intraperitoneal plasmacytomas containing *Myc* translocations within 4-6 weeks [5, 22]. To test efficacy in this model, Bcl-xL tumors were transplanted into syngeneic pristane-primed male and female mice (n = 5) and allowed to grow for two weeks, at which time daily treatment with vehicle, single agent, or the dinaciclib/entinostat combination began. Cytologic evaluation of abdominocentesis samples was performed every other week to monitor peritoneal tumor presence and burden (Fig. S3.3C). Single agent treatment with dinaciclib (7.5 mg/kg, IP, 2x/week), entinostat (15 mg/kg, PO, 2x/week), and combined CDK/HDAC treatment all showed significant improvement in survival (log rank test, $p < 0.05$) – (Fig 3.2C). However, combined CDK/HDAC inhibition was not superior to single agent treatment.

Figure 3.2. *In vivo* evaluation of combined targeted CDK/HDAC inhibition. A) Representative WB analysis of L363 MM cell lysates from mice treated for 5 days with dinaciclib (15 mg/kg, IP, 2x/week), entinostat (15 mg/kg, PO, 2x/week) or both drugs. Each lane represents a lysate from a single animal. Tumor lysates were probed for MYC, p16, total and cleaved caspase 3, and β-actin. B) *In vivo* efficacy of combined CDK/HDAC inhibition versus single agent or control treated NSG mice. C) B) *In vivo* efficacy of combined CDK/HDAC inhibition versus single agent or control treatment in Bcl-xL transgenic mice with intraperitoneal plasma cell tumors. Shaded areas around each survival curve represent survival probability. * = significantly prolonged survival versus control ($p < 0.01$, Log-Rank test). ** = significantly prolonged survival versus control and single agent treatment ($p < 0.001$, Log-Rank test).

Figure 3.2 continued

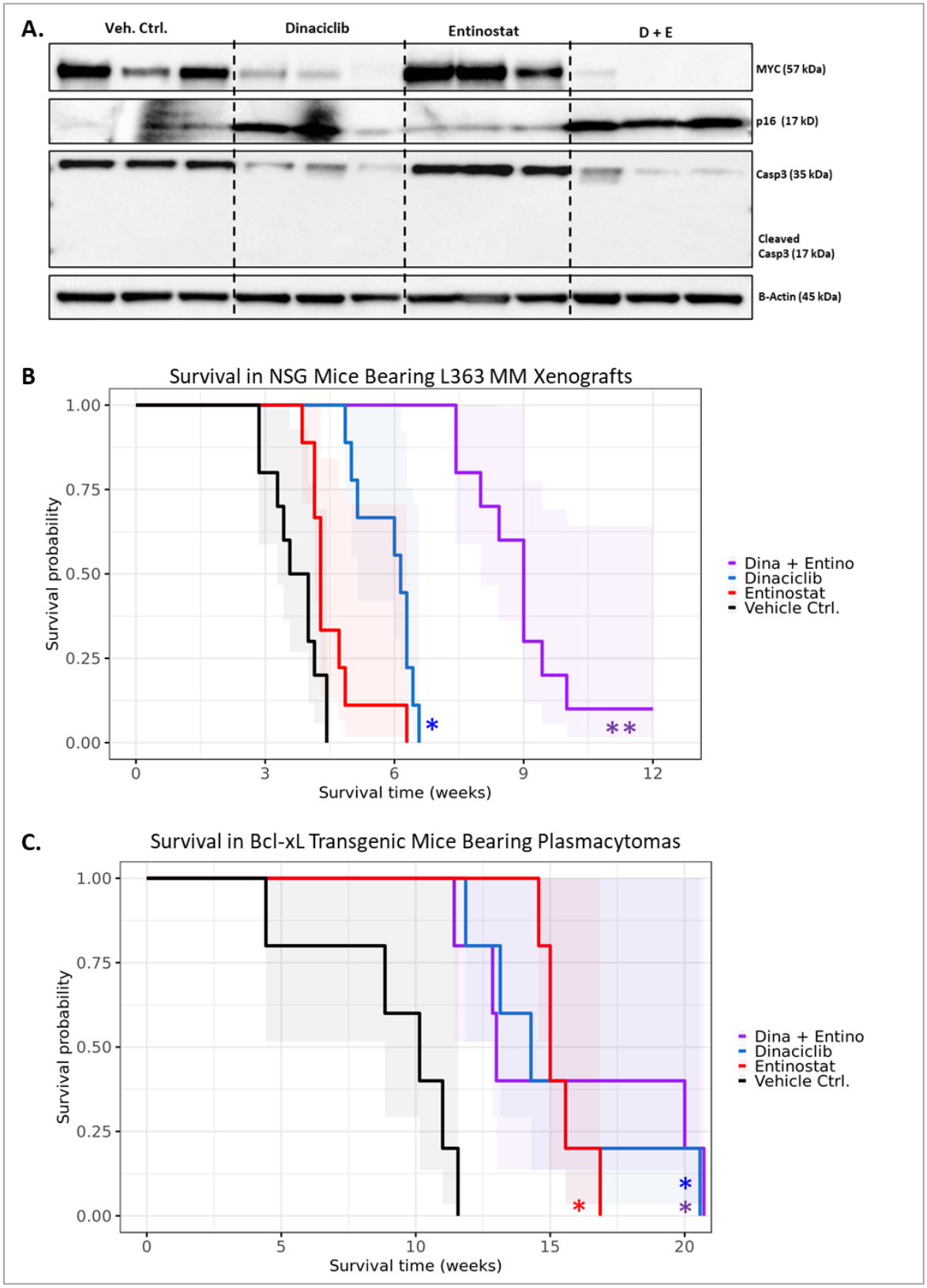

3.3.4 Combined CDK/HDAC inhibition cooperatively and selectively reduces MM patient cell viability ex vivo

Selective reduction of the viability of MM cells was evaluated in bone marrow biopsy samples obtained from patients with confirmed smoldering multiple myeloma (SMM). Cells were selected for CD138 status using magnetic-activated cell sorting (MACS). CD138 positive and negative cells from 3 SMM patients were treated for 48 hours with dinaciclib (10 nM), entinostat (500 nM) or the combination. Viability of SMM cells, normalized to control-treated CD138 positive and negative cell optical densities, was assessed via MTS assay in a 96-well plate in 4 wells per treatment. Combined CDK/HDAC inhibition with dinaciclib and entinostat more effectively reduced viability of SMM patient CD138-positive cells compared to single agent (Fig. 3.3), with relative sparing of non-neoplastic CD138-negative cells.

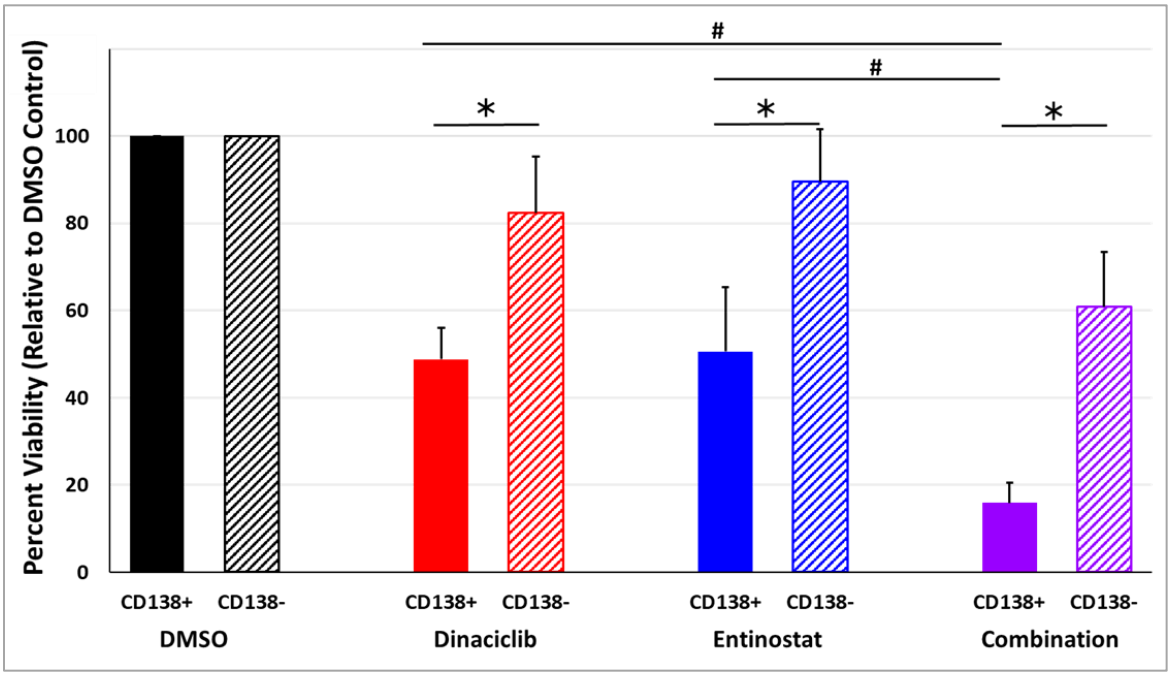

Figure 3.3. Selective efficacy of combined CDK/HDAC inhibition in smoldering multiple myeloma (SMM) patient cells ex vivo. Viability of human CD138+ (MM) and CD138- cells extracted from bone marrow of SMM patients (n=3). Cells were selected for CD138 status using magnetic-activated cell sorting (MACS). CD138+ and CD138- cells were treated with dinaciclib (10 nM), entinostat (500 nM), or the combination of the two. Solid bars indicate the average viability for each combination in CD138+ cells; hash-marked bars represent the average viability for CD138- cells. Error bars = standard deviation. ∗ = $p < 0.0001$; # = $p < 0.005$ by unpaired two-tailed Student's t test.

3.3.5 RNA-seq identifies genes differentially expressed by combined CDKi/HDACi

To gain understanding of the differential gene expression induced by combined CDK/HDAC inhibition and to identify the top pathways affected by the combination, RNA sequencing (RNA-seq) with subsequent genetic analysis was performed in myeloma cells treated with combination or single-agent therapy. The L363 MM cell line, with a known synergistic response to combined CDK/HDAC inhibition [chapter 2], was utilized for the RNA sequencing experiment. L363 MM cells were treated with dinaciclib (4 nM), entinostat (250 nM), or the combination of both drugs for 48 hours. Lower doses of each drug were used based on results from previous dose matrix synergy analysis in L363 cells [Chapter 2] suggesting lower, less toxic, doses of both drugs still provide combination synergy. For total RNA-seq, samples/cells from three replicates were isolated and analyzed. Counts-per-million (CPM) of low-expressed genes across all samples were filtered out ensuring that in at least one treatment group all replicates met the cutoff of 1 CPM.

Two-way analysis of variance (ANOVA) with interaction was performed to determine whether the combined drugs influence gene expression in a synergistic or antagonistic manner as described by Slinker [28]. One-way ANOVA contrasts were fitted to each gene to estimate the treatment effects of each single drug and their combination. Of the total number of significantly affected genes (≥2-fold increased/decreased expression compared to DMSO control), 404 genes were found via two-way ANOVA for simple effects if dinaciclib or entinostat is present to operate in a synergistic or antagonistic manner in the combination versus single agent treatment (Fig 3.4A). Furthermore, as shown in the heatmaps based on the intersections comparing lists of significant genes with combination treatment and interaction, 78 genes in total were found to be synergistically downregulated by the combination and 101 genes were synergistically upregulated compared to single agent treatment (Fig 3.4B-C).

Figure 3.4. RNA-seq identified genes synergistically changed compared to single agent treatment. L363 MM cells were treated for 48h with dinaciclib (4 nM), entinostat (250 nM) or the combination of the two. A) Intersection bar chart of all significantly upregulated or downregulated genes. Sets (with corresponding set sizes) represent the number of the genes non-additively upregulated or downregulated versus single agent treatments, along with number of genes with additive upregulation or downregulation versus single agent treatments. B-C) Heatmaps of $\log_2$ fold change expression of significant genes (2-fold versus control) that were synergistically downregulated (B) or upregulated (C) by the combination compared to single agent dinaciclib or entinostat treatment via two-way ANOVA. Columns represent expression levels for each treatment (3 technical replicates). $p < 0.05$.

Figure 3.4 continued

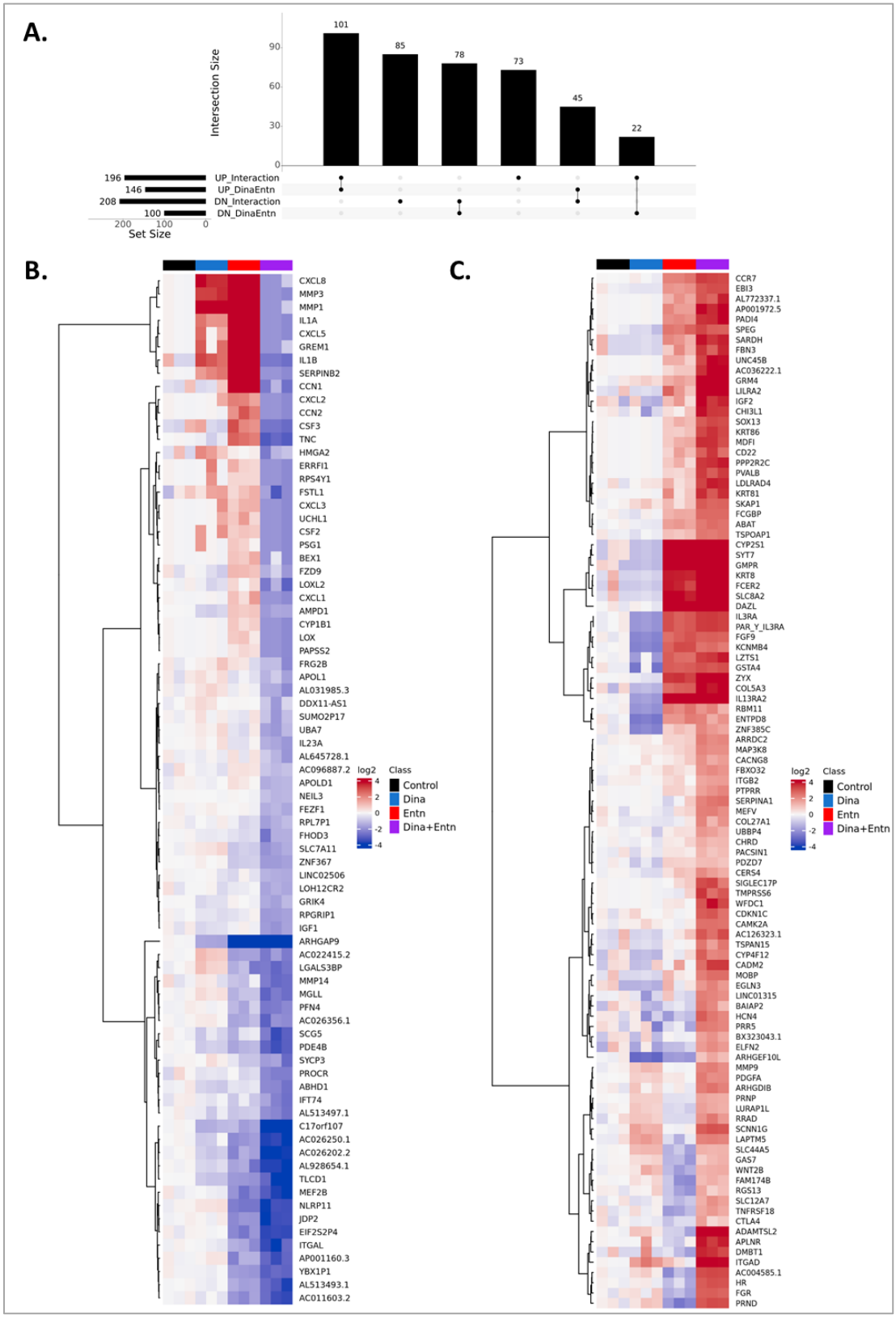

3.3.6 GSEA identifies pathways associated with CDKi/HDACi synergy

Gene set enrichment analysis (GSEA) was employed to investigate genetic pathways enriched in a synergistic CDKi/HDACi response in L363 cells [29]. From the RNA-seq results of significant (≥ 2-fold versus DMSO control) differentially expressed genes; GSEA was performed on the 14998 gene sets derived from the Gene Ontology (GO) dataset provided by the Molecular Signatures Database (MSigDB). 114 gene sets were cooperatively downregulated, and 20 gene sets were cooperatively upregulated, by the CDKi/HDACi combination of dinaciclib and entinostat compared to single agent treatments (Fig. 3.5A). Enrichment scores (ES) were defined as the degree to which genes in the gene set are over-represented at either the top (positive ES) or bottom (negative ES) of the ranked gene list [30], ranged between +1 and -1. Leading edge (LE) subsets (comprised of genes that contributed most to the enrichment signal) were required to contain at least one cooperatively upregulated gene determined from the pre-ranked ANOVA statistic. A significant ES was indicative of coordinated upregulation or downregulation of genes in the gene set.

Within the Biological Process (BP) subset of the GO gene set, comprised of 7481 gene sets, the five most significantly enriched downregulated and upregulated gene sets were selected for evaluation (Fig 3.5B-C, Fig. S3.4A-J, Appendix B). The most significantly enriched downregulated gene sets were those involving DNA replication and protein folding/localization (ES ranging from -0.63 to -0.78 and adjusted p-value ≤ 0.0041) and were as follows (with synergistically downregulated LE genes): DNA Replication Checkpoint (CDC6, CDC45, TICRR, ORC1, CDT1, TIMELESS, TIPIN, ZNF830, DNA2), DNA Replication Initiation (CDC6, MCM5, MCM7, CDC45, POLA2, TICRR, ORC1, PRIM1, CDT1, MCM10, Protein Folding in Endoplasmic Reticulum (HSPA5, HSP90B1, PDIA3, CALR, ERO1A, EMC1, EMC4, CANX), Protein Localization to Kinetochore (RCC2, BUB3, NDC80, MTBP, CDT1, CDK1, HASPIN, SPDL1, TTK, CENPQ), and Telomere Maintenance Via Semiconservative Replication (FEN1, POLA2, RRIM1, POLD3, POLE3, ACD, POLD2, RFC3, DNA2, RFC4).

The most significantly enriched upregulated gene sets (ES ranging from 0.33 to 0.48 and adjusted p-value = 0.0033) were those involved in cell adhesion, antigen presentation, immune response, and GTPase/RAS signal transduction and were as follows: Positive Regulation of Cell

Adhesion (EMP2, SOX2, JUP, CD44, CCL5, IL4R, RSU1, SMAD3, CD47, ITGA3), Immune Response Regulating Signaling Pathway and Activation of Immune Response (LGMN, TFNAIP3, MAPKAPK2, DUSP3, CD38, PRNP, CD47, NFKBIZ, PKRCD, PIK3CD; same LE genes in both gene sets), Regulation of Small GTPase Mediated Signal Transduction (RHOBTB2, ARHGAP17, MAPRE2, CYTH1, RALGPS1, AMOT, SPRY1, ITGA3, CYTH3, ARHGAP42) and Regulation of RAS Protein Signal Transduction (Leading edge genes: MAPRE2, CYTH1, RALGPS1, SPRY1, ITGA3, CYTH3, ARHGAP42, F2R, HEG, NET1).

Figure 3.5 GSEA reveals enriched pathways associated with cooperative CDKi/HDACi response. A) Intersection bar chart [30] of all enriched upregulated or downregulated pathways in the Gene Ontology (GO) dataset provided by the Molecular Signatures Database (MSigDB). Sets (with corresponding set sizes) represent the number of enriched pathways non-additively upregulated or downregulated versus single agent treatments, along with number of enriched pathways with additive upregulation or downregulation versus single agent treatments. B-C) Two example enrichment plots from GSEA [30] of the Gene Ontology (GO) Biological Process (BP) ontology database. B) Downregulated pathway: DNA Replication Checkpoint. C) Upregulated pathway: Positive Regulation of Cell Adhesion. Within each figure are separate subfigures a-c. a) Running enrichment score (ES) calculated along the ranked gene list represented by the red-blue horizontal bar (the ANOVA statistic ranked from the highest positive to the highest negative value); the vertical black bars in the plot indicate the position of the genes from the respective GO terms; the vertical red/blue line indicates the positive and negative ES, respectively. NES = observed ES / mean(null ES). b) Ranking statistic and top ten GSEA leading edge genes (LE). c) Heatmap of the GSEA leading edge genes generated with hierarchical clustering of genes using the Ward distance and complete linkage; in each gene the mean expression of the control group was subtracted in the treatment samples prior to clustering. The GSEA plot was generated using custom R scripts and *fgsea* [31], ggplot2 [32], and ComplexHeatmap [33] packages.

Figure 3.5 continued

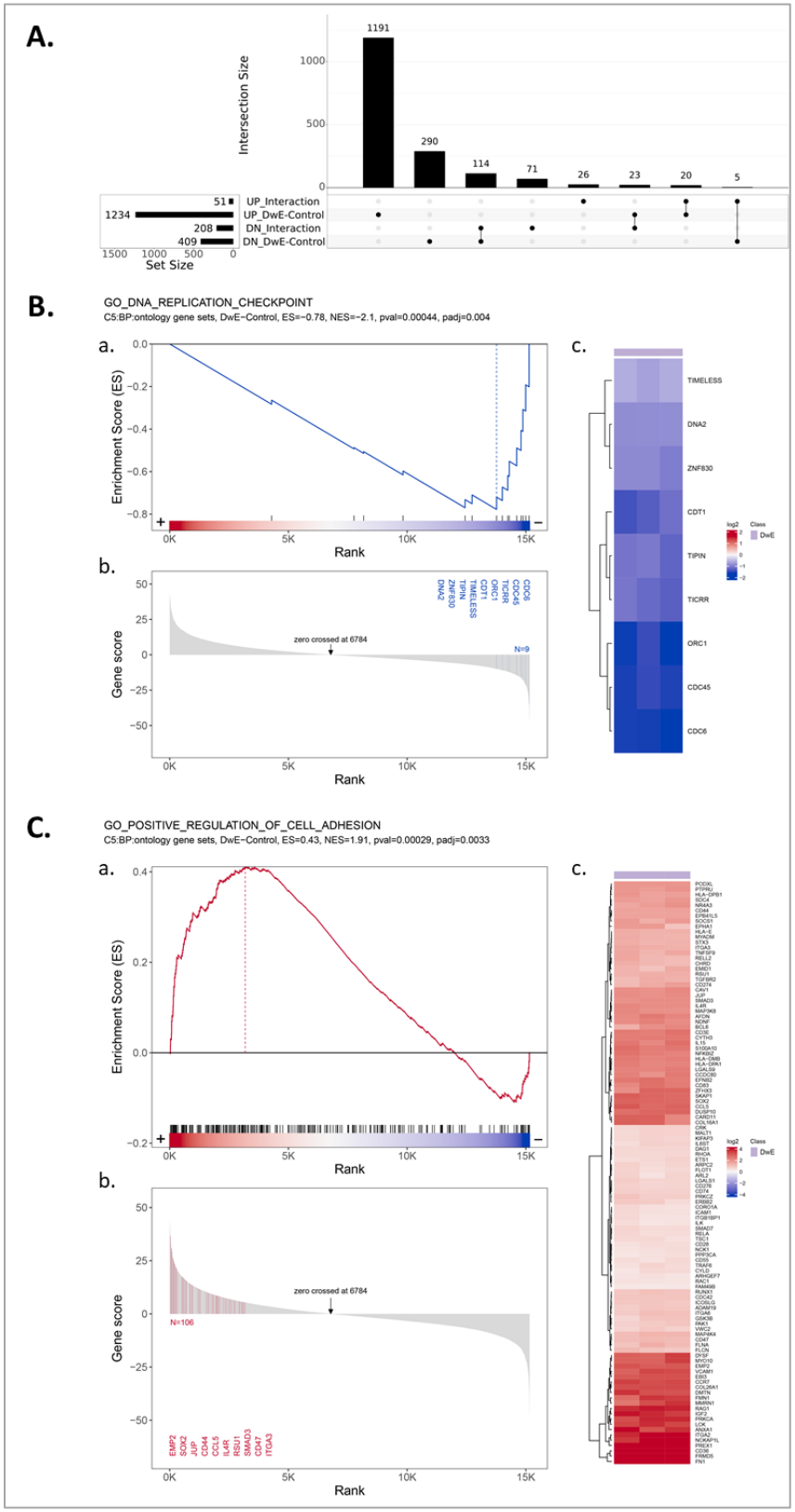

3.3.7 DAVID pathway analysis identifies function-related gene groups enriched in a synergistic CDKi/HDACi response

The Database for Annotation, Visualization, and Integrated Discovery (DAVID) was used to analyze the synergistic genes (determined via two-way ANOVA of RNA-seq results) with at least two-fold upregulation or downregulation (101 and 78, respectively). This tool uses an algorithm to determine overlaps that are greater than that expected by chance between the synergistically upregulated or downregulated gene lists and the gene ontology (GO) database. A modified Fisher's exact test was utilized to determine the overrepresented GO functions of a synergistic response signature and enriched GO terms were selected with a 5% false discovery rate. Upregulation or downregulation of over-represented pathways was determined with pathway z-scores. For each over-represented GO term, a z-score was computed based on the number of up-regulated and down-regulated genes according to the formula (up or down)/sqrt(total) proposed by Walter et al. [34] and visualized with bubble-plots. The absolute z-score cutoff of <-1 or >1 left 102 total enriched pathways (53 downregulated and 49 upregulated). The 10 most downregulated and upregulated pathways in a synergistic CDKi/HDACi response, based on p-value are shown in figure 3.6B and GO pathways are provided in Appendix C.

The downregulated pathways with the lowest z-scores, as determined by the modified Fisher's exact test and shown in the bubble volcano plot (Fig. 3.6A), were those involved in cytokine activity (GO:0005125) and cytokine receptor binding (GO:0005126). Genes synergistically downregulated by combined CDKi/HDACi, common to both pathways, include: GREM1, IL1A, CSF3, CXCL8, CSF2, IL23A, IL1B, CXCL1, CXCL3, CXCL2, and CXCL5. An upregulated gene, common to both pathways is EBI3. Eight of the ten most downregulated pathways, based on significance (lowest p-value) and number of hits within the gene set, were those related to leukocyte (primarily neutrophil) migration. Downregulated genes within these pathways include: IL1A, CXCL8, IL23A, CXCL1, CXCL3, CXCL2, PDE4B, GREM1, and CXCL5. Upregulated genes common to these pathways include CCR7, ITGB2, TNFRSF18, and PDGFA. The degree of overlap among the top downregulated pathways was striking.

The upregulated pathways with the highest z-scores, as determined by them modified Fisher's exact test and shown in the bubble volcano plot (Fig. 3.6A), were those involved in cell

signaling (GO:0010646 and GO:0023051, respectively). Genes synergistically upregulated by combined CDKi/HDACi, common to both pathways, include CDKN1C, PRR5, PTPRR, WNT2B, ABAT, SLC8A2, GRM4, FGF9, and MAP3K8 (Fig. 3.6A, Appendix C). Likewise, eight of the ten most significantly upregulated pathways are those involved in cell surface adhesion and signaling (Fig. 3.6C). Synergistically upregulated genes within these pathways include PRR5, PRNP, EBI3, IGF2, SOX13, CTLA4, ABAT, CCR7, and MAP3K8.

Figure 3.6. Modified Fisher's test reveals enriched function-related gene groups in a synergistic CDKi/HDACi response. The Database for Annotation, Visualization, and Integrated Discovery (DAVID) was used to analysis the pathways most commonly affected by combined CDKi/HDACi. Genes that were synergistically changed in the same direction by the combination treatment and that reached 2-fold change were selected for Fisher's exact test to determine overrepresented Gene Ontology (GO) functions. Enriched GO terms were selected with a 5% false discovery rate. A) For each over-represented GO term a z-score was computed based on the number of up-regulated and down-regulated genes according to the formula (up-down)/sqrt(total) proposed by Walter et al. [34] and visualized with bubble-plots. B-C) Enriched pathways based on a modified Fisher's exact test (EASE score) using DAVID [35, 36] and GO_FAT pathways for the list of differentially expressed genes common between all combination treatments. B = top 10 pathways downregulated by synergistic CDK/HDAC inhibition with z-score < -1, C = top 10 pathways upregulated by synergistic CDK/HDAC inhibition with z-score > 1.

Figure 3.6. Continued

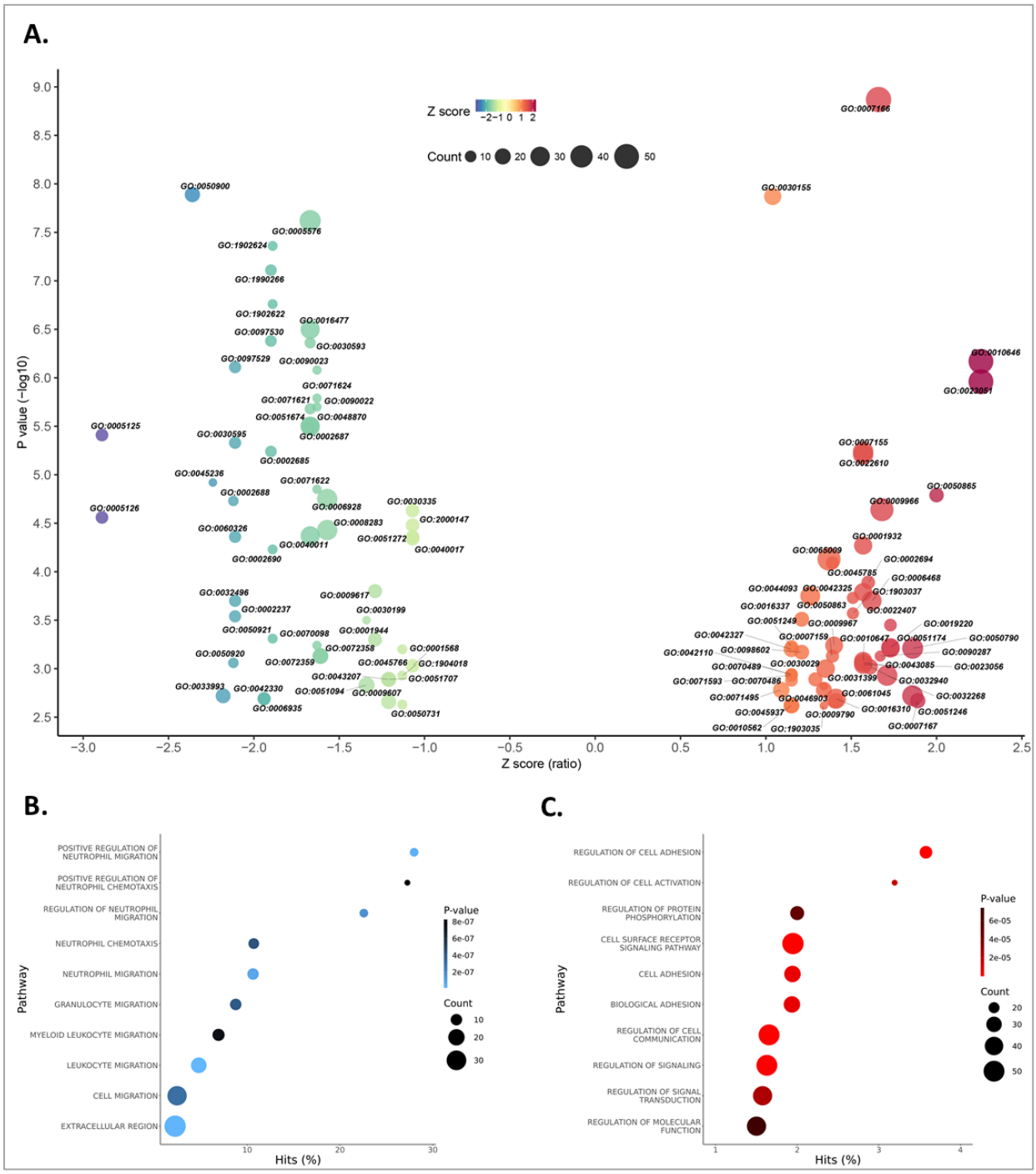

3.3.8 Master regulators of a combined CDKi/HDACi response

Ingenuity Upstream Regulator Analysis (IURA), an application within Ingenuity Pathway Analysis® (IPA, Qiagen) was used to identify the upstream transcriptional regulators of combined CDKi/HDACi synergy from the RNA-seq data. The lists of differentially expressed genes from the L363 MM cells treated with dinaciclib (4 nM) and entinostat (250 nM) were imported into IPA. A cutoff of 1.5-fold significance was selected to provide a broad dataset for analysis. 747 significant genes associated with either single agent treatment or combined CDKi/HDACi were used as the input dataset to provide a broad list of genes with adequate coverage for analysis [5]. IURA examines the number of known targets of each transcription regulator present in the imported dataset, and also compares their direction of change to what is expected from the literature (from information stored in the Ingenuity® Knowledge Base) to predict likely relevant transcriptional regulators. For each potential transcriptional regulator an overlap p-value and activation z-score were calculated (Table 3.1).

A total of fourteen transcriptional regulators were identified with highly significant p-values for overlap and activation z-scores between -2 and 2 (Table 3.1, Fig. 3.7): Five "inhibited" transcriptional regulators (ANKRD42, TGIF1, FLI1, NFKBIZ, ATF4) and nine "activated" transcriptional regulators (LEF1, ZBTB16, ZFP36, ID1, CBX5, ERG2, CITED2, Tcf7, and TP53). The master transcriptional regulators with predicted inhibition consist primarily of those involved in cell adhesion and leukocyte migration. Among the regulators with predicted activation, several are known tumor suppressors or activate/potentiate other tumor suppressors, such as TP53, ZBTB16, and ZFP36 [37-39]. Several target molecules of the upstream regulators were also identified by GSEA as synergistic leading edge genes of enriched upregulated/downregulated pathways; and/or by Fisher's exact testing of GO datasets as components of enriched pathways (Table 3.1). The downregulated molecules, based on this test, were primarily involved in cell adhesion, antigen presentation, leukocyte trafficking, and chemotaxis and include CXCL1, CXCL2, CXCL3, CXCL5, CXCL8, IL1A, IL1B, CSF2, and CSF3, among others. The upregulated molecules are involved in antigen presentation, immune response, and bone remodeling and include SPRY1, SOX13, and PRNP, among others.

Table 3.1. Upstream master regulators of a combined CDKi/HDACi response

Upstream Regulator	Predicted Activation State	Activation z-score	p-value of overlap	Target Molecules in Dataset
ANKRD42	Inhibited	-2	3.92E-06	CSF2,CSF3,CXCL3,IL1B
TGIF1	Inhibited	-2.185	1.23E-06	CCL3,CXCL1,CXCL2,CXCL3,CXCL8,IL1B
FLI1	Inhibited	-2.114	0.0000368	CCN2,CSF2,CSF3,EGR1,LOX,MMP1,SRGN,TNC
NFKBIZ	Inhibited	-2.415	0.0000084	CSF2,CSF3,CXCL3,CXCL8,IL23A,MMP3
ATF4	Inhibited	-3	0.0000268	AMPD1,CHAC1,CTH,CXCL1,CXCL2,CXCL8,DDIT3,DDR2,LAMP3,PSAT1,SLC3A2,SLC7A11, SLC7A5,WNT11
LEF1	Activated	2.2	0.031	CD274,CDH1,ITGB8,PPM1L,SGK1,SH3BGRL2,**SPRY1**
ZBTB16	Activated	2.138	0.00857	CD274,CSF2,IL1A,IL3RA,KLF2,MMP9,MPI,**NFKBIZ**,SOX13,TSC22D3
ZFP36	Activated	2.442	1.54E-07	**CDC6**,CSF2,CXCL2,CXCL3,E2F8,IL1A,IL1B,IL23A,MEFV,MMP1,PBK,TRAF1
ID1	Activated	2.236	0.0000559	ALDH1A1,CCN2,EGR1,IGF2,MMP14,MMP9,NOTCH1,TMPRSS6
CBX5	Activated	2	0.0213	CDC25A,**CDC6**,CXCL5,CYP1B1,PLAAT4,SCG5
EGR2	Activated	2.158	0.0000526	CBLB,CCL1,DMBT1,EGR1,FCER2,IGF2,IL1A,IL1B,MME,NOTCH1,RRAD,TNFSF10
CITED2	Activated	2.1	0.0000209	ARL4A,CD274,CXCL1,CXCL2,CXCL3,CXCL8,EGLN3,IL1A,IL1B,LCP2,MMP1,NAMPT,SAT1,SERPINB2,ZBP1
Tcf7	Activated	2.333	0.0228	CSF2,IL1R1,ITGB8,PAPSS2,PPM1L,SH3BGRL2,SOX13,**SPRY1**,STAT1
TP53	Activated	2.866	2.25E-13	ABAT,ALDH1A1,APOL1,CCN1,CCN2,CDC25A,**CDC6**,CDH1,CERS6,CSF2,CXCL1,CXCL2,CXCL3, CXCL8,DDIT3,DNMT3B,E2F8,EGR1,ENTPD8,FSTL1,GAS7,GPM6B,H2AZ1,IDH2,IGF1,IGF2, IL16,IL1A,IL1B,IL4I1,KRT8,LAMP3,LOX,MAFB,MAP3K8,MB,MIS18A,MMP1,MMP3,MMP9,MPI,NAMPT,NCAPG,NOTCH1,PACSIN1,PADI4,PBK,PDE4B,PDGFA,PFKFB4,PIK3CG,PLAAT4,PRKG1, **PRNP**,PTPRU,RAB11FIP1,**RFC3**,RGS13,RND3,RRAD,SAT1,SERPINB2,SERPINE1,SESN1,SGK1 ,SH3BGRL2,SLC7A11,SLC7A5,SPHK2,STAT1,TMOD1,TNC,TNFAIP2,TNFRSF18,TNFSF10,TRAF1,TSC22D3,**TTK**,TTN,TUBB3,VRK1,WDHD1,ZFP36L1,ZYX

As shown in Table 3.1, Ingenuity Upstream Regulator analysis was performed on the lists of differentially expressed genes from the L363 MM cells treated with dinaciclib (4 nM) and entinostat (250 nM) or the combination of both imported into IPA. Upstream regulator analysis revealed five CDKi/HDACi synergy-associated "inhibited" transcriptional regulators and nine "activated" transcriptional regulators. **Bold gene** = synergistic gene identified as LE gene in GSEA of GO_BP dataset. Underlined gene = synergistic gene identified in top 10 enriched pathways (upregulated or downregulated) from Fisher's exact testing of GO_FAT dataset.

Figure 3.7. Ingenuity upstream regulator analysis identifies predicted master transcriptional regulators of combined CDK/HDAC inhibition. A total of fourteen transcriptional regulators were identified with highly significant p-values for overlap and activation z-scores between -2 and 2. Transcriptional regulators, and their target genes, are arranged by subcellular localization (nucleus, cytoplasm, plasma membrane, or secreted into extracellular space). Master transcriptional regulators are shown in orange ("activated": LEF1, ZBTB16, ZFP36, ID1, CBX5, ERG2, CITED2, Tcf7, and TP53) and blue ("inhibited": ANKRD42, TGIF1, FLI1, NFKBIZ, ATF4). Target genes of the predicted master regulators are shown in red (synergistically upregulated by combined CDKi/HDACi) or green (synergistically downregulated by combined CDKi/HDACi).

Fig 3.7. Continued

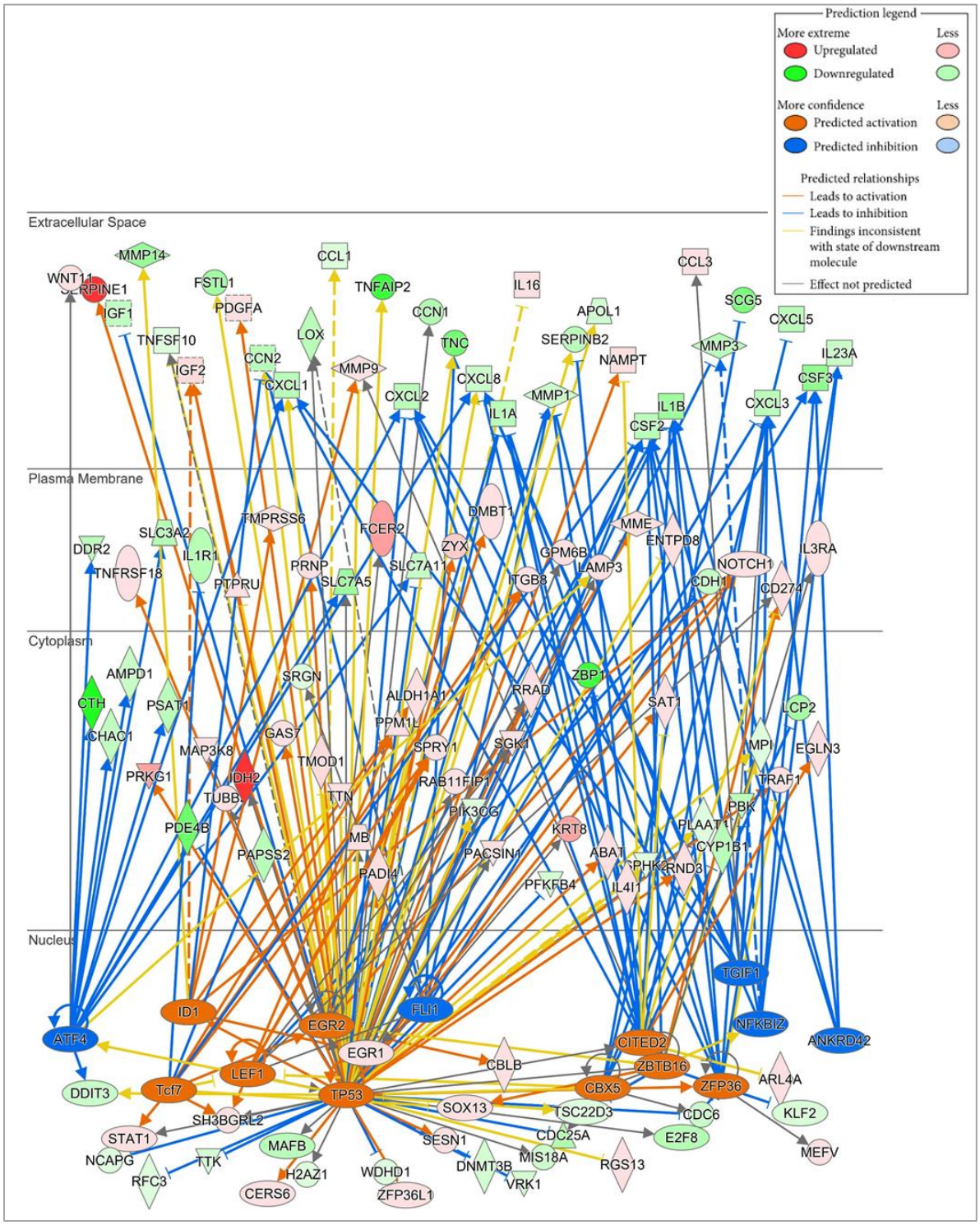

3.4 Discussion

Combined indirect targeting of oncogenic MYC and tumor suppressors such as p16 may be a useful strategy in cancer therapy, especially as activation of oncogenes and inactivation of tumor suppressors act in combination to promote cancer cell growth and contribute to malignancy (8, 9, 40). Combined targeted CDK/HDAC inhibition by dinaciclib and entinostat was effective at reducing oncogenic MYC and its effector molecules, as well as increasing p16 activity, *in vitro* and *in vivo*. Moreover, combined dinaciclib/entinostat was effective at reducing both the rate of L363 tumor growth *in vivo* in NSG mice and in myeloma patient cells treated *ex vivo*. Additionally, GSEA and upstream regulator analysis will help reveal a response signature of combined CDK/HDAC inhibition by highlighting the top pathway affected by the combination.

MYC binds and recruits the positive transcription elongation factor b (P-TEFb; comprised of activated CDK9 and cyclin T1) to its target genes and activates RNA polymerase II (Pol II) transcription complexes by phosphorylation of Pol II at serine 2 in its carboxy-terminal domain (CTD) to initiate elongation of its target genes [23, 24]. As dinaciclib is known to inhibit CDK9 by decreasing phosphorylation of threonine 186 [14], a decrease in p-CDK9^{Thr186} and resultant decrease in phosphorylated Pol II at serine 2 (pPol II^{ser2}) were noted by 48 hours in L363 MM cells treated with dinaciclib alone. Interestingly though, pPol II^{ser2} is effectively reduced by combined CDK/HDAC as early as 24 hours and is almost undetectable at 48 hours, implying that the combination may be more effective at reducing transcription of MYC targets *in vitro*. Additionally, cooperative reduction of CDK9 activity by the combination, as indicated by reduced expression of pCDK9^{Thr186} in MM cells, implies that combined CDK/HDAC inhibition is more effective at decreasing downstream MYC target effects.

In vitro data also shows that targeted CDK/HDAC inhibition is effective in MM cells with induced resistance to proteasome inhibitors (PIs) - (Fig. 3.1, Fig. S3.2). PI resistance is an important driver in increasing oncogenic MYC activity and can result in overexpression of the drug efflux transporter P-glycoprotein/ABCB1 and thereby reducing the efficacy of other potential therapeutics [16, 41, 42]. As such, it is important that a drug combination, likely to be evaluated in clinical trials in patients who have developed PI resistance, be effective in PI-resistant MM as is the case with the proposed novel CDKi/HDACi combination of dinaciclib and entinostat.

The use and outcome of validated and predictive animal models is pivotal in translating the preclinical findings to the clinic. Therefore, target engagement and efficacy of combined CDKi/HDACi were investigated in two separate models, each fulfilling a specific purpose. First, after assessing tolerability of combination treatment, NSG mice bearing subcutaneous L363 MM xenografts were assessed for combination target engagement, indicated by reduction of MYC protein and increased activity of p16, and efficacy as determined by delayed development of tumor burden. The data show that not only is combined CDK/HDAC inhibition with dinaciclib and entinostat tolerated, but the combination reduced MYC protein expression and increased p16 activity slightly better than single agent treatment. More importantly, the combination significantly reduced the rate of tumor growth in xenografts (Fig 3.2). Second, the Bcl-xL transgenic mouse study allowed detection of combination effects in an immunocompetent model of plasma cell tumors with features of human MM and Burkitt lymphoma [5, 22]. Although combined CDK/HDAC inhibition prolonged survival, it was no more effective than single agent treatment. A possible reason for this is that enhanced toxicity in Bcl-xL transgenic mice necessitated a lower dose than in NSG mice.

Cooperative effects of combined CDK/HDAC inhibition were assessed in freshly isolated patient myeloma cells to provide evidence that efficacy was not limited to cultured cell lines and mouse models. The data suggest that the combination was more effective at reducing the viability of human CD138+ myeloma cells than single agent treatment while still showing selectivity for CD138+ myeloma cells; suggesting that combined therapy may spare patients from the detrimental effects of bone marrow depletion because of chemotherapy.

Analysis of the RNA-seq results from L363 myeloma cells treated with dinaciclib and/or entinostat provided insight into mechanisms and potential biomarkers of a combined CDKi/HDACi response, as well as master regulators of synergy. Based on the ANOVA statistical analysis of differentially expressed genes and subsequent gene set enrichment analysis of the GO Biological Process gene sets, downregulated genes and pathways included those involving DNA replication and protein folding/localization (Fig 3.5B, Fig. S3.4A-E). These effects are in line with expected pharmacologic effects of individual CDK and HDAC inhibition [14, 21, 43], but also provide insight into new potential mechanisms of synergy and biomarkers of a combined response. For example, it is known that dinaciclib inhibits the unfolded protein response through a CDK1-

and 5-dependent mechanism [43]. However, GSEA identifying synergistic downregulation of protein folding machinery suggests that combining dinaciclib with the HDAC inhibitor entinostat may enhance UPR-mediated cell death in MM. Further studies are necessary to confirm this, however. Similarly, the GO_BP gene set "Positive Regulation of Cell Adhesion" was among enriched upregulated pathways identified in a synergistic CDKi/HDACi response. One of the synergistically upregulated leading-edge genes in this pathway was SMAD3 (Fig. 3.5C, Fig. S. 3.4F). Increased signaling of the TGFβ/SMAD pathway is a potentially negative consequence associated with combined CDK/HDAC inhibition. This provides further rationale for investigating the addition of TGFβ pathway inhibitors to the combination to help abrogate TGFβ receptor signaling in check and further enhance decreases in myeloma cell proliferation *in vitro* to prolong survival in animal models of MM.

Additionally, Fisher's exact testing of the significant genes, using a wider data set (GO_FAT) provided additional information on upregulated and downregulated functionally-related gene groups and interactions. The ten most downregulated pathways were those related to leukocyte migration, which correlates largely with the results from Ingenuity upstream regulator analysis (IURA). Downregulated genes within these pathways include: IL1A, CXCL8, IL23A, CXCL1, CXCL3, CXCL2, PDE4B, GREM1, and CXCL5. Upregulated genes common to these pathways include CCR7, ITGB2, TNFRSF18, and PDGFA. Interestingly, TNFRSF18, which was synergistically upregulated by CDK/HDAC inhibition, has been identified as a tumor suppressor in MM and may enhance sensitivity of MM cells to proteasome inhibitors by inhibiting NF-κB activation [44]. TNFRSF18 was also a target gene predicted to be upregulated by TP53 in the Ingenuity upstream regulator analysis (Table 3.1)

Ingenuity upstream regulator analysis, based on over-representation in knowledge-based transcriptional networks, was employed to identify master regulators controlling synergistically upregulated/downregulated target genes. The master transcriptional regulators predicted to be inhibited by combined CDK/HDAC inhibition were mainly those involved in regulating cell adhesion molecules and work both intracellularly and as part of the extracellular matrix to promote metastasis. A master regulator of combined CDK/HDAC inhibition with predicted activation was TP53 (Table 3.1, Fig. 3.7). This molecule obviously has a broad set of activities as it relates to cancer, but its dysregulation is implicated in the pathogenesis and progression of MM [37].

Activating TP53, therefore, is a likely beneficial effect of combined CDKi/HDACi interaction. Another known tumor suppressor predicted to be activated by the combination, ZBTB16 [38], is also an important gene involved in bone formation [45]. Its activation, therefore, may be beneficial in patients to help prevent one of the most deleterious consequences of MM progression, bony lysis. TCF7 and LEF1, both upstream transcriptional regulators with predicted activation by synergistic CDK/HDAC inhibition were predicted to activate SPRY1, an enriched gene in GSEA analysis on the leading edge of two of the top 5 upregulated gene sets (Fig.S.3.4). SPRY1 (Sprouty 1) promotes osteogenesis and is regulated by miR-21 [46], thus providing more evidence that the combination may prevent bone-loss/lysis in vivo. However, a recent study has proposed that upregulated LEF1 may promote MM cell growth [47]. It is important to note though, that LEF1 was not found to be one of the synergistically upregulated genes from the RNA-seq results and was actually only upregulated with single agent entinostat treatment in L363 cells. Further studies, including validation of predicted changes to master regulators via RT-PCR, are necessary to evaluate the effects of combined CDK/HDAC inhibition on the master regulators and their targets.

3.5 Future Directions and Limitations

Further investigation into a combined genetic signature will aid in discovering mechanisms of drug synergy and provide biomarkers for a combined response that may translate to clinics. Concurrent to the L363 cells treated in monoculture with either single agent or the combination, RNA samples were obtained from treated L363 cells co-cultured with HS-5 bone marrow stromal cells (BMSCs); as well as L363 cells (with and without BMSC co-culture) treated with the TGFβR inhibitor SB505124. RNA-seq and subsequent data analysis from these experiments will help provide insight into the interplay between myeloma and the microenvironment of supportive stroma and may help elucidate novel mechanisms of drug sensitivity and/or resistance in MM. Weighted gene co-expression network analysis (WGCNA) of the RNA-seq data from these experiments will aid in elucidating a signature of combined CDKi/HDACi response in MM and provide biomarkers for future preclinical development.

Experimental validation of activation or inhibition of the predicted master regulators via RT-PCR of RNA from treated cells is necessary. Also, it will be important to determine which of the predicted transcriptional regulators show a trend in expression upwards/downwards during disease

progression from monoclonal gammopathy of undetermined significance (MGUS) to SMM to MM based on patient data.

More investigations into the effects of CDKi/HDACi combination therapy on patient myeloma cells *ex vivo* are also necessary, particularly as the samples in this study were limited to those from smoldering (asymptomatic) myeloma patients and not from those who are symptomatic or refractory to first line therapies. Investigating the efficacy of combined CDK/HDAC inhibitor therapy in relapsed and/or refractory MM patient cells is necessary as this patient population would be most likely to receive combination therapy and may be the most likely to benefit. Additionally, evaluation of the effects of the combination in a CD138+ and CD138 negative coculture setting could give insight into possible resistance to treatment that bone marrow stromal cells may impart [48]; especially as the RNA-seq data has elucidated the important changes in cell-cell interaction, leukocyte trafficking, and other pathways that contextual understanding of the microenvironment may impart.

A potential limitation of the GSEA strategy was that the Gene Ontology (GO) results summarized in this study were restricted to gene sets derived from the Biological Process (BP) ontology. Gene sets not included in the summary but included in the full GSEA of the RNA-seq data include Cellular Component (CC) and Molecular Function (MF) ontology gene sets, comprised of 996 and 1708 gene sets, respectively. A future direction will be to incorporate GSEA of these gene sets into the analysis of important enriched gene sets in a combined CDKi/HDACi response.

In summary, these studies have provided rationale for combined CDK/HDAC inhibition in treating human MM. The cooperative effects on targets and limited off-target effects as shown in *in vitro*, *in vivo*, and *ex vivo* studies support that the combination may have therapeutic utility for patients.

3.6 Materials and Methods

3.6.1 Human MM and other cell lines

L363 human MM cells were obtained in 2014, cultured, and authenticated as described previously [6]. LP-1 oprozomib-resistant MM cells were generated from parental MM cell lines

(obtained from M. Kuehl, NCI) by exposure to increasing concentrations of oprozomib (up to 1μM) over a period of up to 45 weeks. Resistance to oprozomib was confirmed via dose-response assay before experiments. Cells were cultured in RPMI 1640 with GlutaMAX L-glutamine (Life Technologies) supplemented with 10% fetal bovine serum (Cambrex BioScience), 100 U/ml penicillin and 100 μg/ml streptomycin (life technologies).

3.6.2 Western blot analysis

For western blot (WB) experiments, cells were seeded at 1.5x10^6 cells/ml, 3 ml/well in six-well plates and treated with DMSO (10 nM), dinaciclib (10 nM), entinostat (500 nM) or the combination of dinaciclib and entinostat for 24, 48 or 72 hours. Immunoblot analyses were performed on cells lysed with RIPA buffer (Thermo Fisher Scientific), electrophoresed on 4-20% Tris-Glycine SDSPAGE gels (Novex), and blotted on to nitrocellulose using iBlot (Invitrogen). Each experiment was repeated at least three times, and a representative blot is shown in the figure. Antibodies for β-actin, were obtained from Cell Signaling and used at 1:1000 dilutions.

3.6.3 Cell viability assays in human MM cell lines and primary human MM cells

For cell viability assays MM cell lines (LP1, LP1-OpzR) were treated with increasing doses of a single agent or a combination of two drugs (1:1 molar ratio). Cells were seeded in 96-well plates at 50,000 cells per well in 200 mL media and treated for 48 hours and MTS assay using CellTiter96® Aqueous One Solution Cell Proliferation Assay (Promega) was performed to determine cell titers. Ratios of inhibitor-treated to untreated control cell titers were calculated. Activity and synergy analyses were performed on a dose matrix comprised of eight single agent concentrations for each compound, and the 64 combinations thereof. MM cells were seeded in 96-well plates at 50,000 cells per well in 200m media with four replicates per dose. Viability was assessed after 48 h of treatment with CellTiter96® Aqueous One MTS reagent (Promega).

For *ex vivo* viability assays, bone marrow aspirates were collected from patients with confirmed smoldering multiple myeloma (SMM) enrolled in clinical trials at the NCI/NIH. Informed consent forms were reviewed and signed by all patients prior to admission. Ficoll-Paque PLUS density gradient sedimentation (Cytiva) was utilized to isolate bone marrow mononuclear

cells and primary SMM cells as per the manufacturer's protocol. CD138 positive cells were further separated from bone marrow samples by antibody-mediated positive selection using anti-CD138 magnetic-activated cell separation microbeads (Miltenyi Biotech). The percentage of CD138 positive cells in the positive fraction was quantified by flow cytometric analysis using FlowJo software and found to be greater than 98%. *Ex vivo* patient cell viability was determined in CD138 positive and CD138 negative cells treated with the three top combinations (at IC50 doses of each drug) compared to DMSO-treated control cells.

3.6.4 Flow cytometry assay for apoptosis in human MM cell lines

L363, LP-1-Parental, or LP-1-OpzR MM cells were seeded at 1.5x10^6 cells/ml, 3 ml/well in six-well plates and treated with DMSO (10 nM), dinaciclib (10 nM), entinostat (500 nM) or the combination of dinaciclib and entinostat for 24, 48 or 72 hours. Cells were stained for apoptosis using FITC Annexin V and propridium iodide (PI) reagents as per the manufacturer's protocol (#556547BD Biosciences). After incubation, cells were quantified by flow cytometric analysis using FlowJo software.

3.6.5 *In vivo* experiments

All animal experiments were conducted in accordance with the Guide for the Care and Use of Laboratory Animals and institutionally approved (LCBG-009, ACUC, NCI) in a facility approved by the Association for Assessment and Accreditation of Laboratory Animal Care. Tolerability and dose ranging of combined CDK/HDAC inhibition with dinaciclib and entinostat was evaluated in both naïve NSG mice and naïve Bcl-xL transgenic mice prior to starting studies.

For target engagement and efficacy studies in NSG mice bearing L363 MM xenografts, 5x10^6 cells were inoculated onto each flank (2 tumors per mouse) of NSG (NOD scid gamma) mice (NCI, Frederick, MD) and allowed to grow for 11 days prior to randomization into treatment groups (4 groups; 10 mice per group). For visualization, L363 cells were transfected with the pSicoLV-luciferase-green fluorescent protein fusion gene (luc/GFP+) [21]. Mice were treated with 15 mg/kg dinaciclib (intraperitoneal [IP], in 20% β-Cyclodextrin, 3x/week) and 15 mg/kg entinostat (oral gavage [PO] or IP, in 20% β-Cyclodextrin, 5x/week). Tumor volumes and animal

weights were measured twice weekly, and growth of luc/GFP positive L363 cells was measured weekly manually with calipers and by bioluminescence using a XenogenIVIS100® system. For the target engagement study, mice were humanely euthanized on the fifth day and tumors were collected for histology and western blotting. For the long-term efficacy study, NSG mice were humanely euthanized an tumors collected for histology if animals were observed in moribund condition or if one of the tumor dimensions met or exceeded 1 cm in diameter. Kaplan-Meier survival curves were generated for overall survival between the four groups. Survival probability distributions were compared using the log rank test.

For the long-term *in vivo* efficacy in the Bcl-xl transgenic model, BALB/c-Bcl-xL transgenic mice were generated as previously described [22]. Tumor transplants were initiated by injecting finely minced oil granuloma tissue from donor mice into intraperitoneally into syngeneic BALB/c-Bcl-xL recipient mice that had primed with 0.2 ml pristane oil 14 days prior to transplantation. Tumors were allowed to grow for 14 days prior to randomization into treatment groups (4 groups, 5 animals per group). Mice were administered DMSO 7.5 mg/kg dinaciclib (IP, 2x/week), 15 mg/kg entinostat (PO, 2x/week) or the combination. Mice were treated until criteria for humane euthanasia were met [27]. Plasma cell tumors were diagnosed via Wright-Geimsa staining of ascites fluid cytofuge preparations. The criterion for a positive sample was ten tumor cells per high-powered field. Survival probability distributions were compared among Kaplan-Meier survival curves generated for each treatment and compared using the log rank test.

3.6.6 RNA-seq and differential gene expression analysis of combined CDK-HDAC inhibition

L363 MM cells were cultured either alone or in co-culture with bone marrow stromal cells (BMSC-HS5) and treated with dinaciclib (4nM), entinostat (250nM), SB505125 (5μM); dinaciclib and entinostat combination, and dinaciclib, entinostat and SB505125 triple combination. For total RNA sequencing (RNA-seq) of samples/cells from three replicates cultured in above conditions were harvested, and RNA were isolated using the RNeasy Mini Kit (Qiagen) using manufacturers protocol. Briefly, 3 million cells were harvested, lysed by RLT buffer, and loaded on QIAshredder spin column homogenizer (Qiagen). The filtrate was proceeded for RNA isolation as per the RNA mini kit guidelines. RNA was eluted in RNAse free water provided in the kit and stored at -80℃.

RNA concentration was measured 260/280 and 230/260 ratios using DeNovix DS-11 Spectrophotometers/Fluorometers machine. For quality control (QC) of the RNA samples, automated electrophoresis via the Agilent Tape Station system with regular sensitivity (25-500 ng/ul), at Center for Cancer Research (CCR)'s Genomics core, was performed. The RNA samples were diluted to approximately 100 ng/µl in PCR strip tubes in a total volume of 10 µl. The QC of RNA is described as RNA integrity number (RIN) ranging from intact (10) to degraded (1). All the 36 RNA samples had RIN ≥8. and at a concentration of 50 ng/ul in a volume of 10ul were sent to CCR's Genomic core at Frederick for sequencing on the NovaSeq 6000® system using Illumina TruSeq Stranded mRNA Library Prep and paired-end sequencing. Reads of the samples were trimmed for adapters and low-quality bases using Cutadapt before alignment with the reference genome (hg38) and the annotated transcripts using STAR. The mapping statistics were calculated using Picard software. Library complexity was measured in terms of unique fragments in the mapped reads using Picard's MarkDuplicate utility. In addition, the gene expression quantification analysis was performed for all samples using STAR/RSEM tools.

Gene-level raw counts (RSEM) were transformed to counts-per-million (CPM) with library size normalization [49]. Low-expressed genes across all samples were filtered out assuring that in at least one treatment group all replicates met the cutoff of 1 CPM. Subsequently, limma-voom [50] was used for quantile normalization and empirical Bayes extension of Analysis of Variance (ANOVA). Univariate two-way ANOVA with interaction was performed to determine whether the combined drugs influence gene expression in a synergistic or antagonistic manner as described by Slinker [28]. One-way ANOVA contrasts were also fitted to each gene to estimate the treatment effects of each single drug and their combination. The univariate p-values were adjusted for false discovery rate (FDR) using the method of Benjamini and Hochberg [51]. An adjusted p-value <0.05 and absolute fold change >1.5 were used as the cutoffs to identify significant genes. The analyses were done using the R programming language version 3.5.1, EdgeR version 3.24.3, limma version 3.38.3 Bioconductor packages, and the NIH Integrated Data Analysis Platform (NIDAP).

3.6.7 Gene set enrichment analysis

Gene Set Enrichment Analysis (GSEA) [29] was performed using Bioconductor *fgsea* package [30] and GO Ontology collections from The Molecular Signatures Database (MSigDB

v7.0). In the GSEA analysis, genes were pre-ranked with the ANOVA statistic for the combination treatment effect and the interaction term. For each gene set, p-value was calculated with 5000 random gene permutations. Gene sets with the FDR less than 5% were considered significantly enriched. The GSEA plot was generated using custom R scripts and fast gene set enrichment analysis (*fgsea*) implementation method (open-source R package in Bioconductor) – [31], ggplot2 [32], and ComplexHeatmap [33] packages.

3.6.8 DAVID enrichment analysis of GO data set

The Database for Annotation, Visualization, and Integrated Discovery (DAVID, https://david.ncifcrf.gov/) [35, 36] was used to determine overrepresented Gene Ontology (GO) functions in the lists of significant genes. GO_FAT functional categories (comprised of GO subsets with the broadest terms filtered out) were tested. Enriched GO terms were selected with nominal p-value less than 0.05 with the synergistically upregulated or downregulated genes from RNA-seq and the false discovery rate less than 5% [51]. For each over-represented GO term a z-score was computed based on the number of up-regulated and down-regulated genes according to the formula (up-down)/sqrt(total) proposed by Walter et.al [34] and visualized with bubble-plots.

3.7 References and Notes

[1] Gulla A, Anderson KC. Multiple myeloma: the (r)evolution of current therapy and a glance into future. *Haematologica*. 2020 Oct 1;105(10):2358-2367.

[2] Kazandjian D. Multiple myeloma epidemiology and survival: A unique malignancy. *Semin Oncol*. 2016 Dec;43(6):676-681.

[3] Bazarbachi AH, Al Hamed R, Malard F, Harousseau JL, Mohty M. Relapsed refractory multiple myeloma: a comprehensive overview. *Leukemia*. 2019 Oct;33(10):2343-2357.

[4] Zhang S, DuBois W, Zhang K, Simmons JK, Hughitt VK, Gorjifard S, Gaikwad S, Peat TJ, Mock BA. Mouse tumor susceptibility genes identify drug combinations for multiple myeloma. *J Cancer Metastasis Treat*. 2020;6:21.

[5] Simmons JK, Michalowski AM, Gamache BJ, DuBois W, Patel J, Zhang K, Gary J, Zhang S, Gaikwad SM, Connors D, Watson N, Leon E, Chen JQ, Kuehl WM, Lee MP, Zingone A, Landgren O, Ordentlich P, Huang J, Mock BA. Cooperative targets of combined mTOR/HDAC inhibition promote MYC degradation. *Mol Cancer Ther*. 2017 Sep;16(9):2008-21.

[6] Jovanović KK, Roche-Lestienne C, Ghobrial IM, Facon T, Quesnel B, Manier S. Targeting MYC in multiple myeloma. *Leukemia*. 2018 Jun;32(6):1295-306.

[7] Chesi M, Robbiani DF, Sebag M, Chng WJ, Affer M, Tiedemann R, Valdez R, Palmer SE, Haas SS, Stewart AK, Fonseca R, Kremer R, Cattoretti G, Bergsagal PL. AID-dependent activation of a MYC transgene induces multiple myeloma in a conditional mouse model of postgerminal center malignancies. *Cancer Cell*. 2008 Feb;13:167–80.

[8] Chng WJ, Huang GF, Chung TH, Ng SB, Gonzalez-Paz N, Troska-Price T, Mulligan G, Chesi M, Bergsagel PL, Fonseca R. Clinical and biological implications of MYC activation: a common difference between MGUS and newly diagnosed multiple myeloma. *Leukemia*. 2011 Jun;25(6):1026–35.

[9] Whitfield JR, Beaulieu ME, Soucek L. Strategies to inhibit Myc and their clinical applicability. *Front Cell Dev Biol*. 2017 Feb 23;5:10.

[10] Dang CV, Reddy EP, Shokat KM, Soucek L. Drugging the 'undruggable' cancer targets. *Nat Rev Cancer*. 2017 Aug;17(8):502-08.

[11] Wen Z, Rajagopalan A, Flietner ED, Yun G, Chesi M, Furumo Q, Burns RT, Papadas A, Ranheim EA, Pagenkopf AC, Morrow ZT, Finn R, Zhou Y, Li S, You X, Jensen J, Yu M, Cicala A, Menting J, Mitsiades CS, Callander NS, Bergsagel PL, Wang D, Asimakopoulos F, Zhang J. Expression of NrasQ61R and MYC transgene in germinal center B cells induces a highly malignant multiple myeloma in mice. *Blood*. 2021 Jan 7;137(1):61-74.

[12] Rajan AM, Kumar S. New investigational drugs with single-agent activity in multiple myeloma. *Blood Cancer J*. 2016 Jul 29;6(7):e451.

[13] Alagpulinsa DA, Ayyadevara S, Yaccoby S, Shmookler Reis RJ. A Cyclin-Dependent Kinase Inhibitor, Dinaciclib, Impairs Homologous Recombination and Sensitizes Multiple Myeloma Cells to PARP Inhibition. *Mol Cancer Ther*. 2016 Feb;15(2):241-50.

[14] Parry D, Guzi T, Shanahan F, Davis N, Prabhavalkar D, Wiswell D, Seghezzi W, Paruch K, Dwyer MP, Doll R, Nomeir A, Windsor W, Fischmann T, Wang Y, Oft M, Chen T, Kirschmeier P, Lees EM. Dinaciclib (SCH 727965), a novel and potent cyclin-dependent kinase inhibitor. *Mol Cancer Ther*. 2010 Aug;9(8):2344-53.

[15] Kumar SK, Rajkumar V, Kyle RA, van Duin M, Sonneveld P, Mateos MV, Gay F, Anderson K. Multiple myeloma. *Nat Rev Dis Primers*. 2017 Jul 20;3:17046.

[16] De Souza C, Chatterji BP. HDAC inhibitors as novel anti-cancer therapeutics. *Recent Pat Anticancer Drug Discov*. 2015;10(2):145-62.

[17] Connolly RM, Rudek MA, Piekarz R. Entinostat: a promising treatment option for patients with advanced breast cancer. *Future Oncol*. 2017 Jun;13(13):1137-1148.

[18] Kumar SK, LaPlant B, Chng WJ, Zonder J, Callander N, Fonseca R, Fruth B, Roy V, Erlichman C, Stewart AK; Mayo Phase 2 Consortium. Dinaciclib, a novel CDK inhibitor, demonstrates encouraging single-agent activity in patients with relapsed multiple myeloma. *Blood*. 2015 Jan 15;125(3):443-8.

[19] Connolly RM, Zhao F, Miller KD, Lee MJ, Pikarz RL, Smith KL, Brown-Glaberman UA, Winn JS, Faller BA, Adedayo AO, Burkard ME, Budd GT, Levine EG, Royce ME, Kaufman PA, Thomas A, Trepel JB, Wolff AC, Sparano JA. E2112: Randomized phase III trial of endocrine therapy plus entinostat or placebo in hormone receptor–positive advanced breast cancer. A trial of the ECOG-ACRIN cancer research group. *Am J Clin Oncol.* 2021 39:28, 3171-3181.

[20] Hellmann MD, Jänne PA, Opyrchal M, Hafez N, Raez LE, Gabrilovich DI, Wang F, Trepel JB, Lee MJ, Yuno A, Lee S, Brouwer S, Sankoh S, Wang L, Tamang D, Schmidt EV, Meyers ML, Ramalingam SS, Shum E, Ordentlich P. Entinostat plus pembrolizumab in patients with metastatic NSCLC previously treated with anti-PD-(L)1 therapy. *Clin Cancer Res*. 2021 Feb 15;27(4):1019-1028.

[21] Simmons JK, Patel J, Michalowski AM, Zhang S, Wei BR, Sullivan P, Gamache B, Felsenstein K, Kuehl WM, Simpson RM, Zingone A, Landgren O, Mock BA. TORC1 and class I HDAC inhibitors synergize to suppress mature B cell neoplasms. *Mol Oncol*. 2014 Mar;8(2):261-72.

[22] Kovalchuk AL, duBois W, Mushinski E, McNeil NE, Hirt C, Qi CF, Li Z, Janz S, Honjo T, Muramatsu M, Ried T, Behrens T, Potter M. AID-deficient Bcl-xL transgenic mice develop delayed atypical plasma cell tumors with unusual Ig/Myc chromosomal rearrangements. *J Exp Med*. 2007 Nov 26;204(12):2989–3001.

[23] Gregory GP, Hogg SJ, Kats LM, Vidacs E, Baker AJ, Gilan O, Lefebure M, Martin BP, Dawson MA, Johnstone RW, Shortt J. CDK9 inhibition by dinaciclib potently suppresses Mcl-1 to induce durable apoptotic responses in aggressive MYC-driven B-cell lymphoma in vivo. *Leukemia*. 2015 Jun;29(6):1437-41.

[24] Marshall NF, Peng J, Xie Z, Price DH. Control of RNA polymerase II elongation potential by a novel carboxyl-terminal domain kinase. *J Biol Chem*. 1996 Oct 25;271(43):27176-83.

[25] Kurmasheva RT, Bandyopadhyay A, Favours E, Del Pozo V, Ghilu S, Phelps DA, Erickson SW, Peer CJ, Figg WD, Smith MA, Houghton PJ. Evaluation of entinostat alone and in combination with standard-of-care cytotoxic agents against rhabdomyosarcoma xenograft models. *Pediatr Blood Cancer*. 2019 Oct;66(10):e27933.

[26] Yeh YY, Chen R, Hessler J, Mahoney E, Lehman AM, Heerema NA, Grever MR, Plunkett W, Byrd JC, Johnson AJ. Up-regulation of CDK9 kinase activity and Mcl-1 stability contributes to the acquired resistance to cyclin-dependent kinase inhibitors in leukemia. *Oncotarget*. 2015 Feb 20;6(5):2667-79.

[27] Talbot SR, Biernot S, Bleich A, van Dijk RM, Ernst L, Häger C, Helgers SOA, Koegel B, Koska I, Kuhla A, Miljanovic N, Müller-Graff FT, Schwabe K, Tolba R, Vollmar B, Weegh N, Wölk T, Wolf F, Wree A, Zieglowski L, Potschka H, Zechner D. Defining body-weight reduction as a humane endpoint: a critical appraisal. *Lab Anim*. 2020 Feb;54(1):99-110.

[28] Slinker BK. The statistics of synergism. *J Mol Cell Cardiol*. 1998 Apr;30(4):723-31.

[29] Subramanian A, Tamayo P, Mootha VK, Mukherjee S, Ebert BL, Gillette MA, Paulovich A, Pomeroy SL, Golub TR, Lander ES, Mesirov JP. Gene set enrichment analysis: a knowledge-based approach for interpreting genome-wide expression profiles. *Proc Natl Acad Sci U S A*. 2005 Oct 25;102(43):15545-50.

[30] Conway JR, Lex A, Gehlenborg N. UpSetR: an R package for the visualization of intersecting sets and their properties. *Bioinformatics*. 2017 Sep 15;33(18):2938-2940.

[31] Korotkevich G, Sukhov V, Sergushichev A. Fast gene set enrichment analysis. *bioRxiv*. 2019. http://biorxiv.org/content/early/2016/06/20/060012.

[32] Wickham H. ggplot2: elegant graphics for data analysis. 2nd ed. New York (NY). Springer International Publishing; 2016. 41-135 p.

[33] Gu Z, Eils R, Schlesner M. Complex heatmaps reveal patterns and correlations in multidimensional genomic data. *Bioinformatics*. 2016 Sep 15;32(18):2847-9.

[34] Walter W, Sánchez-Cabo F, Ricote M. GOplot: an R package for visually combining expression data with functional analysis. *Bioinformatics*. 2015 Sep 1;31(17):2912-4.

[35] Huang DW, Sherman BT, Lempicki RA. Systematic and integrative analysis of large gene lists using DAVID Bioinformatics Resources. *Nature Protoc*. 2009;4(1):44-57.

[36] Huang DW, Sherman BT, Lempicki RA. Bioinformatics enrichment tools: paths toward the comprehensive functional analysis of large gene lists. *Nucleic Acids Res*. 2009;37(1):1-13.

[37] Flynt E, Bisht K, Sridharan V, Ortiz M, Towfic F, Thakurta A. Prognosis, biology, and targeting of *TP53* dysregulation in multiple myeloma. *Cells*. 2020 Jan 24;9(2):287.

[38] He J, Wu M, Xiong L, Gong Y, Yu R, Peng W, Li L, Li L, Tian S, Wang Y, Tao Q, Xiang T. BTB/POZ zinc finger protein ZBTB16 inhibits breast cancer proliferation and metastasis through upregulating ZBTB28 and antagonizing BCL6/ZBTB27. *Clin Epigenetics*. 2020 Jun 9;12(1):82.

[39] Chen W, Chen M, Zhao Z, Weng Q, Song J, Fang S, Wu X, Wang H, Zhang D, Yang W, Wang Z, Xu M, Ji J. ZFP36 Binds with PRC1 to inhibit tumor growth and increase 5-Fu chemosensitivity of hepatocellular carcinoma. *Front Mol Biosci*. 2020 Jul 14;7:126.

[40] Guo XE, Ngo B, Modrek AS, Lee WH. Targeting tumor suppressor networks for cancer therapeutics. *Curr Drug Targets*. 2014 Jan;15(1):2-16.

[41] Gandolfi S, Laubach JP, Hideshima T, Chauhan D, Anderson KC, Richardson PG. The proteasome and proteasome inhibitors in multiple myeloma. *Cancer Metastasis Rev*. 2017 Dec;36(4):561-584.

[42] Besse A, Stolze SC, Rasche L, Weinhold N, Morgan GJ, Kraus M, Bader J, Overkleeft HS, Besse L, Driessen C. Carfilzomib resistance due to ABCB1/MDR1 overexpression is overcome by nelfinavir and lopinavir in multiple myeloma. *Leukemia*. 2018 Feb;32(2):391.

[43] Nguyen TK, Grant S. Dinaciclib (SCH727965) inhibits the unfolded protein response through a CDK1- and 5-dependent mechanism. *Mol Cancer Ther*. 2014 Mar;13(3):662-74.

[44] Zhao Y, Zhang K, Li G, Zhang X, Shi D. Expression of GITR Enhances Multiple Myeloma Cell Sensitivity to Bortezomib. PLoS One. 2015 May 14;10(5):e0127334.

[45] Boylan KL, Gosse MA, Staggs SE, Janz S, Grindle S, Kansas GS, Van Ness BG. A transgenic mouse model of plasma cell malignancy shows phenotypic, cytogenetic, and gene expression heterogeneity similar to human multiple myeloma. *Cancer Res*. 2007 May 1;67(9):4069-78.

[46] Hu CH, Sui BD, Du FY, Shuai Y, Zheng CX, Zhao P, Yu XR, Jin Y. miR-21 deficiency inhibits osteoclast function and prevents bone loss in mice. *Sci Rep*. 2017 Feb 27;7:43191.

[47] Zhang G, Miao F, Liu K, Wu J, Xu J. Downregulation of LEF1 Impairs Myeloma Cell Growth Through Modulating CYLD/NF-κB Signaling. *Technol Cancer Res Treat*. 2021 Jan-Dec;20:15330338211034270.

[48] Ria R, Vacca A. Bone marrow stromal cells-induced drug resistance in multiple myeloma. *Int J Mol Sci*. 2020 Jan 17;21(2):613.

[49] Robinson MD, McCarthy DJ, Smyth GK. edgeR: a Bioconductor package for differential expression analysis of digital gene expression data. *Bioinformatics*. 2010 Jan 1;26(1):139.

[50] Ritchie ME, Phipson B, Wu D, Hu Y, Law CW, Shi W, Smyth GK. limma powers differential expression analyses for RNA-sequencing and microarray studies. *Nucleic Acids Res*. 2015 Apr 20;43(7):e47.

[51] Benjamini Y, Hochberg, Y. Controlling the false discovery rate: a practical and powerful approach to multiple testing. *J R Stat Soc Series B*. 1995 57(1), 289–300.

3.8 Supplemental Figures and Tables:

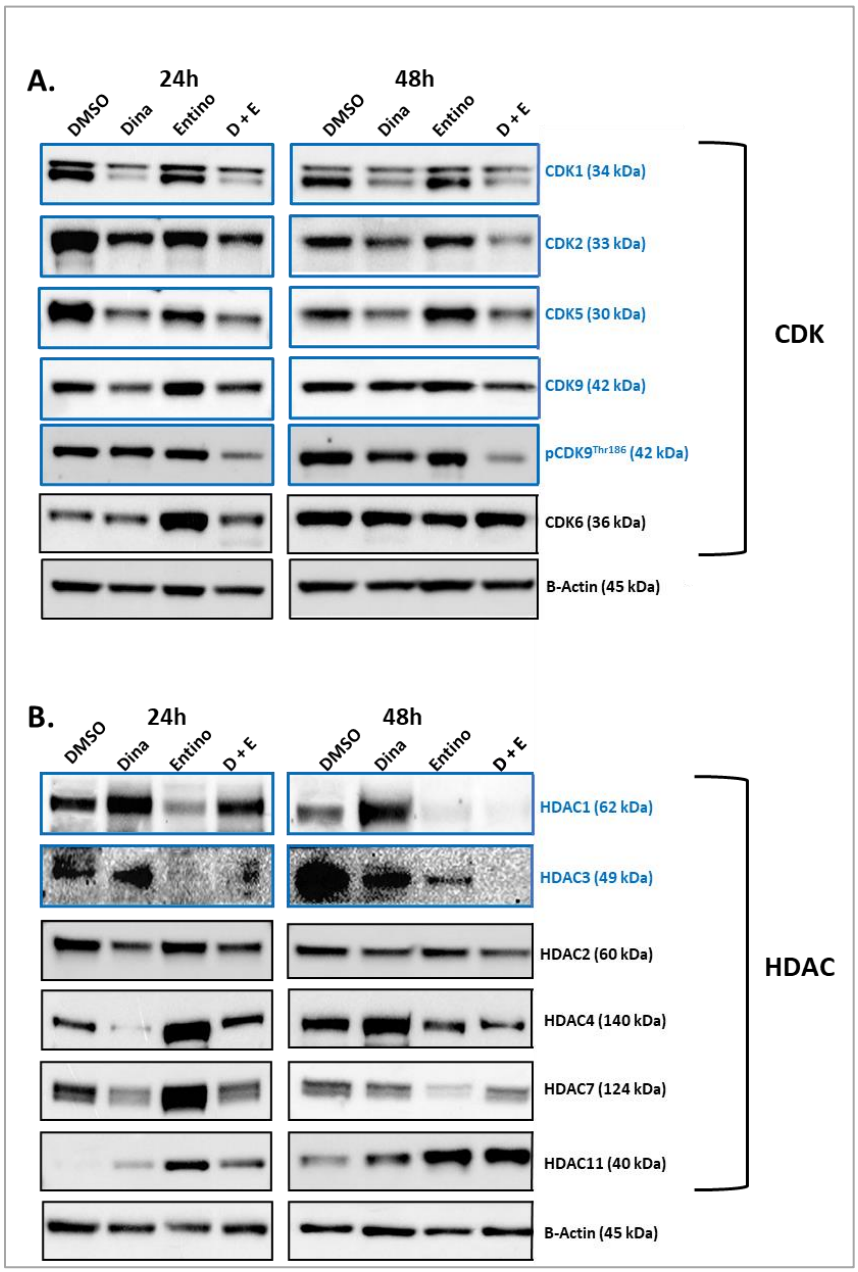

Figure S. 3.1. Evaluation of on- and off-target CDK and HDAC effects by dinaciclib and/or entinostat treatment. L363 MM Cells were treated for 24 or 48 hours with dinaciclib (Dina – 10 nM) or entinostat (Entino – 500 nM), singly or in combination (D + E). A) Representative western blot (WB) images of target CDKs 1, 2, 5 and 9 (including phospho-CDK9^{Thr186} (blue labels and boxes) versus non-target CDK6 (black box and labels). B) Representative WB images of entinostat targeted HDACs 1 and 3 (blue labels and boxes) versus non-target HDACs 2, 4, 7 and 11 (black box and labels).

Figure S. 3.2. Evaluation of targeted combined CDK/HDAC inhibition in LP-1 parental and oprozomib resistant MM cell lines. A) Representative bar charts of western blot (WB) ratiometric analysis, normalized to β-Actin and DMSO-treated control cells, of bands representing MYC, p16, HDAC1, HDAC3, CDK1, CDK2, CDK5, and CDK9 in LP-1-Parental and proteasome inhibitor resistant (LP-1-OpzR) cells treated for 24, 48, or 72 hours with IC50 concentrations of dinaciclib (LP-1-P and LP-1-OpzR = 5 nM) and entinostat (LP-1-P = 62.5 nM, LP-1-OpzR = 250 nM) as determined by dose matrix synergy analysis (Fig. 3.1G-H). B-C) Dose-response curves for dinaciclib and entinostat in LP-1-P (B) and LP-1-OpzR (C) cells. Cell viability was assessed with MTS assay 48h after treatment with escalated dose concentrations of either drug individually or in combination at a 1:1 molar ratio. Each data point represents mean of 4 wells and error bars indicate replicate standard deviation. IC50 (in nM) for individual drugs and combination in each table. D-E) Matrix dose response testing for activity and synergy with representative heat maps and topographical graphs of excess of highest single agent (EOSHA) showing the amount of additional activity achieved combined dinaciclib/entinostat treatment achieved over the highest single agent dose in each respective row. LP-1P (D) or LP-1-OpzR (E) MM cells were treated with the top 3 combinations for 48 hours at 8 different doses (64 total dose combination). HSA Score = highest single agent synergy score (>10 indicates synergy).

Fig S. 3.2 Continued

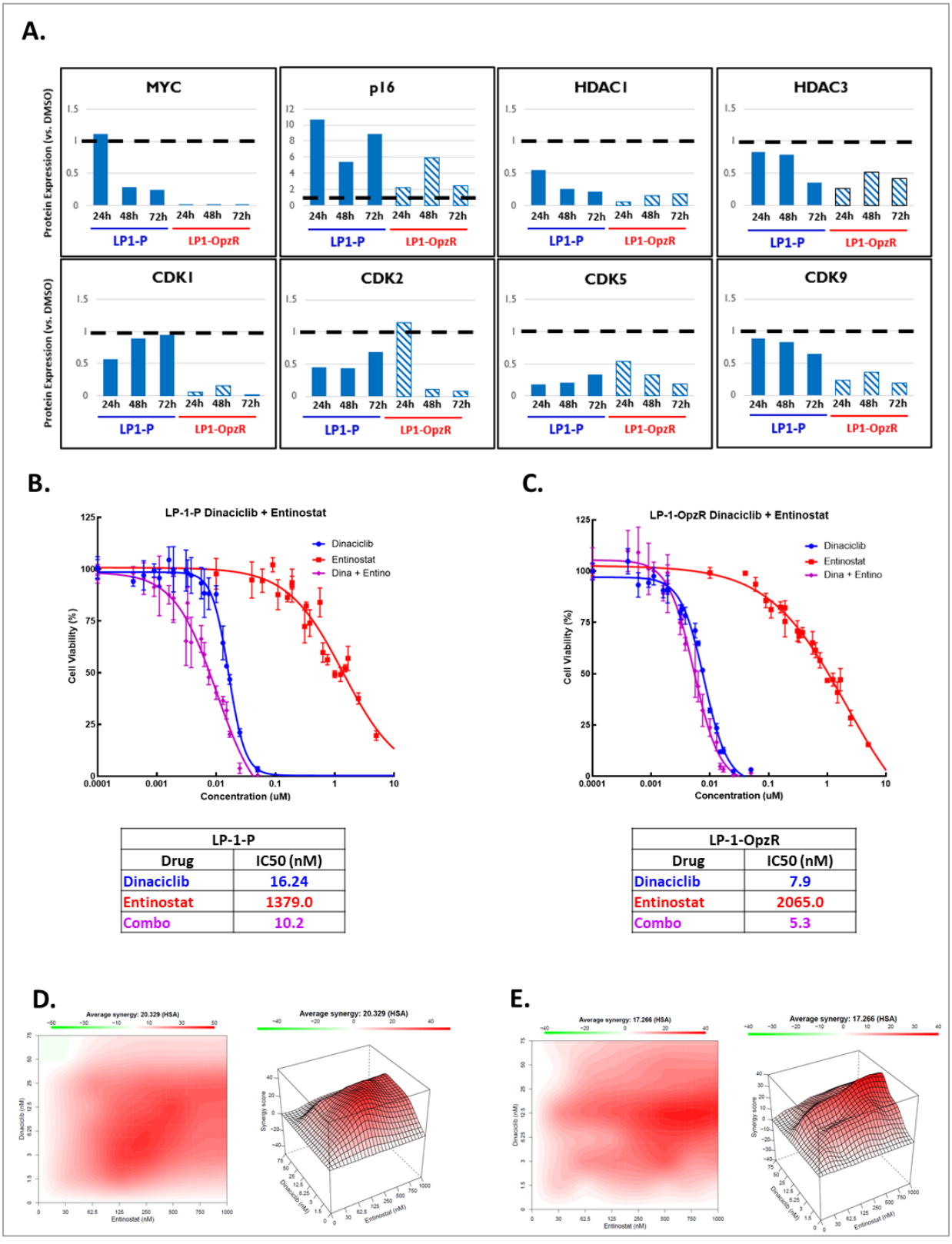

LP-1-P	
Drug	IC50 (nM)
Dinaciclib	16.24
Entinostat	1379.0
Combo	10.2

LP-1-OpzR	
Drug	IC50 (nM)
Dinaciclib	7.9
Entinostat	2065.0
Combo	5.3

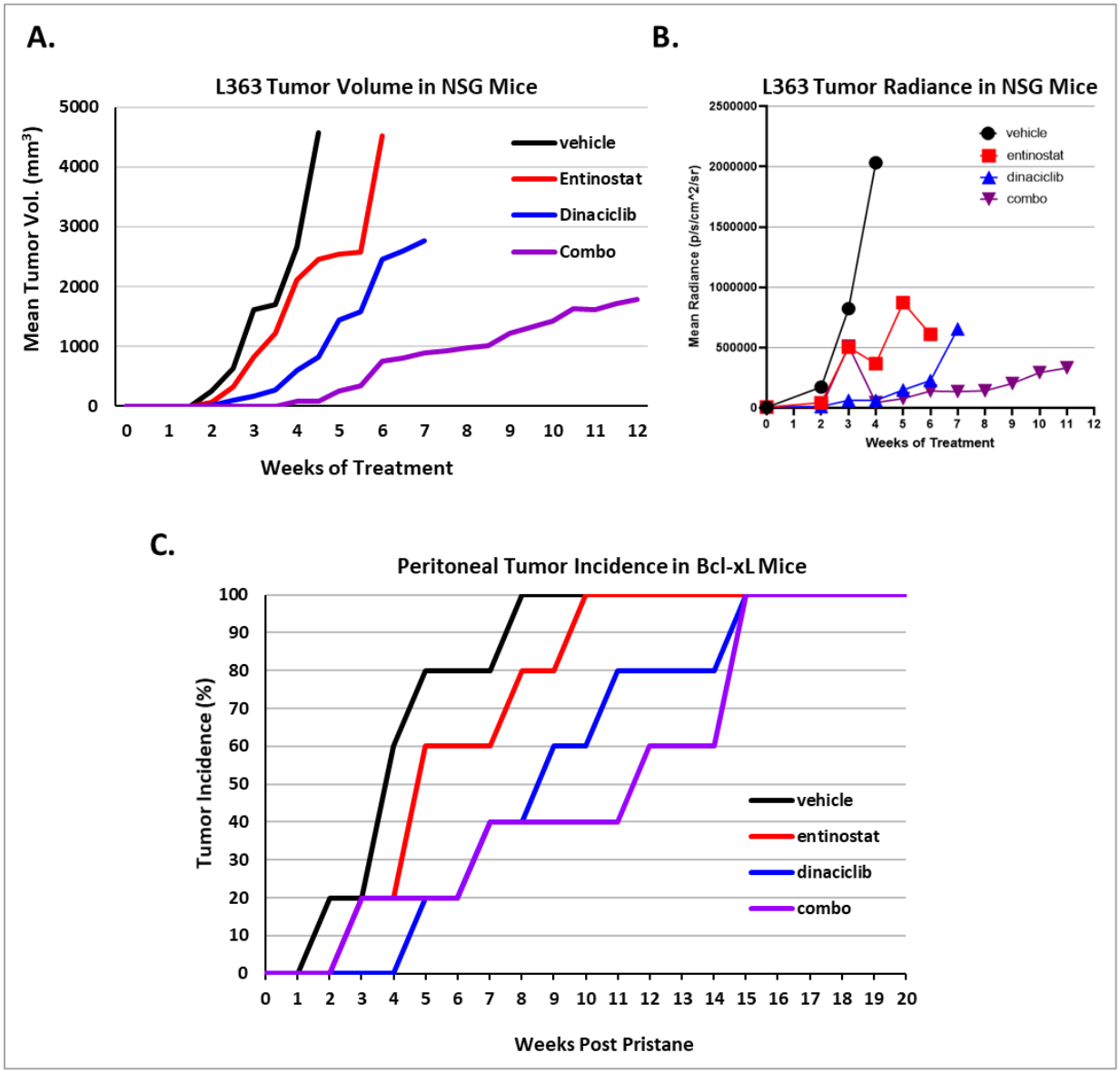

Figure S. 3.3. Evaluating efficacy of combined CDK/HDAC inhibition in mouse models of MM. A-B) Mean tumor volume (A) and mean tumor radiance (B) over time in NSG mice bearing GFP/Luc+ L363 xenografts (n = 10). A) tumor volume expressed in mm^3. Black line = vehicle control, red line = entinostat (15 mg/kg, PO, 5x/week), blue line = dinaciclib (15 mg/kg, IP, 3x/week), purple line = combo. B) Mean tumor radiance over time expressed as $p/s/cm^2/sr$. C) Peritoneal tumor incidence in pristane-induced Bcl-xL mice over time.

Figure S. 3.4 GSEA reveals enriched pathways associated with cooperative CDKi/HDACi response. A-J) Enrichment plots from GSEA [30] of the Gene Ontology (GO) Biological Process (BP) ontology database. A-E) Synergistically downregulated GO BP pathways: DNA Replication Checkpoint (A), DNA Replication Initiation (B), Protein Folding in Endoplasmic Reticulum (C), Protein Localization to Kinetochore (D), Telomere Maintenance Via Semi Conservative Replication (E). F-J) Synergistically upregulated pathways: Positive Regulation of Cell Adhesion (F), Immune Response Regulating Signaling Pathway (G), Activation of Immune Response (H), Regulation of Immune Response (I), Regulation of Small GTPase-Mediated Signal Transduction (J). Within each figure, separate are separate subfigures a-c. a) Running enrichment score calculated along the ranked gene list represented by the red-blue horizontal bar (the ANOVA statistic ranked from the highest positive to the highest negative value); the vertical black bars in the plot indicate the position of the genes from the respective GO terms; the vertical red/blue line indicates the positive and negative enrichment score (ES), respectively. b) Ranking statistic and top ten GSEA leading edge genes (LE). c) Heatmap of the GSEA leading edge genes generated with hierarchical clustering of genes using the Ward distance and complete linkage; in each gene the mean expression of the control group was subtracted in the treatment samples prior to clustering. The GSEA plot was generated using custom R scripts and fgsea [32], ggplot2 [33], and ComplexHeatmap [34] packages.

Figure S. 3.4. Continued

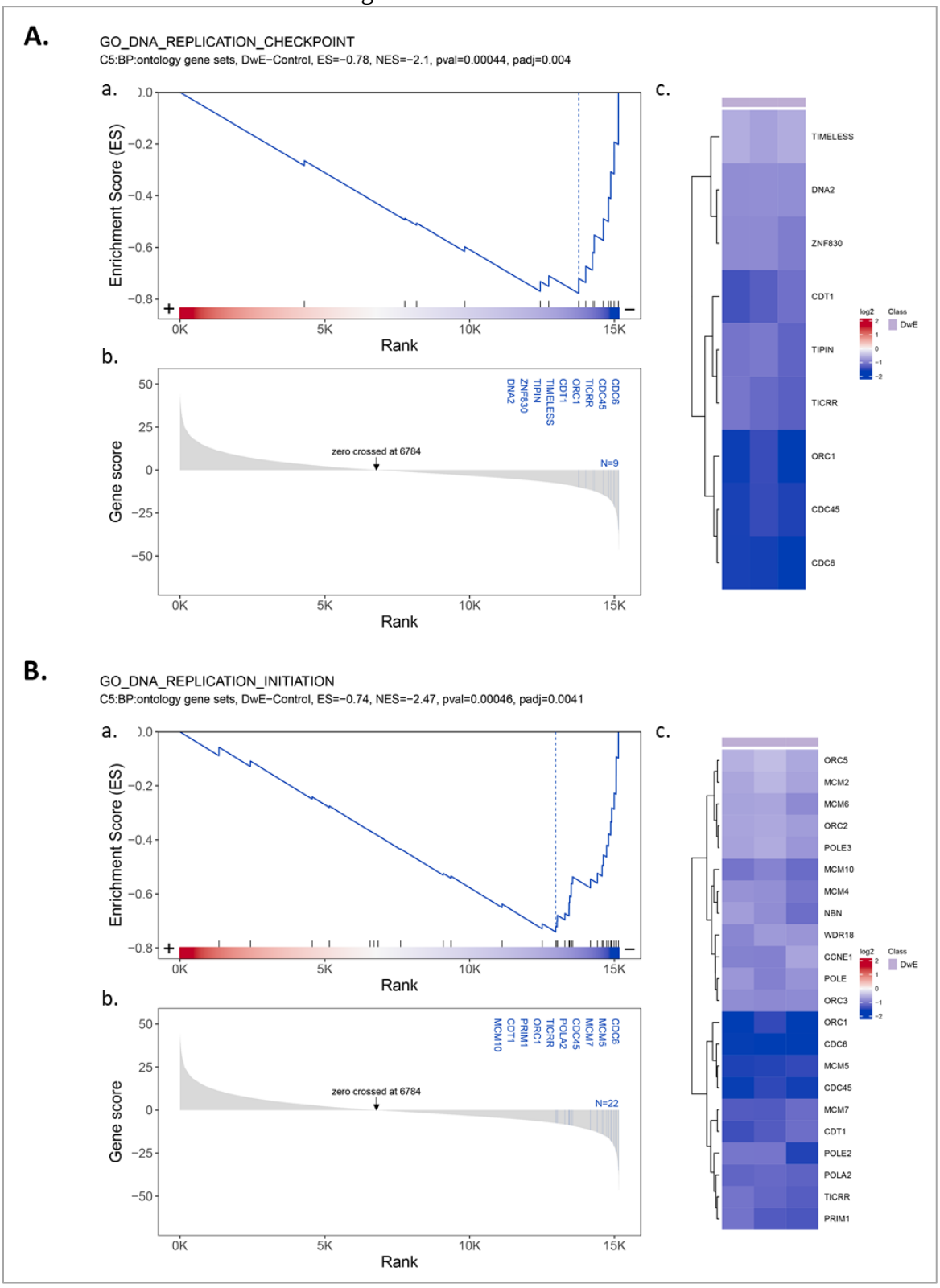

Figure S. 3.4. Continued

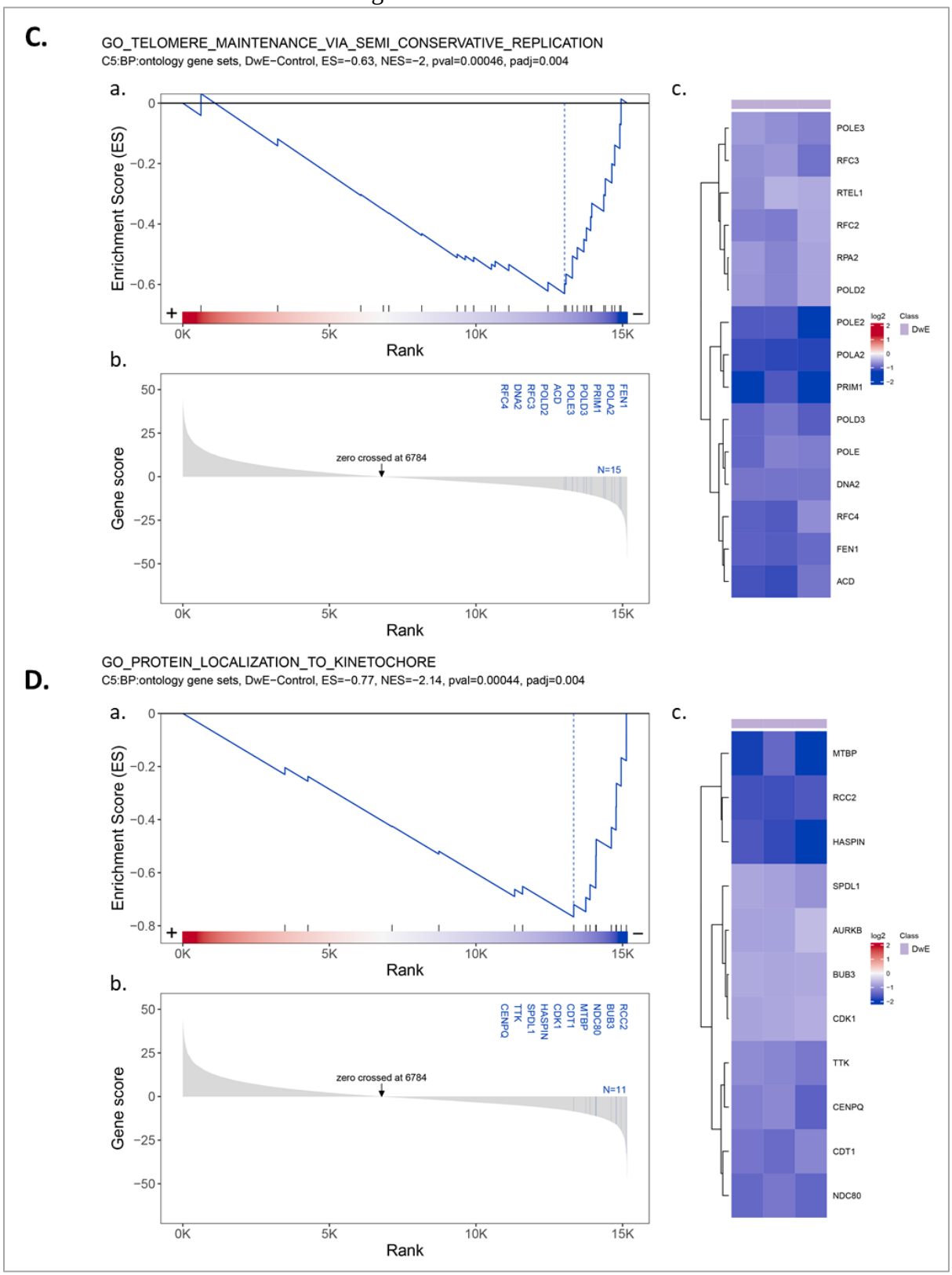

Figure S. 3.4. Continued

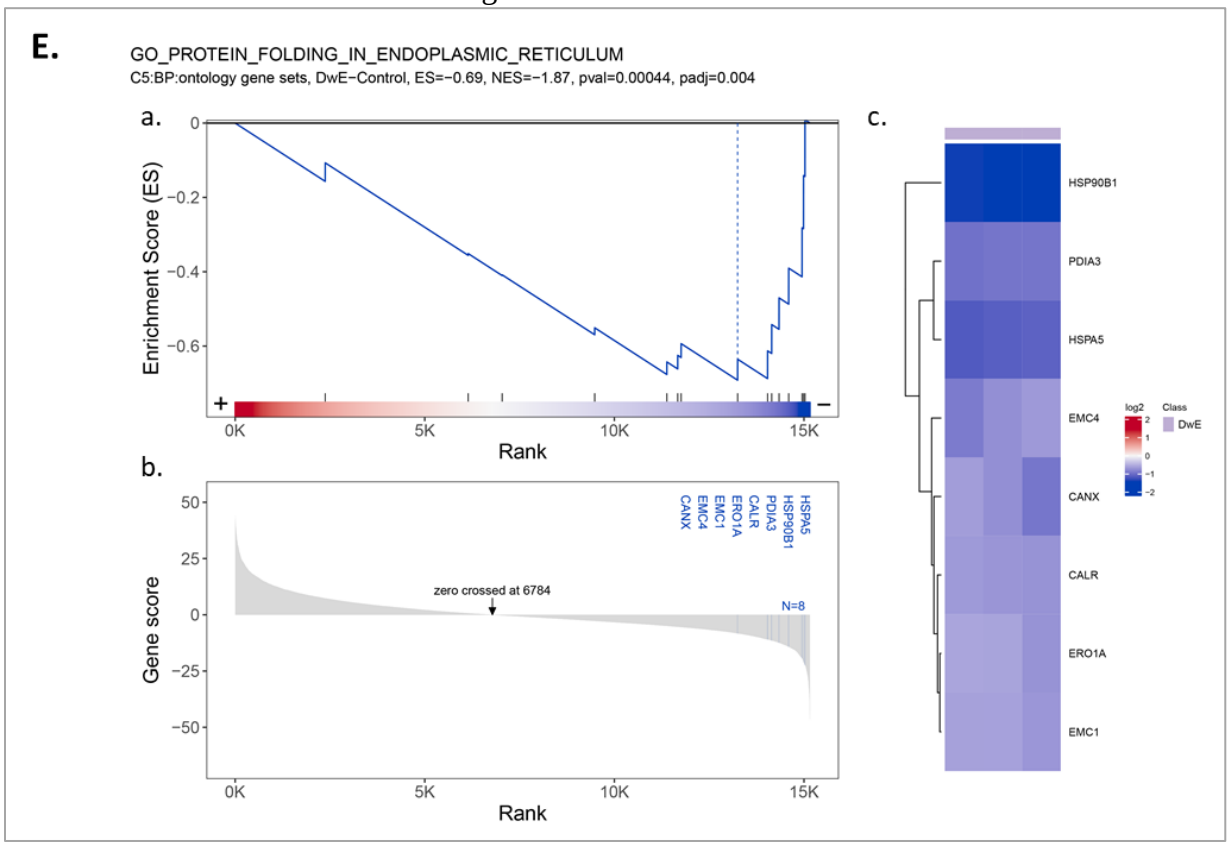

Figure S. 3.4. Continued

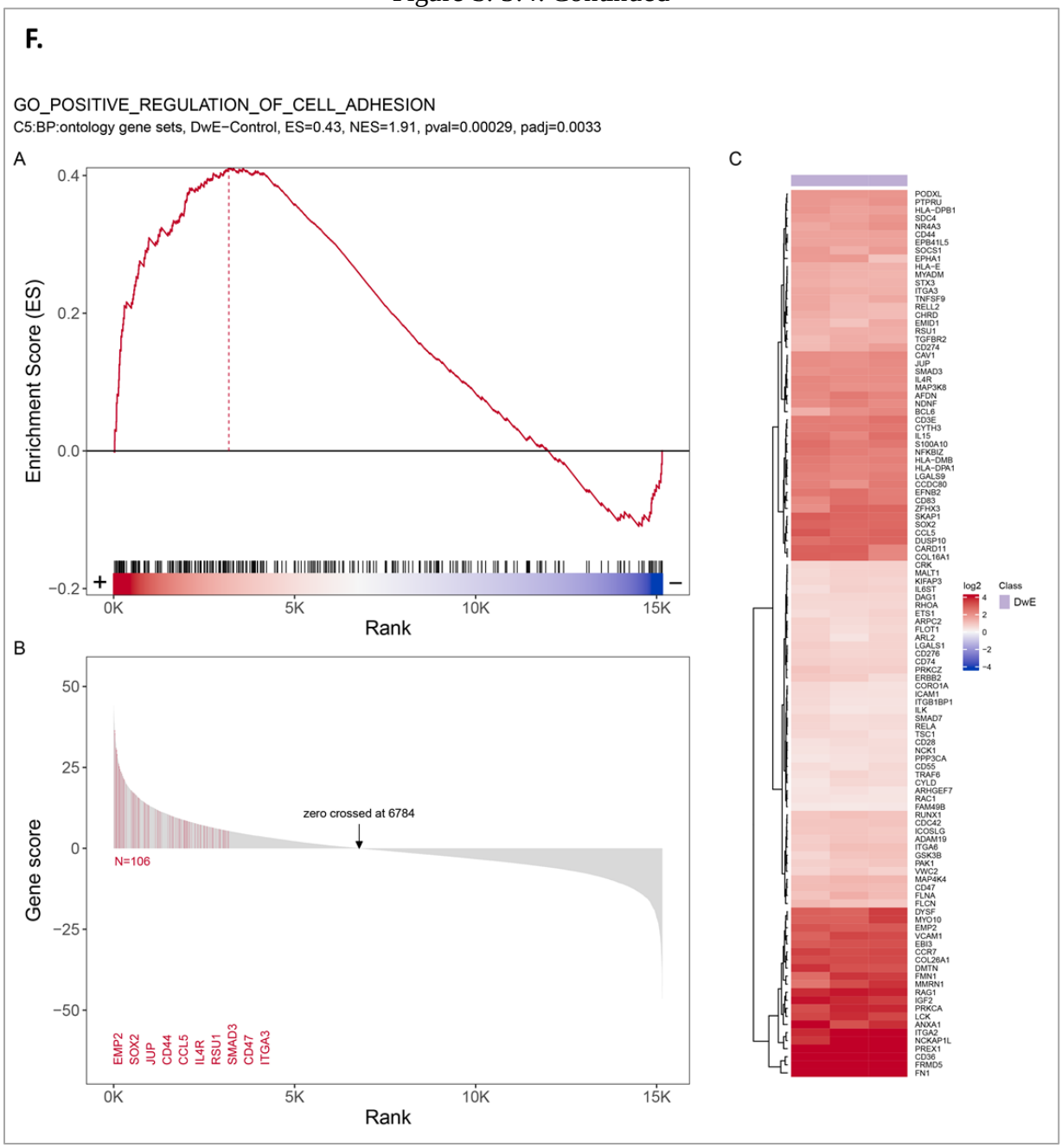

Figure S. 3.4. Continued

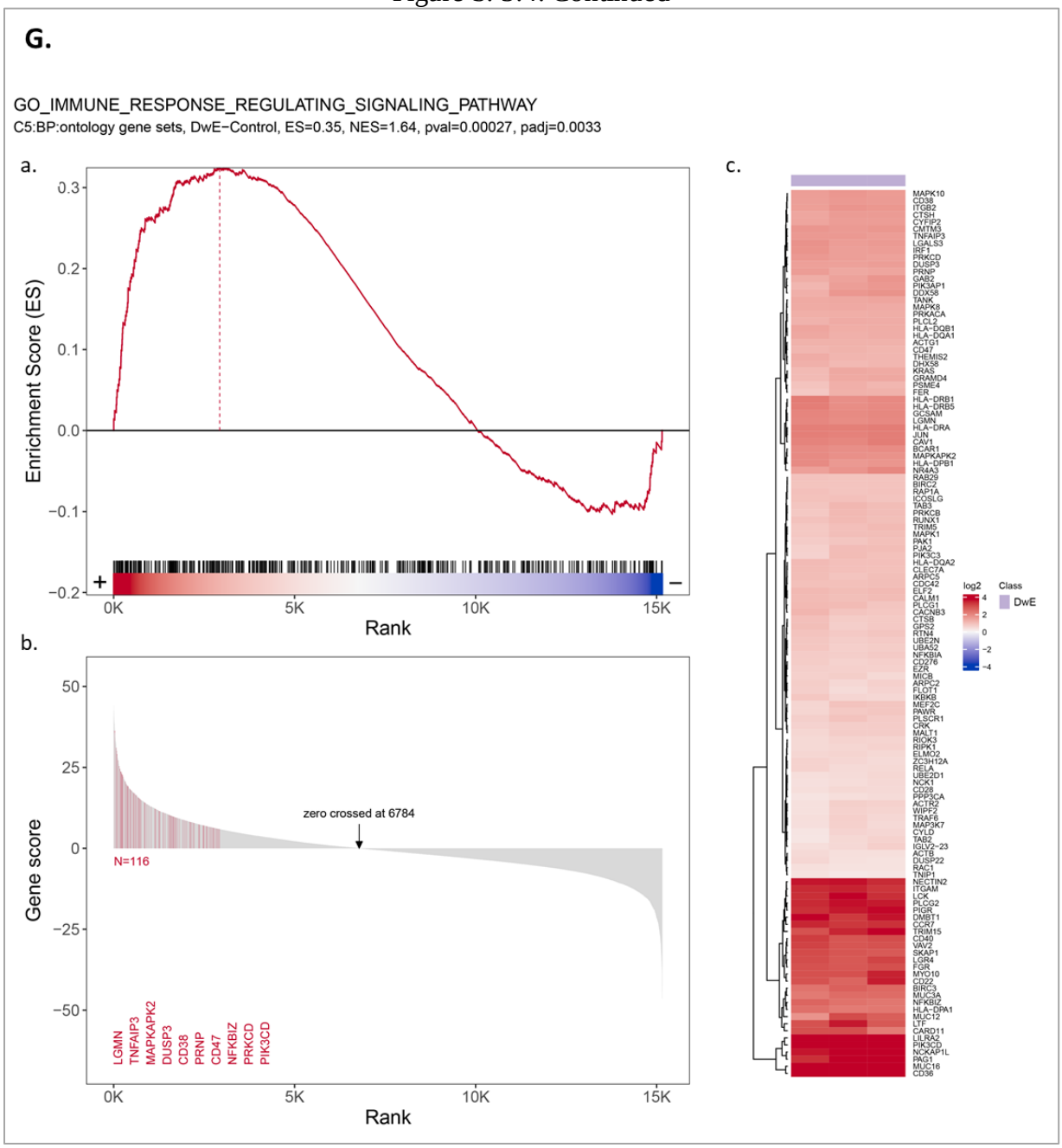

Figure S. 3.4. Continued

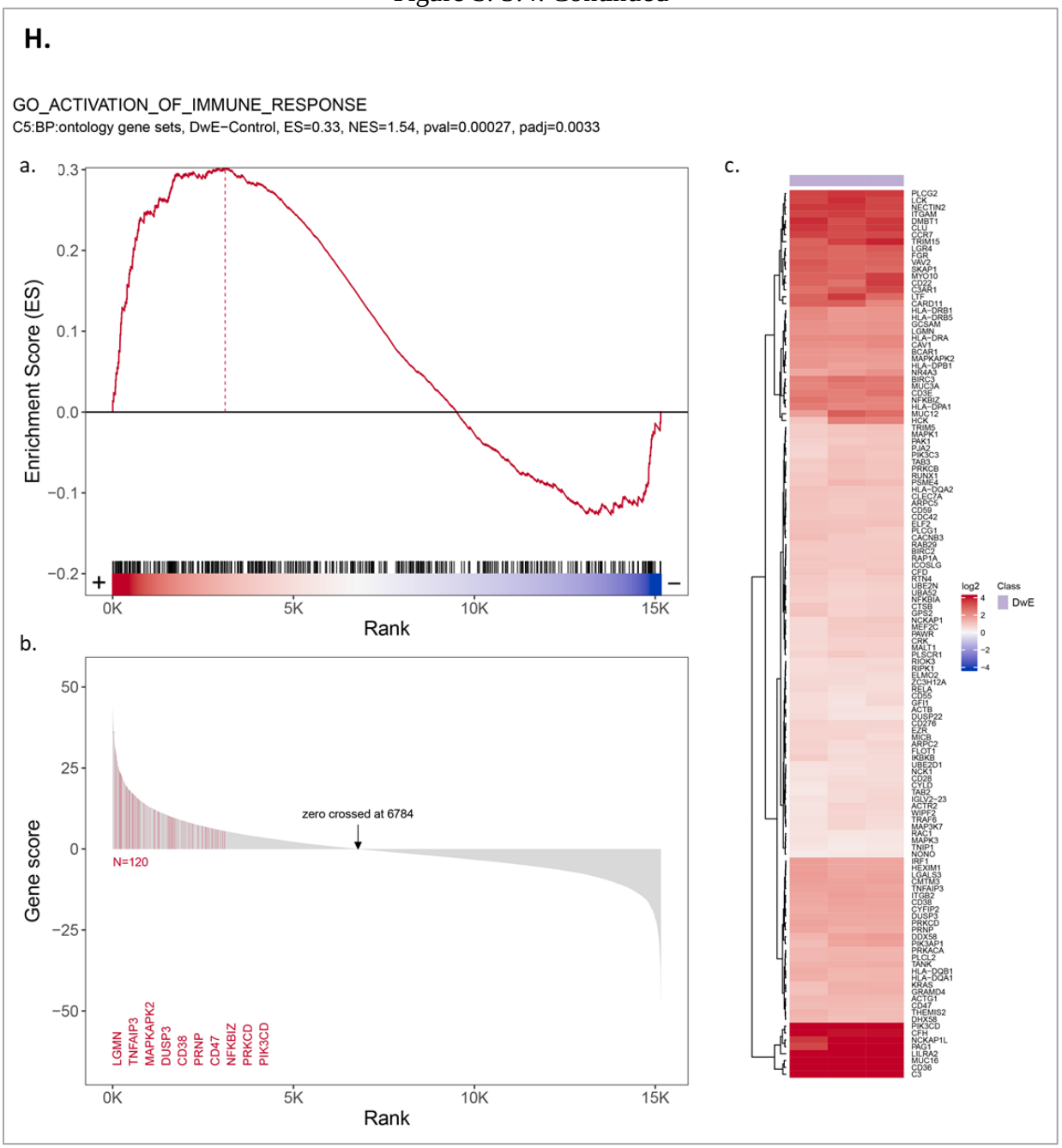

Figure S. 3.4. Continued

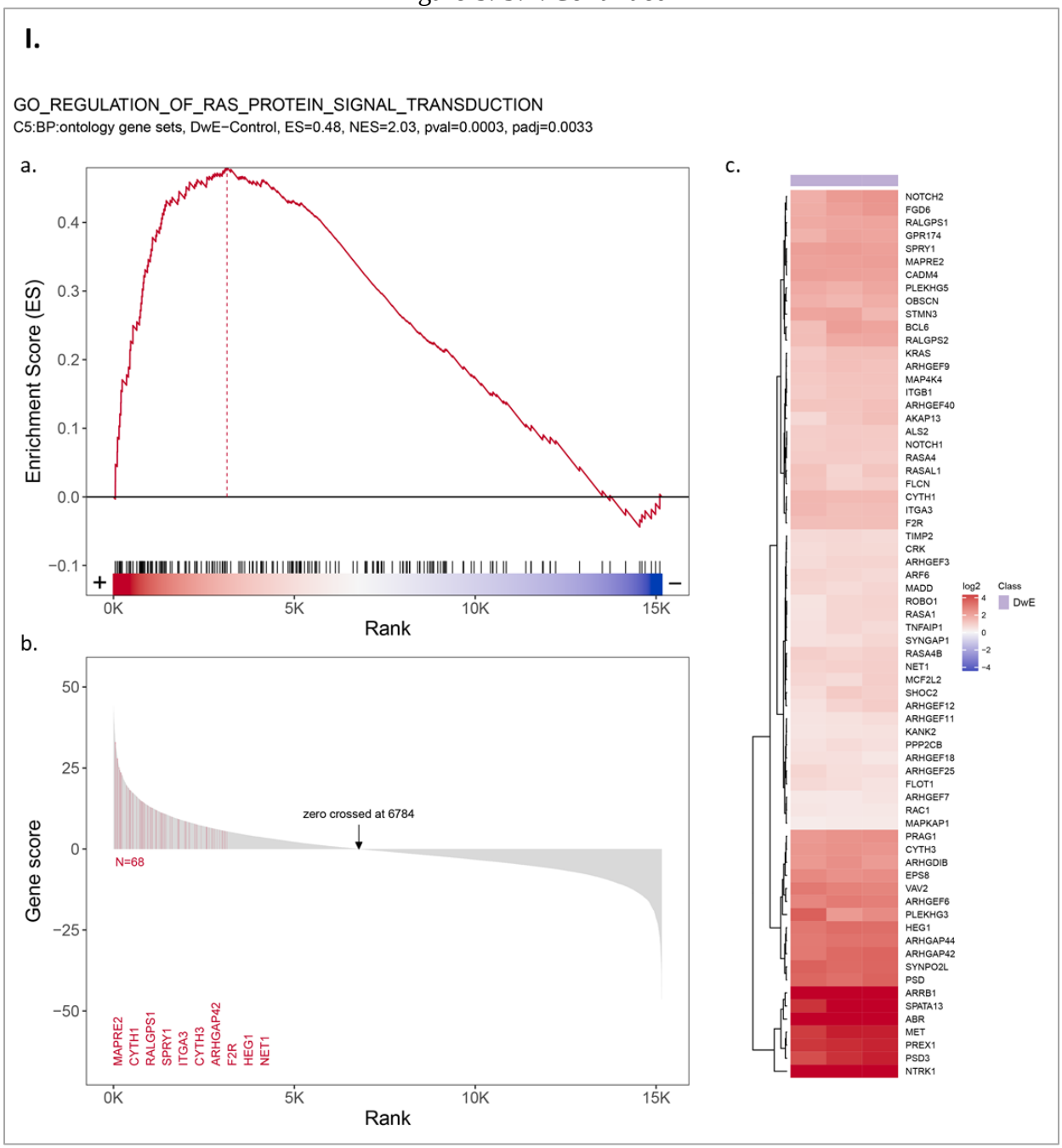

Figure S. 3.4. Continued

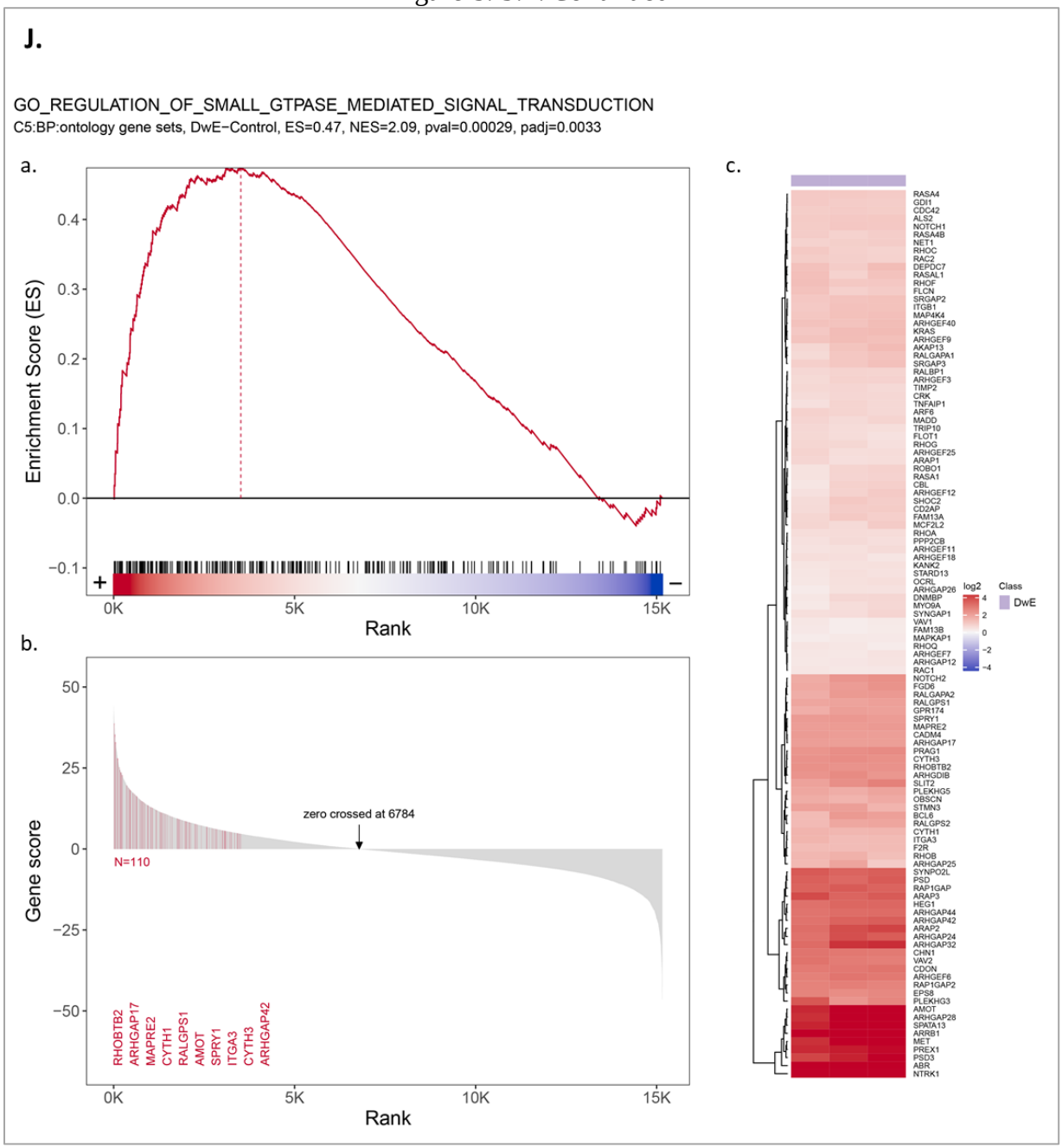

Table S. 3.1. Tolerability of combined CDK/HDAC inhibition in naïve NSG mice

Group	# Animals	Dinaciclib Dose	Dinaciclib Route	Entinostat Dose	Entinostat Route	Mean % Weight Gain/Loss	St. Dev.	Decreased BM Cellularity	Clinical Observations
1	3	control - 20% BCD, IP, 3x/week				↑2.17	1.21	--	--
2	3	10 mg/kg	IP	10 mg/kg	PO	↓4.17	4.4	--	--
3	3	10 mg/kg	IP	10 mg/kg	IP	↓2.02	6.6	--	--
4	3	20 mg/kg	IP	20 mg/kg	PO	↓6.24	1.15	minimal	--
5	3	20 mg/kg	IP	20 mg/kg	IP	↓9.15	5.86	slight	--
Dinaciclib- 2x/week (Tu, Th)									
Entinostat - 2 x/week (M, W)									

Table S.3.1 illustrates the tolerability of combined dinaciclib and entinostat therapy in female NSG mice when administered at different doses and via different routes (IP = intraperitoneal, PO = oral gavage). The duration of the study was 5 days. ↑ = Increased; ↓ = Decreased; -- = finding not observed.

Table S. 3.2. Tolerability of combined CDK/HDAC inhibition in naïve Bcl-xL mice

Group	# Animals	Dinaciclib Dose	Dinaciclib Route	Mean % Weight Gain/Loss	St. Dev.	Decreased BM Cellularity	Clinical Observations
1	3	control - 20% BCD, IP, 3x/week		↑2.97	3.25	--	--
2	3	2.5 mg/kg	IP	↑4.13	4.37	--	--
3	3	5.0 mg/kg	IP	↓3.47	3.54	--	--
4	3	7.5 mg/kg	IP	↓0.65	1.41	minimal	--
5	3	10.0 mg/kg	IP	↑2.65	1	minimal	liquid feces in 2/3
6	3	15.0 mg/kg	IP	↓15.03	2.52	minimal	liquid feces in 3/3, hunched on Day 5 in 3/3
Dinaciclib- 2x/week (Tu, Th)							
Entinostat - 2 x/week (M, W)							

Table S.3.2 illustrates the tolerability of combined dinaciclib and entinostat therapy in NSG mice (mixture of males and females) when administered at different doses of dinaciclib IP (2.5 mg/kg – 15 mg/kg) and a consistent dose of 15 mg/kg entinostat PO. The duration of the study was 5 days. ↑ = Increased; ↓ = Decreased; -- = finding not observed.

APPENDIX A. ENRICHED GO DATASETS OF CONCORDANT GENES AMONG TOP COMBINATIONS

GO id	GO term	GO category	P-value	Hit in pathway	Not in pathway	Total pathway	Hit% in pathway	Genes in pathway	Down genes	Up genes	Z-score(ratio)
GO:0007050	cell cycle arrest	BP	0.01191952	14	54	68	20.6	PML, CNOT10, SMAD3, UBB, ID2, TGFB1, WNT10B, CDK4, MAP2K6, CDKN1C, CDKN1A, CHEK2, E2F1, RB1	(-5) CNOT10 WNT10B CDK4 E2F1 RB1	(+9) PML SMAD3 UBB ID2 TGFB1 MAP2K6 CDKN1C CDKN1A CHEK2	1.07
GO:0044843	cell cycle G1/S phase transition	BP	0.00126334	16	51	67	23.9	PML, CNOT10, MNAT1, UBB, ID2, PKMYT1, CDK4, BCL2, CDC25A, TCF3, CCND2, CDKN1A, CHEK2, E2F1, EIF4EBP1, RB1	(-11) CNOT10 MNAT1 PKMYT1 CDK4 BCL2 CDC25A TCF3 CCND2 E2F1 EIF4EBP1 RB1	(+5) PML UBB ID2 CDKN1A CHEK2	-1.50
GO:0044770	cell cycle phase transition	BP	0.0021184	19	73	92	20.7	PML, CNOT10, MNAT1, UBB, ID2, TGFB1, WNT10B, PKMYT1, CDK4, BCL2, CDC25A, TCF3, CCND2, CDKN1A, CHEK1, CHEK2, E2F1, EIF4EBP1, RB1	(-13) CNOT10 MNAT1 WNT10B PKMYT1 CDK4 BCL2 CDC25A TCF3 CCND2 CHEK1 E2F1 EIF4EBP1 RB1	(+6) PML UBB ID2 TGFB1 CDKN1A CHEK2	-1.61
GO:0022402	cell cycle process	BP	0.03005028	26	152	178	14.6	CNOT10, MNAT1, FANCA, TGFB1, WNT10B, PKMYT1, CDK4, BCL2, TCF3, CDC25A, CCND2, CHEK1, CHEK2, EIF4EBP1, PML, SMAD3, UBB, ID2, PBRM1, FLNA, MAP2K6, PTTG2, CDKN1C, CDKN1A, E2F1, RB1	(-14) CNOT10 MNAT1 WNT10B PKMYT1 CDK4 BCL2 TCF3 CDC25A CCND2 CHEK1 EIF4EBP1 PBRM1 E2F1 RB1	(+12) FANCA TGFB1 CHEK2 PML SMAD3 UBB ID2 FLNA MAP2K6 PTTG2 CDKN1C CDKN1A	-0.39
GO:0000082	G1/S transition of mitotic cell cycle	BP	0.00240211	15	49	64	23.4	PML, CNOT10, MNAT1, UBB, ID2, PKMYT1, CDK4, BCL2, CDC25A, CCND2, CDKN1A, CHEK2, E2F1, EIF4EBP1, RB1	(-10) CNOT10 MNAT1 PKMYT1 CDK4 BCL2 CDC25A CCND2 E2F1 EIF4EBP1 RB1	(+5) PML UBB ID2 CDKN1A CHEK2	-1.29
GO:0072332	intrinsic apoptotic signaling pathway by p53 class mediator	BP	0.04235759	5	9	14	35.7	PML, CDKN1A, UBB, CHEK2, E2F1	(-1) E2F1	(+4) PML CDKN1A UBB CHEK2	1.34
GO:0000278	mitotic cell cycle	BP	0.022488	22	117	139	15.8	PML, CNOT10, SMAD3, MNAT1, UBB, ID2, PBRM1, TGFB1, WNT10B, PKMYT1, CDK4, FLNA, BCL2, CDC25A, TCF3, CCND2, CDKN1A, CHEK1, CHEK2, E2F1, EIF4EBP1, RB1	(-14) CNOT10 MNAT1 PBRM1 WNT10B PKMYT1 CDK4 BCL2 CDC25A TCF3 CCND2 CHEK1 E2F1 EIF4EBP1 RB1	(+8) PML SMAD3 UBB ID2 TGFB1 FLNA CDKN1A CHEK2	-1.28
GO:0007093	mitotic cell cycle checkpoint	BP	0.0151602	10	31	41	24.4	PML, CNOT10, CDKN1A, MNAT1, UBB, CHEK1, CHEK2, TGFB1, E2F1, RB1	(-5) CNOT10 MNAT1 CHEK1 E2F1 RB1	(+5) PML CDKN1A UBB CHEK2 TGFB1	0.00

GO:0044772	mitotic cell cycle phase transition	BP	0.00121277	19	69	88	21.6	PML, CNOT10, MNAT1, UBB, ID2, TGFB1, WNT10B, PKMYT1, CDK4, BCL2, CDC25A, TCF3, CCND2, CDKN1A, CHEK1, CHEK2, E2F1, EIF4EBP1, RB1	(-13) CNOT10 MNAT1 WNT10B PKMYT1 CDK4 BCL2 CDC25A TCF3 CCND2 CHEK1 E2F1 EIF4EBP1 RB1	(+6) PML UBB ID2 TGFB1 CDKN1A CHEK2	-1.61
GO:1903047	mitotic cell cycle process	BP	0.01062014	21	101	122	17.2	PML, CNOT10, MNAT1, UBB, ID2, PBRM1, TGFB1, WNT10B, PKMYT1, CDK4, FLNA, BCL2, CDC25A, TCF3, CCND2, CDKN1A, CHEK1, CHEK2, E2F1, EIF4EBP1, RB1	(-14) CNOT10 MNAT1 PBRM1 WNT10B PKMYT1 CDK4 BCL2 CDC25A TCF3 CCND2 CHEK1 E2F1 EIF4EBP1 RB1	(+7) PML UBB ID2 TGFB1 FLNA CDKN1A CHEK2	-1.53
GO:0045786	negative regulation of cell cycle	BP	0.0407752	17	87	104	16.3	PML, CNOT10, SMAD3, MNAT1, UBB, ID2, TGFB1, WNT10B, CDK4, MAP2K6, CDKN1C, BCL2, CDKN1A, CHEK1, CHEK2, E2F1, RB1	(-8) CNOT10 MNAT1 WNT10B CDK4 BCL2 CHEK1 E2F1 RB1	(+9) PML SMAD3 UBB ID2 TGFB1 MAP2K6 CDKN1C CDKN1A CHEK2	0.24
GO:1902807	negative regulation of cell cycle G1/S phase transition	BP	0.03234748	8	24	32	25.0	PML, BCL2, CNOT10, CDKN1A, UBB, CHEK2, E2F1, RB1	(-4) BCL2 CNOT10 E2F1 RB1	(+4) PML CDKN1A UBB CHEK2	0.00
GO:1901988	negative regulation of cell cycle phase transition	BP	0.03722979	9	31	40	22.5	PML, BCL2, CNOT10, CDKN1A, MNAT1, UBB, CHEK2, E2F1, RB1	(-5) BCL2 CNOT10 MNAT1 E2F1 RB1	(+4) PML CDKN1A UBB CHEK2	-0.33
GO:0010948	negative regulation of cell cycle process	BP	0.0424324	11	45	56	19.6	CDK4, PML, BCL2, CNOT10, CDKN1A, MNAT1, UBB, CHEK1, CHEK2, E2F1, RB1	(-7) CDK4 BCL2 CNOT10 MNAT1 CHEK1 E2F1 RB1	(+4) PML CDKN1A UBB CHEK2	-0.90
GO:2000134	negative regulation of G1/S transition of mitotic cell cycle	BP	0.02306211	8	22	30	26.7	PML, BCL2, CNOT10, CDKN1A, UBB, CHEK2, E2F1, RB1	(-4) BCL2 CNOT10 E2F1 RB1	(+4) PML CDKN1A UBB CHEK2	0.00
GO:0045930	negative regulation of mitotic cell cycle	BP	0.01490402	12	43	55	21.8	PML, BCL2, CNOT10, CDKN1A, SMAD3, MNAT1, UBB, CHEK1, CHEK2, TGFB1, E2F1, RB1	(-6) BCL2 CNOT10 MNAT1 CHEK1 E2F1 RB1	(+6) PML CDKN1A SMAD3 UBB CHEK2 TGFB1	0.00
GO:1901991	negative regulation of mitotic cell cycle phase transition	BP	0.02794285	9	29	38	23.7	PML, BCL2, CNOT10, CDKN1A, MNAT1, UBB, CHEK2, E2F1, RB1	(-5) BCL2 CNOT10 MNAT1 E2F1 RB1	(+4) PML CDKN1A UBB CHEK2	-0.33
GO:0045787	positive regulation of cell cycle	BP	0.02667714	14	61	75	18.7	PML, CNOT10, UBB, ID2, TGFB1, WNT10B, CDK4, TCF3, CCND2, CDKN1A, CHEK2, E2F1, EIF4EBP1, RB1	(-8) CNOT10 WNT10B CDK4 TCF3 CCND2 E2F1 EIF4EBP1 RB1	(+6) PML UBB ID2 TGFB1 CDKN1A CHEK2	-0.53
GO:0071158	positive regulation of cell cycle arrest	BP	0.01919859	8	21	29	27.6	PML, CNOT10, CDKN1A, UBB, ID2, CHEK2, TGFB1, E2F1	(-2) CNOT10 E2F1	(+6) PML CDKN1A UBB ID2 CHEK2 TGFB1	1.41
GO:0090068	positive regulation of cell cycle process	BP	0.01705164	12	44	56	21.4	CDK4, PML, CNOT10, CCND2, CDKN1A, UBB, ID2, CHEK2, TGFB1, WNT10B, E2F1, RB1	(-12) CDK4 CNOT10 CCND2 WNT10B E2F1 RB1 CDK4 CNOT10 CCND2 WNT10B E2F1 RB1	(+12) PML CDKN1A UBB ID2 CHEK2 TGFB1 PML CDKN1A UBB ID2 CHEK2 TGFB1	0.00
GO:0090068	positive regulation of cell cycle process	BP	0.01705164	12	44	56	21.4	CDK4, PML, CNOT10, CCND2, CDKN1A, UBB, ID2, CHEK2, TGFB1, WNT10B, E2F1, RB1	(-12) CDK4 CNOT10 CCND2 WNT10B E2F1 RB1 CDK4 CNOT10 CCND2 WNT10B E2F1 RB1	(+12) PML CDKN1A UBB ID2 CHEK2 TGFB1 PML CDKN1A UBB ID2 CHEK2 TGFB1	0.00

GO:0051726	regulation of cell cycle	BP	0.02987281	25	144	169	14.8	CNOT10, MNAT1, TGFB1, WNT10B, PKMYT1, CDK4, E2F5, BCL2, TCF3, CDC25A, CCND2, FGF2, CHEK1, CHEK2, EIF4EBP1, PML, SMAD3, UBB, ID2, MAP2K6, CDKN1C, CDKN1A, E2F1, GADD45B, RB1	(-15) CNOT10 MNAT1 WNT10B PKMYT1 CDK4 E2F5 BCL2 TCF3 CDC25A CCND2 FGF2 CHEK1 EIF4EBP1 E2F1 RB1	(+10) TGFB1 CHEK2 PML SMAD3 UBB ID2 MAP2K6 CDKN1C CDKN1A GADD45B	-1.00
GO:0071156	regulation of cell cycle arrest	BP	0.01446228	9	25	34	26.5	CDK4, PML, CNOT10, CDKN1A, UBB, ID2, CHEK2, TGFB1, E2F1	(-3) CDK4 CNOT10 E2F1	(+6) PML CDKN1A UBB ID2 CHEK2 TGFB1	1.00
GO:1902806	regulation of cell cycle G1/S phase transition	BP	0.00679674	11	32	43	25.6	PML, BCL2, CNOT10, TCF3, CCND2, CDKN1A, UBB, ID2, CHEK2, E2F1, RB1	(-6) BCL2 CNOT10 TCF3 CCND2 E2F1 RB1	(+5) PML CDKN1A UBB ID2 CHEK2	-0.30
GO:1901987	regulation of cell cycle phase transition	BP	0.00328719	15	51	66	22.7	PML, CNOT10, MNAT1, UBB, ID2, TGFB1, WNT10B, CDK4, BCL2, TCF3, CCND2, CDKN1A, CHEK2, E2F1, RB1	(-9) CNOT10 MNAT1 WNT10B CDK4 BCL2 TCF3 CCND2 E2F1 RB1	(+6) PML UBB ID2 TGFB1 CDKN1A CHEK2	-0.77
GO:0010564	regulation of cell cycle process	BP	0.0407752	17	87	104	16.3	PML, CNOT10, MNAT1, UBB, ID2, TGFB1, WNT10B, PKMYT1, CDK4, BCL2, TCF3, CCND2, CDKN1A, CHEK1, CHEK2, E2F1, RB1	(-11) CNOT10 MNAT1 WNT10B PKMYT1 CDK4 BCL2 TCF3 CCND2 CHEK1 E2F1 RB1	(+6) PML UBB ID2 TGFB1 CDKN1A CHEK2	-1.21
GO:2000045	regulation of G1/S transition of mitotic cell cycle	BP	0.00386501	11	29	40	27.5	PML, BCL2, CNOT10, TCF3, CCND2, CDKN1A, UBB, ID2, CHEK2, E2F1, RB1	(-6) BCL2 CNOT10 TCF3 CCND2 E2F1 RB1	(+5) PML CDKN1A UBB ID2 CHEK2	-0.30
GO:0007346	regulation of mitotic cell cycle	BP	0.00173523	20	78	98	20.4	PML, CNOT10, SMAD3, MNAT1, UBB, ID2, TGFB1, WNT10B, PKMYT1, CDK4, CDKN1C, BCL2, TCF3, CCND2, CDKN1A, CHEK1, CHEK2, E2F1, EIF4EBP1, RB1	(-12) CNOT10 MNAT1 WNT10B PKMYT1 CDK4 BCL2 TCF3 CCND2 CHEK1 E2F1 EIF4EBP1 RB1	(+8) PML SMAD3 UBB ID2 TGFB1 CDKN1C CDKN1A CHEK2	-0.89
GO:1901990	regulation of mitotic cell cycle phase transition	BP	0.00204022	15	48	63	23.8	PML, CNOT10, MNAT1, UBB, ID2, TGFB1, WNT10B, CDK4, BCL2, TCF3, CCND2, CDKN1A, CHEK2, E2F1, RB1	(-9) CNOT10 MNAT1 WNT10B CDK4 BCL2 TCF3 CCND2 E2F1 RB1	(+6) PML UBB ID2 TGFB1 CDKN1A CHEK2	-0.77
GO:0031327	negative regulation of cellular biosynthetic process	BP	0.04745529	24	143	167	14.4	PML, FZD8, HIST1H3B, SMAD3, VEGFA, NF2, NSD1, UBB, SFRP2, HIST1H3H, ID2, ID1, TGFB1, WNT10B, FLNA, CDKN1C, TCF3, HDAC10, BMP6, NOTCH1, CHEK2, E2F1, EIF4EBP1, RB1	(-10) HIST1H3B VEGFA NSD1 HIST1H3H WNT10B TCF3 BMP6 E2F1 EIF4EBP1 RB1	(+14) PML FZD8 SMAD3 NF2 UBB SFRP2 ID2 ID1 TGFB1 FLNA CDKN1C HDAC10 NOTCH1 CHEK2	0.82

GO:2000113	negative regulation of cellular macromolecule biosynthetic process	BP	0.02199751	24	132	156	15.4	PML, FZD8, HIST1H3B, SMAD3, VEGFA, NF2, NSD1, UBB, SFRP2, HIST1H3H, ID2, ID1, TGFB1, WNT10B, FLNA, CDKN1C, TCF3, HDAC10, BMP6, NOTCH1, CHEK2, E2F1, EIF4EBP1, RB1	(-10) HIST1H3B VEGFA NSD1 HIST1H3H WNT10B TCF3 BMP6 E2F1 EIF4EBP1 RB1	(+14) PML FZD8 SMAD3 NF2 UBB SFRP2 ID2 ID1 TGFB1 FLNA CDKN1C HDAC10 NOTCH1 CHEK2	0.82
GO:0031324	negative regulation of cellular metabolic process	BP	0.03908824	34	222	256	13.3	SOCS1, HIST1H3B, VEGFA, NF2, HIST1H3H, TGFB1, WNT10B, PKMYT1, BCL2, TCF3, HDAC10, HSPB1, BMP6, DUSP8, CHEK2, TRIM39, EIF4EBP1, PML, FZD8, SMAD3, NSD1, UBB, SFRP2, ID2, ID1, FLNA, PTTG2, CDKN1C, CDKN1A, HSPA1A, NOTCH1, E2F1, GADD45B, RB1	(-14) HIST1H3B VEGFA HIST1H3H WNT10B PKMYT1 BCL2 TCF3 BMP6 DUSP8 TRIM39 EIF4EBP1 NSD1 E2F1 RB1	(+20) SOCS1 NF2 TGFB1 HDAC10 HSPB1 CHEK2 PML FZD8 SMAD3 UBB SFRP2 ID2 ID1 FLNA PTTG2 CDKN1C CDKN1A HSPA1A NOTCH1 GADD45B	1.03
GO:0010629	negative regulation of gene expression	BP	0.03401328	24	138	162	14.8	PML, CNOT10, FZD8, HIST1H3B, SMAD3, VEGFA, NSD1, UBB, SFRP2, HIST1H3H, ID2, ID1, TGFB1, WNT10B, FLNA, CDKN1C, TCF3, HDAC10, CDKN1A, BMP6, NOTCH1, E2F1, EIF4EBP1, RB1	(-11) CNOT10 HIST1H3B VEGFA NSD1 HIST1H3H WNT10B TCF3 BMP6 E2F1 EIF4EBP1 RB1	(+13) PML FZD8 SMAD3 UBB SFRP2 ID2 ID1 TGFB1 FLNA CDKN1C HDAC10 CDKN1A NOTCH1	0.41
GO:0010558	negative regulation of macromolecule biosynthetic process	BP	0.0416681	24	141	165	14.5	PML, FZD8, HIST1H3B, SMAD3, VEGFA, NF2, NSD1, UBB, SFRP2, HIST1H3H, ID2, ID1, TGFB1, WNT10B, FLNA, CDKN1C, TCF3, HDAC10, BMP6, NOTCH1, CHEK2, E2F1, EIF4EBP1, RB1	(-10) HIST1H3B VEGFA NSD1 HIST1H3H WNT10B TCF3 BMP6 E2F1 EIF4EBP1 RB1	(+14) PML FZD8 SMAD3 NF2 UBB SFRP2 ID2 ID1 TGFB1 FLNA CDKN1C HDAC10 NOTCH1 CHEK2	0.82
GO:0009892	negative regulation of metabolic process	BP	0.04492285	35	233	268	13.1	SOCS1, CNOT10, HIST1H3B, VEGFA, NF2, HIST1H3H, TGFB1, WNT10B, PKMYT1, BCL2, TCF3, HDAC10, HSPB1, BMP6, DUSP8, CHEK2, TRIM39, EIF4EBP1, PML, FZD8, SMAD3, NSD1, UBB, SFRP2, ID2, ID1, FLNA, PTTG2, CDKN1C, CDKN1A, HSPA1A, NOTCH1, E2F1, GADD45B, RB1	(-15) CNOT10 HIST1H3B VEGFA HIST1H3H WNT10B PKMYT1 BCL2 TCF3 BMP6 DUSP8 TRIM39 EIF4EBP1 NSD1 E2F1 RB1	(+20) SOCS1 NF2 TGFB1 HDAC10 HSPB1 CHEK2 PML FZD8 SMAD3 UBB SFRP2 ID2 ID1 FLNA PTTG2 CDKN1C CDKN1A HSPA1A NOTCH1 GADD45B	0.85
GO:0051172	negative regulation of nitrogen compound metabolic process	BP	0.04745529	24	143	167	14.4	PML, FZD8, HIST1H3B, SMAD3, VEGFA, NF2, NSD1, UBB, SFRP2, HIST1H3H, ID2, ID1, TGFB1, WNT10B, FLNA, CDKN1C, TCF3, HDAC10, BMP6, NOTCH1, CHEK2, E2F1, EIF4EBP1, RB1	(-10) HIST1H3B VEGFA NSD1 HIST1H3H WNT10B TCF3 BMP6 E2F1 EIF4EBP1 RB1	(+14) PML FZD8 SMAD3 NF2 UBB SFRP2 ID2 ID1 TGFB1 FLNA CDKN1C HDAC10 NOTCH1 CHEK2	0.82

GO:1903507	negative regulation of nucleic acid-templated transcription	BP	0.04012801	21	117	138	15.2	PML, FZD8, HIST1H3B, SMAD3, VEGFA, NSD1, UBB, SFRP2, HIST1H3H, ID2, ID1, TGFB1, WNT10B, FLNA, CDKN1C, TCF3, HDAC10, BMP6, NOTCH1, E2F1, RB1	(-9) HIST1H3B VEGFA NSD1 HIST1H3H WNT10B TCF3 BMP6 E2F1 RB1	(+12) PML FZD8 SMAD3 UBB SFRP2 ID2 ID1 TGFB1 FLNA CDKN1C HDAC10 NOTCH1	0.65
GO:1902679	negative regulation of RNA biosynthetic process	BP	0.04012801	21	117	138	15.2	PML, FZD8, HIST1H3B, SMAD3, VEGFA, NSD1, UBB, SFRP2, HIST1H3H, ID2, ID1, TGFB1, WNT10B, FLNA, CDKN1C, TCF3, HDAC10, BMP6, NOTCH1, E2F1, RB1	(-9) HIST1H3B VEGFA NSD1 HIST1H3H WNT10B TCF3 BMP6 E2F1 RB1	(+12) PML FZD8 SMAD3 UBB SFRP2 ID2 ID1 TGFB1 FLNA CDKN1C HDAC10 NOTCH1	0.65
GO:0051253	negative regulation of RNA metabolic process	BP	0.04621822	21	119	140	15.0	PML, FZD8, HIST1H3B, SMAD3, VEGFA, NSD1, UBB, SFRP2, HIST1H3H, ID2, ID1, TGFB1, WNT10B, FLNA, CDKN1C, TCF3, HDAC10, BMP6, NOTCH1, E2F1, RB1	(-9) HIST1H3B VEGFA NSD1 HIST1H3H WNT10B TCF3 BMP6 E2F1 RB1	(+12) PML FZD8 SMAD3 UBB SFRP2 ID2 ID1 TGFB1 FLNA CDKN1C HDAC10 NOTCH1	0.65
GO:0045892	negative regulation of transcription; DNA-templated	BP	0.03466248	21	115	136	15.4	PML, FZD8, HIST1H3B, SMAD3, VEGFA, NSD1, UBB, SFRP2, HIST1H3H, ID2, ID1, TGFB1, WNT10B, FLNA, CDKN1C, TCF3, HDAC10, BMP6, NOTCH1, E2F1, RB1	(-9) HIST1H3B VEGFA NSD1 HIST1H3H WNT10B TCF3 BMP6 E2F1 RB1	(+12) PML FZD8 SMAD3 UBB SFRP2 ID2 ID1 TGFB1 FLNA CDKN1C HDAC10 NOTCH1	0.65
GO:0010468	regulation of gene expression	BP	0.04280819	46	329	375	12.3	CNOT10, HIST1H3B, VEGFA, MNAT1, HIST1H3H, FANCA, TGFB1, WNT10B, CDK4, E2F5, BCL2, BRAF, TCF3, HDAC10, HSPB1, FGF2, BMP6, CHEK1, MAPK8, PLCG2, CHEK2, EIF4EBP1, PML, NFE2L2, FZD8, SMAD3, NSD1, UBB, SFRP2, MLLT3, ID2, PBRM1, ID1, MAP3K13, PIK3CD, ETV4, FLNA, MAP2K6, PTTG2, CDKN1C, CDKN1A, HSPA1A, FUT8, NOTCH1, E2F1, RB1	(-23) CNOT10 HIST1H3B VEGFA MNAT1 HIST1H3H WNT10B CDK4 E2F5 BCL2 BRAF TCF3 FGF2 BMP6 CHEK1 MAPK8 EIF4EBP1 NFE2L2 NSD1 MLLT3 PBRM1 ETV4 E2F1 RB1	(+23) FANCA TGFB1 HDAC10 HSPB1 PLCG2 CHEK2 PML FZD8 SMAD3 UBB SFRP2 ID2 ID1 MAP3K13 PIK3CD FLNA MAP2K6 PTTG2 CDKN1C CDKN1A HSPA1A FUT8 NOTCH1	0.00
GO:0030336	negative regulation of cell migration	BP	0.00650414	9	21	30	30.0	BRAF, BCL2, NFE2L2, FGF2, NF2, SFRP2, ACVR1C, NOTCH1, TGFB1	(-4) BRAF BCL2 NFE2L2 FGF2	(+5) NF2 SFRP2 ACVR1C NOTCH1 TGFB1	0.33
GO:2000146	negative regulation of cell motility	BP	0.00806578	9	22	31	29.0	BRAF, BCL2, NFE2L2, FGF2, NF2, SFRP2, ACVR1C, NOTCH1, TGFB1	(-4) BRAF BCL2 NFE2L2 FGF2	(+5) NF2 SFRP2 ACVR1C NOTCH1 TGFB1	0.33
GO:0051271	negative regulation of cellular component movement	BP	0.01446228	9	25	34	26.5	BRAF, BCL2, NFE2L2, FGF2, NF2, SFRP2, ACVR1C, NOTCH1, TGFB1	(-4) BRAF BCL2 NFE2L2 FGF2	(+5) NF2 SFRP2 ACVR1C NOTCH1 TGFB1	0.33

GO:0040013	negative regulation of locomotion	BP	0.01201864	9	24	33	27.3	BRAF, BCL2, NFE2L2, FGF2, NF2, SFRP2, ACVR1C, NOTCH1, TGFB1	(-4) BRAF BCL2 NFE2L2 FGF2	(+5) NF2 SFRP2 ACVR1C NOTCH1 TGFB1	0.33
GO:0043534	blood vessel endothelial cell migration	BP	0.00569715	7	11	18	38.9	HSPB1, NFE2L2, FGF2, VEGFA, NOTCH1, ID1, TGFB1	(-3) NFE2L2 FGF2 VEGFA	(+4) HSPB1 NOTCH1 ID1 TGFB1	0.38
GO:0090101	negative regulation of transmembrane receptor protein serine/threonine kinase signaling pathway	BP	0.03306225	6	13	19	31.6	HSPA1A, SMAD3, UBB, SFRP2, NOTCH1, TGFB1	(-0)	(+6) HSPA1A SMAD3 UBB SFRP2 NOTCH1 TGFB1	2.45
GO:0043536	positive regulation of blood vessel endothelial cell migration	BP	0.01761194	5	6	11	45.5	HSPB1, NFE2L2, FGF2, VEGFA, TGFB1	(-3) NFE2L2 FGF2 VEGFA	(+2) HSPB1 TGFB1	-0.45
GO:0043535	regulation of blood vessel endothelial cell migration	BP	0.03306225	6	13	19	31.6	HSPB1, NFE2L2, FGF2, VEGFA, NOTCH1, TGFB1	(-3) NFE2L2 FGF2 VEGFA	(+3) HSPB1 NOTCH1 TGFB1	0.00
GO:0007179	transforming growth factor beta receptor signaling pathway	BP	0.03782063	8	25	33	24.2	PML, CDKN1C, HSPA1A, SMAD3, UBB, FUT8, ID1, TGFB1	(-0)	(+8) PML CDKN1C HSPA1A SMAD3 UBB FUT8 ID1 TGFB1	2.83
GO:0007178	transmembrane receptor protein serine/threonine kinase signaling pathway	BP	0.04810211	12	53	65	18.5	PML, CDKN1C, HSPA1A, SMAD3, BMP6, UBB, SFRP2, FUT8, ACVR1C, NOTCH1, ID1, TGFB1	(-1) BMP6	(+11) PML CDKN1C HSPA1A SMAD3 UBB SFRP2 FUT8 ACVR1C NOTCH1 ID1 TGFB1	2.89
GO:0044839	cell cycle G2/M phase transition	BP	0.02041265	9	27	36	25.0	CDK4, CDC25A, CDKN1A, MNAT1, UBB, CHEK1, CHEK2, WNT10B, PKMYT1	(-6) CDK4 CDC25A MNAT1 CHEK1 WNT10B PKMYT1	(+3) CDKN1A UBB CHEK2	-1.00
GO:0030003	cellular cation homeostasis	BP	0.0438765	8	26	34	23.5	PML, BCL2, CACNB3, FGF2, SMAD3, BMP6, PLCG2, TGFB1	(-3) BCL2 FGF2 BMP6	(+5) PML CACNB3 SMAD3 PLCG2 TGFB1	0.71
GO:0006875	cellular metal ion homeostasis	BP	0.03782063	8	25	33	24.2	PML, BCL2, CACNB3, FGF2, SMAD3, BMP6, PLCG2, TGFB1	(-3) BCL2 FGF2 BMP6	(+5) PML CACNB3 SMAD3 PLCG2 TGFB1	0.71
GO:0000086	G2/M transition of mitotic cell cycle	BP	0.01201864	9	24	33	27.3	CDK4, CDC25A, CDKN1A, MNAT1, UBB, CHEK1, CHEK2, WNT10B, PKMYT1	(-6) CDK4 CDC25A MNAT1 CHEK1 WNT10B PKMYT1	(+3) CDKN1A UBB CHEK2	-1.00
GO:1901989	positive regulation of cell cycle phase transition	BP	0.03268109	5	8	13	38.5	CDK4, CCND2, TGFB1, WNT10B, RB1	(-4) CDK4 CCND2 WNT10B RB1	(+1) TGFB1	-1.34
GO:1901992	positive regulation of mitotic cell cycle phase transition	BP	0.0244453	5	7	12	41.7	CDK4, CCND2, TGFB1, WNT10B, RB1	(-4) CDK4 CCND2 WNT10B RB1	(+1) TGFB1	-1.34
GO:0010608	posttranscriptional regulation of gene expression	BP	0.00906544	10	28	38	26.3	CDK4, PML, CNOT10, HSPB1, HSPA1A, SMAD3, UBB, TGFB1, E2F1, EIF4EBP1	(-8) CDK4 CNOT10 E2F1 EIF4EBP1 CDK4 CNOT10 E2F1 EIF4EBP1	(+12) PML HSPB1 HSPA1A SMAD3 UBB TGFB1 PML HSPB1 HSPA1A SMAD3 UBB TGFB1	0.63
GO:0010608	posttranscriptional regulation of gene expression	BP	0.00906544	10	28	38	26.3	CDK4, PML, CNOT10, HSPB1, HSPA1A, SMAD3, UBB, TGFB1, E2F1, EIF4EBP1	(-8) CDK4 CNOT10 E2F1 EIF4EBP1 CDK4 CNOT10 E2F1 EIF4EBP1	(+12) PML HSPB1 HSPA1A SMAD3 UBB TGFB1 PML HSPB1 HSPA1A SMAD3 UBB TGFB1	0.63
GO:0050821	protein stabilization	BP	0.01010038	7	13	20	35.0	PML, FLNA, CDKN1A, HSPA1A, SMAD3, CHEK2, WNT10B	(-1) WNT10B	(+6) PML FLNA CDKN1A HSPA1A SMAD3 CHEK2	1.89
GO:0034248	regulation of cellular amide metabolic process	BP	0.02743604	8	23	31	25.8	CDK4, PML, CNOT10, HSPB1, NFE2L2, SMAD3, TGFB1, EIF4EBP1	(-4) CDK4 CNOT10 NFE2L2 EIF4EBP1	(+4) PML HSPB1 SMAD3 TGFB1	0.00
GO:0031063	regulation of histone deacetylation	BP	0.00826968	4	1	5	80.0	PML, VEGFA, MAPK8, TGFB1	(-2) VEGFA MAPK8	(+2) PML TGFB1	0.00

GO:0090311	regulation of protein deacetylation	BP	0.01535537	4	2	6	66.7	PML, VEGFA, MAPK8, TGFB1	(-2) VEGFA MAPK8	(+2) PML TGFB1	0.00
GO:0031647	regulation of protein stability	BP	0.00155447	10	20	30	33.3	PML, FLNA, BCL2, CDKN1A, HSPA1A, SMAD3, NF2, ID1, CHEK2, WNT10B	(-2) BCL2 WNT10B	(+8) PML FLNA CDKN1A HSPA1A SMAD3 NF2 ID1 CHEK2	1.90
GO:0043276	anoikis	BP	0.03709778	4	4	8	50.0	BCL2, NOTCH1, CHEK2, E2F1	(-2) BCL2 E2F1	(+2) NOTCH1 CHEK2	0.00
GO:0010761	fibroblast migration	BP	0.02495672	4	3	7	57.1	PML, BRAF, FGF2, TGFB1	(-2) BRAF FGF2	(+2) PML TGFB1	0.00
GO:0008631	intrinsic apoptotic signaling pathway in response to oxidative stress	BP	0.03709778	4	4	8	50.0	PML, BCL2, HSPB1, NFE2L2	(-2) BCL2 NFE2L2	(+2) PML HSPB1	0.00
GO:2001243	negative regulation of intrinsic apoptotic signaling pathway	BP	0.03268109	5	8	13	38.5	BCL2, HSPB1, NFE2L2, HSPA1A, SFRP2	(-2) BCL2 NFE2L2	(+3) HSPB1 HSPA1A SFRP2	0.45
GO:0044092	negative regulation of molecular function	BP	0.03363832	20	107	127	15.7	SOCS1, PML, VEGFA, NF2, UBB, SFRP2, ID2, ID1, PKMYT1, FLNA, PTTG2, CDKN1C, HSPB1, CDKN1A, DUSP8, NOTCH1, MAPK8, E2F1, RB1, GADD45B	(-6) VEGFA PKMYT1 DUSP8 MAPK8 E2F1 RB1	(+14) SOCS1 PML NF2 UBB SFRP2 ID2 ID1 FLNA PTTG2 CDKN1C HSPB1 CDKN1A NOTCH1 GADD45B	1.79
GO:0030279	negative regulation of ossification	BP	0.03306225	6	13	19	31.6	BCL2, SMAD3, NOTCH1, ID2, ID1, TGFB1	(-1) BCL2	(+5) SMAD3 NOTCH1 ID2 ID1 TGFB1	1.63
GO:2000177	regulation of neural precursor cell proliferation	BP	0.03306225	6	13	19	31.6	FGF2, VEGFA, NF2, NOTCH1, ID2, TGFB1	(-2) FGF2 VEGFA	(+4) NF2 NOTCH1 ID2 TGFB1	0.82
GO:0031960	response to corticosteroid	BP	0.03071856	7	18	25	28.0	BCL2, CDKN1A, BMP6, NOTCH1, CASP3, TGFB1, EIF4EBP1	(-4) BCL2 BMP6 CASP3 EIF4EBP1	(+3) CDKN1A NOTCH1 TGFB1	-0.38
GO:0070482	response to oxygen levels	BP	0.04378226	13	59	72	18.1	PML, NFE2L2, SMAD3, VEGFA, UBB, TGFB1, CDK4, BCL2, CDKN1A, NOTCH1, CASP3, E2F1, EIF4EBP1	(-7) NFE2L2 VEGFA CDK4 BCL2 CASP3 E2F1 EIF4EBP1	(+6) PML SMAD3 UBB TGFB1 CDKN1A NOTCH1	-0.28
GO:0031965	nuclear membrane	CC	0.00748265	6	8	14	42.9	CDK4, PML, BCL2, CCND2, SMAD3, PRPF38A	(-4) CDK4 BCL2 CCND2 PRPF38A	(+2) PML SMAD3	-0.82
GO:0005654	nucleoplasm	CC	0.02878371	36	243	279	12.9	HIST1H3B, MNAT1, HIST1H3H, FANCA, PKMYT1, CDK4, E2F5, TCF3, HDAC10, CDC25A, CCND2, CHEK1, MAPK8, CHEK2, CASP3, EIF4EBP1, PML, SMAD3, NSD1, UBB, MLLT3, ID2, PBRM1, ID1, ETV4, MAP2K6, ALKBH2, DNAJC14, CDKN1A, HSPA1A, FCF1, ALKBH3, NOTCH1, U2AF1, E2F1, RB1	(-23) HIST1H3B MNAT1 HIST1H3H PKMYT1 CDK4 E2F5 TCF3 CDC25A CCND2 CHEK1 MAPK8 CASP3 EIF4EBP1 NSD1 MLLT3 PBRM1 ETV4 ALKBH2 FCF1 ALKBH3 U2AF1 E2F1 RB1	(+13) FANCA HDAC10 CHEK2 PML SMAD3 UBB ID2 ID1 MAP2K6 DNAJC14 CDKN1A HSPA1A NOTCH1	-1.67
GO:0046983	protein dimerization activity	MF	0.0353584	19	108	127	15.0	PML, HIST1H3B, SMAD3, VEGFA, HIST1H3H, ID2, ID1, TGFB1, MAP3K13, FLNA, BRAF, E2F5, BCL2, TCF3, BMP6, NOTCH1, SOS2, CHEK2, E2F1	(-10) HIST1H3B VEGFA HIST1H3H BRAF E2F5 BCL2 TCF3 BMP6 SOS2 E2F1	(+9) PML SMAD3 ID2 ID1 TGFB1 MAP3K13 FLNA NOTCH1 CHEK2	-0.23

APPENDIX B. GSEA ENRICHED GO_BP DATASETS UPON SYNERGISTIC CDK/HDAC INHIBITION

Up or Down	pathway	padj	ES	NES	size	leading Edge	Size leading Edge	fraction Leading Edge
Down	Protein Localization to Kinetochore	0.004	-0.76686	-2.13877	17	RCC2,BUB3,NDC80,MTBP,CDT1,CDK1,HASPIN,SPDL1,TTK,CENPQ,AURKB	11	0.647059
Down	DNA Replication Checkpoint	0.004	-0.77765	-2.10337	15	CDC6,CDC45,TICRR,ORC1,CDT1,TIMELESS,TIPIN,ZNF830,DNA2	9	0.6
Down	Protein Folding in Endoplasmic Reticulum	0.004	-0.69181	-1.8712	15	HSPA5,HSP90B1,PDIA3,CALR,ERO1A,EMC1,EMC4,CANX	8	0.533333
Down	Telomere Maintenance Semiconservative Replication	0.00402	-0.63052	-1.99835	28	FEN1,POLA2,PRIM1,POLD3,POLE3,ACD,POLD2,RFC3,DNA2,RFC4,POLE2,POLE,RPA2,RFC2,RTEL1	15	0.535714
Down	DNA Replication Initiation	0.00406	-0.74117	-2.47033	34	CDC6,MCM5,MCM7,CDC45,POLA2,TICRR,ORC1,PRIM1,CDT1,MCM10,POLE3,ORC2,ORC3,MCM4,MCM2,POLE2,NBN,CCNE1,POLE,ORC5,MCM6,WDR18	22	0.647059
Up	Activation of Immune Response	0.00334	0.332172	1.538157	446	LGMN,HLA-DRA,TNFAIP3,MAPKAPK2,DUSP3,HLA-DPA1,CD38,PRNP,CD47,NFKBIZ,PRKCD,PIK3CD,CDC42,PLCG2,HLA-DRB1,HLA-DRB5,CD59,CAV1,HLA-DPB1,PRKACA,IRF1,TANK,HLA-DQB1,ARPC5,CLEC7A,GCSAM,NECTIN2,CYFIP2,BIRC3,RTN4,RAB29,HEXIM1,HLA-DQA1,EZR,PLCL2,CCR7,ACTG1,CLU,LGALS3,ITGAM,CD36,BIRC2,RUNX1,PAK1,BCAR1,ELF2,PLCG1,CTSB,THEMIS2,RAP1A,UBE2N,VAV2,CMTM3,LILRA2,SKAP1,NFKBIA,PRKCB,MAPK1,HLADQA2,CFH,KRAS,TAB3,PSME4,MUC3A,CD276,C3,CACNB3,PIK3C3,NR4A3,PLSCR1,TRIM15,GPS2,CRK,ELMO2,UBA52,ARPC2,ICOSLG,MALT1,MEF2C,PIK3AP1,IGLV223,PAWR,RIPK1,MUC16,DDX58,FLOT1,RELA,TRIM5,RIOK3,LCK,FGR,NCKAP1L,NCK1,RAC1,MICB,MAP3K7,PJA2,GRAMD4,LGR4,ACTB,DMBT1,PAG1,ZC3H12A,ACTR2,DHX58,CD28,MUC12,JKBKB,CFD,NONO,MYO10,WIPF2,CARD11,TNIP1,LTF,CD22,ITGB2,UBE2D1,DUSP22,TAB2,CYLD,TRAF6,C3AR1,GFI1,CD3E,MAPK3,NCKAP1,CD55,HCK	129	0.289238
Up	Immune Response Regulating Signaling Pathway	0.00334	0.354504	1.636582	433	LGMN,HLA-DRA,TNFAIP3,MAPKAPK2,DUSP3,HLA-DPA1,CD38,PRNP,CD47,NFKBIZ,PRKCD,PIK3CD,CDC42,PLCG2,HLA-DRB1,HLA-DRB5,CAV1,JUN,HLA-DPB1,PRKACA,IRF1,TANK,HLA-DQB1,CALM1,ARPC5,CLEC7A,MAPK8,GCSAM,NECTIN2,CYFIP2,BIRC3,RTN4,RAB29,HLA-DQA1,EZR,PLCL2,CCR7,ACTG1,LGALS3,ITGAM,CD36,BIRC2,RUNX1,PAK1,BCAR1,ELF2,PLCG1,CTSB,THEMIS2,RAP1A,CD40,UBE2N,VAV2,CMTM3,LILRA2,SKAP1,NFKBIA,PRKCB,MAPK1,HLADQA2,KRAS,TAB3,PSME4,MUC3A,CD276,GAB2,CACNB3,PIK3C3,NR4A3,PLSCR1,TRIM15,GPS2,CRK,ELMO2,UBA52,ARPC2,ICOSLG,MALT1,MEF2C,PIK3AP1,IGLV223,PAWR,RIPK1,MUC16,DDX58,FLOT1,RELA,TRIM5,RIOK3,LCK,FGR,NCKAP1L,NCK1,RAC1,PIGR,MICB,MAP3K7,PJA2,GRAMD4,LGR4,FER,ACTB,DMBT1,PAG1,ZC3H12A,ACTR2,PPP3CA,DHX58,CD28,MUC12,JKBKB,MYO10,WIPF2,MAPK10,CARD11,TNIP1,LTF,CD22,CTSH,ITGB2,UBE2D1,DUSP22,TAB2,CYLD,TRAF6	125	0.288684
Up	Positive Regulation of Cell Adhesion	0.00334	0.430148	1.912325	286	EMP2,SOX2,HLA-DMB,JUP,CD44,CCL5,HLA-DPA1,IL4R,RSU1,SMAD3,CD47,ITGA3,HLA-E,NFKBIZ,CYTH3,CDC42,STX3,CAV1,HLA-DPB1,EPB41L5,PODXL,AFDN,S100A10,MYADM,NDNF,SDC4,CCR7,FN1,RHOA,CD36,RUNX1,PAK1,EBI3,DUSP10,MAP4K4,PREX1,PRKCA,CD74,MAP3K8,FRMD5,CD83,FLCN,SKAP1,PTPRU,TNFSF9,PRKCZ,TGFBR2,CD276,LGALS1,SMAD7,NR4A3,KIFAP3,CRK,VWC2,ARPC2,ICOSLG,MALT1,ICAM1,FLOT1,ADAM19,RELA,ITGA6,VCAM1,ZFHX3,RELL2,LCK,TSC1,ANXA1,ITGA2,BCL6,NCKAP1L,LGALS9,IGF2,EFNB2,NCK1,RAC1,EMID1,COL26A1,GSK3B,RAG1,FMN1,IL15,COL16A1,ILK,FLNA,PPP3CA,DAG1,CD28,CD274,DMTN,MYO10,SOCS1,CARD11,ARL2,ERBB2,ARHGEF7,MMRN1,CYLD,TRAF6,JLTS1,FAM49B,CD3E,CORO1A,ITGB1BP1,CD55,DYSF,EPHA1,CCDC80,CHRD	110	0.384615
Up	Regulation of Small GTPase Signal Transduction	0.00334	0.474638	2.093758	266	RHOBTB2,ARHGAP17,MAPRE2,CYTH1,RALGPS1,AMOT,SPRY1,ITGA3,CYTH3,ARHGAP42,CDC42,F2R,CDON,HEG1,NET1,GDI1,ARHGEF9,RAC2,RHOB,ALS2,ITGB1,CADM4,NTRK1,PRAG1,RHOA,CHN1,RAP1GAP,RASA4,SRGAP2,MAP4K4,ARF6,ARHGEF40,OBSCN,PSD,MET,PREX1,VAV2,TIMP2,RALBP1,FLCN,ARRB1,ARHGEF3,RALGAPA2,RALGPS2,ABR,RHOC,KRAS,ARHGDIB,MADD,RHOF,SPATA13,FGD6,NOTCH2,PLEKHG5,TNFAIP1,STMN3,RAP1GAP2,CRK,GPR174,ARAP1,ARHGAP28,FLOT1,PSD3,ARHGEF6,TRIP10,ARAP3,SHOC2,RHOG,BCL6,ARHGAP44,ARHGAP32,RALGAPA1,NOTCH1,RAC1,ARHGAP24,ARHGEF25,ARAP2,RASA4B,AKAP13,ARHGEF11,ROBO1,EPS8,MCF2L2,PPP2CB,MAPKAP1,ARHGEF7,KANK2,ARHGAP26,CD2AP,ARHGEF12,RASA1,OCRL,PLEKHG3,SYNPO2L,RHOQ,RASAL1,STARD13,SYNGAP1,SRGAP3,ARHGEF18,SLIT2,DNMBP,FAM13B,ARHGAP25,DEPDC7,ARHGAP12,FAM13A,VAV1,MYO9A,CBL	110	0.413534
Up	Regulation of Ras Protein Signal Transduction	0.00334	0.480191	2.030598	183	MAPRE2,CYTH1,RALGPS1,SPRY1,ITGA3,CYTH3,ARHGAP42,F2R,HEG1,NET1,ARHGEF9,ALS2,ITGB1,CADM4,NTRK1,PRAG1,RASA4,MAP4K4,ARF6,ARHGEF40,OBSCN,PSD,MET,PREX1,VAV2,TIMP2,FLCN,ARRB1,ARHGEF3,RALGPS2,ABR,KRAS,ARHGDIB,MADD,SPATA13,FGD6,NOTCH2,PLEKHG5,TNFAIP1,STMN3,CRK,GPR174,FLOT1,PSD3,ARHGEF6,SHOC2,BCL6,ARHGAP44,NOTCH1,RAC1,ARHGEF25,RASA4B,AKAP13,ARHGEF11,ROBO1,EPS8,MCF2L2,PPP2CB,MAPKAP1,ARHGEF7,KANK2,ARHGEF12,RASA1,PLEKHG3,SYNPO2L,RASAL1,SYNGAP1,ARHGEF18	68	0.371585

APPENDIX C. FISHER'S EXACT ENRICHED GO_FAT DATASETS UPON SYNERGISTIC CDK/HDAC INHIBITION

GOid	GO term	collection	Zscore	Down_genes	Up_genes	PValue	FDR	Count
GO:0005125	cytokine activity	MF_FAT	-2.88675	(-11) GREM1 IL1A CSF3 CXCL8 CSF2 IL23A IL1B CXCL1 CXCL3 CXCL2 CXCL5	(+1) EBI3	3.89E-06	0.001995	12
GO:0005126	cytokine receptor binding	MF_FAT	-2.88675	(-11) GREM1 IL1A CSF3 CXCL8 CSF2 IL23A IL1B CXCL1 CXCL3 CXCL2 CXCL5	(+1) EBI3	2.72E-05	0.004657	12
GO:0050900	leukocyte migration	BP_FAT	-2.35702	(-14) CXCL8 MMP1 CXCL1 SLC7A11 ITGAL CXCL3 CXCL2 CXCL5 GREM1 IL1A PROCR IL23A IL1B PDE4B	(+4) TNFRSF18 ITGB2 MMP9 CCR7	1.29E-08	1.02E-05	18
GO:0045236	CXCR chemokine receptor binding	MF_FAT	-2.23607	(-5) CXCL8 CXCL1 CXCL3 CXCL2 CXCL5	(+0)	1.21E-05	0.003094	5
GO:0033993	response to lipid	BP_FAT	-2.18282	(-13) ERRFI1 CSF3 CXCL8 CSF2 TNC HMGA2 CXCL1 CXCL3 CXCL2 CXCL5 LOX IL1B PDE4B	(+4) TNFRSF18 WFDC1 FBXO32 CCR7	0.001893	0.038774	17
GO:0002688	regulation of leukocyte chemotaxis	BP_FAT	-2.12132	(-7) GREM1 CXCL8 IL23A CXCL1 CXCL3 CXCL2 CXCL5	(+1) CCR7	1.85E-05	0.001362	8
GO:0050920	regulation of chemotaxis	BP_FAT	-2.12132	(-7) GREM1 CXCL8 IL23A CXCL1 CXCL3 CXCL2 CXCL5	(+1) CCR7	8.80E-04	0.023019	8
GO:0097529	myeloid leukocyte migration	BP_FAT	-2.11058	(-9) GREM1 IL1A CXCL8 IL23A IL1B PDE4B CXCL1 CXCL3 CXCL2	(+2) ITGB2 CCR7	7.70E-07	1.51E-04	11
GO:0030595	leukocyte chemotaxis	BP_FAT	-2.11058	(-9) GREM1 CXCL8 IL23A IL1B PDE4B CXCL1 CXCL3 CXCL2 CXCL5	(+2) ITGB2 CCR7	4.66E-06	5.13E-04	11
GO:0060326	cell chemotaxis	BP_FAT	-2.11058	(-9) GREM1 CXCL8 IL23A IL1B PDE4B CXCL1 CXCL3 CXCL2 CXCL5	(+2) ITGB2 CCR7	4.35E-05	0.002648	11
GO:0032496	response to lipopolysaccharide	BP_FAT	-2.11058	(-9) CSF3 CXCL8 CSF2 IL1B PDE4B CXCL1 CXCL3 CXCL2 CXCL5	(+2) TNFRSF18 CCR7	2.00E-04	0.00827	11
GO:0002237	response to molecule of bacterial origin	BP_FAT	-2.11058	(-9) CSF3 CXCL8 CSF2 IL1B PDE4B CXCL1 CXCL3 CXCL2 CXCL5	(+2) TNFRSF18 CCR7	2.88E-04	0.011323	11
GO:0006935	chemotaxis	BP_FAT	-1.94145	(-10) CXCL8 CXCL1 CXCL3 CXCL2 CXCL5 GREM1 IL23A IL1B PDE4B FEZF1	(+3) ITGB2 PDGFA CCR7	0.002025	0.040585	13
GO:0042330	taxis	BP_FAT	-1.94145	(-10) CXCL8 CXCL1 CXCL3 CXCL2 CXCL5 GREM1 IL23A IL1B PDE4B FEZF1	(+3) ITGB2 PDGFA CCR7	0.002056	0.040843	13
GO:1990266	neutrophil migration	BP_FAT	-1.89737	(-8) IL1A CXCL8 IL23A IL1B PDE4B CXCL1 CXCL3 CXCL2	(+2) ITGB2 CCR7	7.81E-08	3.01E-05	10
GO:0097530	granulocyte migration	BP_FAT	-1.89737	(-8) IL1A CXCL8 IL23A IL1B PDE4B CXCL1 CXCL3 CXCL2	(+2) ITGB2 CCR7	4.14E-07	1.13E-04	10
GO:0002685	regulation of leukocyte migration	BP_FAT	-1.89737	(-8) GREM1 IL1A CXCL8 IL23A CXCL1 CXCL3 CXCL2 CXCL5	(+2) TNFRSF18 CCR7	5.70E-06	5.77E-04	10
GO:1902624	positive regulation of neutrophil migration	BP_FAT	-1.88982	(-6) IL1A CXCL8 IL23A CXCL1 CXCL3 CXCL2	(+1) CCR7	4.33E-08	2.23E-05	7
GO:1902622	regulation of neutrophil migration	BP_FAT	-1.88982	(-6) IL1A CXCL8 IL23A CXCL1 CXCL3 CXCL2	(+1) CCR7	1.73E-07	5.93E-05	7
GO:0002690	positive regulation of leukocyte chemotaxis	BP_FAT	-1.88982	(-6) CXCL8 IL23A CXCL1 CXCL3 CXCL2 CXCL5	(+1) CCR7	5.83E-05	0.003156	7
GO:0050921	positive regulation of chemotaxis	BP_FAT	-1.88982	(-6) CXCL8 IL23A CXCL1 CXCL3 CXCL2 CXCL5	(+1) CCR7	4.93E-04	0.017475	7
GO:0016477	cell migration	BP_FAT	-1.67126	(-19) CXCL8 CXCL1 SLC7A11 ITGAL CXCL3 CXCL2 CXCL5 LOXL2 PDE4B CYP1B1 FEZF1 MMP1 IGF1 GREM1 IL1A PROCR MMP14 IL23A IL1B	(+10) PTPRR ITGB2 CHRD PDGFA LDLRAD4 ARHGDIB CCR7 TNFRSF18 MMP9 FGR	3.15E-07	9.73E-05	29
GO:0048870	cell motility	BP_FAT	-1.67126	(-19) CXCL8 CXCL1 SLC7A11 ITGAL CXCL3 CXCL2 CXCL5 LOXL2 PDE4B CYP1B1 FEZF1 MMP1 IGF1 GREM1 IL1A PROCR MMP14 IL23A IL1B	(+10) PTPRR ITGB2 CHRD PDGFA LDLRAD4 ARHGDIB CCR7 TNFRSF18 MMP9 FGR	3.17E-06	3.84E-04	29

GO:0051674	localization of cell	BP_FAT	-1.67126	(-19) CXCL8 CXCL1 SLC7A11 ITGAL CXCL3 CXCL2 CXCL5 LOXL2 PDE4B CYP1B1 FEZF1 MMP1 IGF1 GREM1 IL1A PROCR MMP14 IL23A IL1B	(+10) PTPRR ITGB2 CHRD PDGFA LDLRAD4 ARHGDIB CCR7 TNFRSF18 MMP9 FGR	3.17E-06	3.84E-04	29
GO:0040011	locomotion	BP_FAT	-1.67126	(-19) CXCL8 CXCL1 SLC7A11 ITGAL CXCL3 CXCL2 CXCL5 LOXL2 PDE4B CYP1B1 FEZF1 MMP1 IGF1 GREM1 IL1A PROCR MMP14 IL23A IL1B	(+10) PTPRR ITGB2 CHRD PDGFA LDLRAD4 ARHGDIB CCR7 TNFRSF18 MMP9 FGR	4.27E-05	0.002648	29
GO:0030593	neutrophil chemotaxis	BP_FAT	-1.66667	(-7) CXCL8 IL23A IL1B PDE4B CXCL1 CXCL3 CXCL2	(+2) ITGB2 CCR7	4.41E-07	1.13E-04	9
GO:0071621	granulocyte chemotaxis	BP_FAT	-1.66667	(-7) CXCL8 IL23A IL1B PDE4B CXCL1 CXCL3 CXCL2	(+2) ITGB2 CCR7	2.11E-06	2.96E-04	9
GO:0002687	positive regulation of leukocyte migration	BP_FAT	-1.66667	(-7) IL1A CXCL8 IL23A CXCL1 CXCL3 CXCL2 CXCL5	(+2) TNFRSF18 CCR7	3.23E-06	3.84E-04	9
GO:0005576	extracellular region	CC_DIRECT	-1.66667	(-23) LGALS3BP CSF3 CSF2 CXCL8 TNC CXCL1 CXCL3 FSTL1 CXCL2 APOLD1 CXCL5 APOL1 SERPINB2 MMP1 MMP3 PSG1 IGF1 IL1A PROCR LOX IL23A IL1B SCG5	(+13) SERPINA1 WNT2B EBI3 PDGFA LILRA2 FGF9 DMBT1 IL13RA2 COL27A1 TNFRSF18 IGF2 MMP9 COL5A3	2.42E-08	2.01E-06	36
GO:0090023	positive regulation of neutrophil chemotaxis	BP_FAT	-1.63299	(-5) CXCL8 IL23A CXCL1 CXCL3 CXCL2	(+1) CCR7	8.25E-07	1.51E-04	6
GO:0071624	positive regulation of granulocyte chemotaxis	BP_FAT	-1.63299	(-5) CXCL8 IL23A CXCL1 CXCL3 CXCL2	(+1) CCR7	1.63E-06	2.65E-04	6
GO:0090022	regulation of neutrophil chemotaxis	BP_FAT	-1.63299	(-5) CXCL8 IL23A CXCL1 CXCL3 CXCL2	(+1) CCR7	2.01E-06	2.96E-04	6
GO:0071622	regulation of granulocyte chemotaxis	BP_FAT	-1.63299	(-5) CXCL8 IL23A CXCL1 CXCL3 CXCL2	(+1) CCR7	1.41E-05	0.001247	6
GO:0070098	chemokine-mediated signaling pathway	BP_FAT	-1.63299	(-5) CXCL8 CXCL1 CXCL3 CXCL2 CXCL5	(+1) CCR7	5.76E-04	0.01945	6
GO:0072359	circulatory system development	BP_FAT	-1.60591	(-13) FHOD3 ERRFI1 CXCL8 IGF1 APOLD1 LOXL2 GREM1 IL1A IFT74 MMP14 LOX IL1B CYP1B1	(+6) TMPRSS6 ITGB2 PDGFA FGF9 APLNR CHI3L1	7.46E-04	0.020576	19
GO:0072358	cardiovascular system development	BP_FAT	-1.60591	(-13) FHOD3 ERRFI1 CXCL8 IGF1 APOLD1 LOXL2 GREM1 IL1A IFT74 MMP14 LOX IL1B CYP1B1	(+6) TMPRSS6 ITGB2 PDGFA FGF9 APLNR CHI3L1	7.46E-04	0.020576	19
GO:0006928	movement of cell or subcellular component	BP_FAT	-1.5667	(-21) CXCL8 CXCL1 SLC7A11 ITGAL CXCL3 CXCL2 CXCL5 LOXL2 IFT74 UCHL1 PDE4B CYP1B1 FEZF1 MMP1 IGF1 GREM1 IL1A PROCR MMP14 IL23A IL1B	(+12) HCN4 PTPRR ITGB2 CHRD PDGFA LDLRAD4 MOBP ARHGDIB CCR7 TNFRSF18 MMP9 FGR	1.79E-05	0.001359	33
GO:0008283	cell proliferation	BP_FAT	-1.5667	(-21) ERRFI1 CSF3 CSF2 CXCL8 TNC CXCL1 CXCL5 LOXL2 IFT74 UCHL1 CYP1B1 FEZF1 FZD9 HMGA2 IGF1 RPGRIP1 GREM1 IL1A MMP14 IL23A IL1B	(+12) CDKN1C WNT2B EBI3 CHRD WFDC1 PDGFA FGF9 CTLA4 SPEG PRNP IGF2 MMP9	3.69E-05	0.002422	33
GO:0030199	collagen fibril organization	BP_FAT	-1.34164	(-4) GREM1 LOX CYP1B1 LOXL2	(+1) COL5A3	3.19E-04	0.011845	5
GO:0051094	positive regulation of developmental process	BP_FAT	-1.34164	(-13) CSF3 CXCL8 FZD9 HMGA2 IGF1 LOXL2 GREM1 IL1A MMP14 IL23A IL1B CYP1B1 FEZF1	(+7) WNT2B ITGB2 PDGFA BAIAP2 FGF9 CHI3L1 PACSIN1	0.001495	0.03254	20
GO:0009617	response to bacterium	BP_FAT	-1.29099	(-10) CSF3 CXCL8 CSF2 CXCL1 CXCL3 CXCL2 CXCL5 IL23A IL1B PDE4B	(+5) TNFRSF18 BAIAP2 FGR DMBT1 CCR7	1.59E-04	0.007197	15
GO:0001944	vasculature development	BP_FAT	-1.29099	(-10) ERRFI1 CXCL8 APOLD1 LOXL2 GREM1 IL1A MMP14 LOX IL1B CYP1B1	(+5) TMPRSS6 ITGB2 PDGFA FGF9 CHI3L1	5.07E-04	0.017758	15
GO:0051707	response to other organism	BP_FAT	-1.21268	(-11) CSF3 CXCL8 CSF2 HMGA2 CXCL1 CXCL3 CXCL2 CXCL5 IL23A IL1B PDE4B	(+6) TNFRSF18 KRT8 BAIAP2 FGR DMBT1 CCR7	0.0013	0.029062	17
GO:0043207	response to external biotic stimulus	BP_FAT	-1.21268	(-11) CSF3 CXCL8 CSF2 HMGA2 CXCL1 CXCL3 CXCL2 CXCL5 IL23A IL1B PDE4B	(+6) TNFRSF18 KRT8 BAIAP2 FGR DMBT1 CCR7	0.0013	0.029062	17
GO:0009607	response to biotic stimulus	BP_FAT	-1.21268	(-11) CSF3 CXCL8 CSF2 HMGA2 CXCL1 CXCL3 CXCL2 CXCL5 IL23A IL1B PDE4B	(+6) TNFRSF18 KRT8 BAIAP2 FGR DMBT1 CCR7	0.002202	0.042199	17
GO:0045766	positive regulation of angiogenesis	BP_FAT	-1.13389	(-5) GREM1 IL1A CXCL8 IL1B CYP1B1	(+2) ITGB2 CHI3L1	6.37E-04	0.01945	7
GO:1904018	positive regulation of vasculature development	BP_FAT	-1.13389	(-5) GREM1 IL1A CXCL8 IL1B CYP1B1	(+2) ITGB2 CHI3L1	0.001182	0.027216	7

GO:0050731	positive regulation of peptidyl-tyrosine phosphorylation	BP_FAT	-1.13389	(-5) GREM1 CSF3 CSF2 IL23A IGF1	(+2) TNFRSF18 IGF2	0.00237	0.044629	7
GO:0030335	positive regulation of cell migration	BP_FAT	-1.06904	(-9) CXCL8 CXCL1 IGF1 CXCL3 CXCL2 CXCL5 IL1A MMP14 IL23A	(+5) TNFRSF18 PDGFA MMP9 FGR CCR7	2.32E-05	0.001626	14
GO:2000147	positive regulation of cell motility	BP_FAT	-1.06904	(-9) CXCL8 CXCL1 IGF1 CXCL3 CXCL2 CXCL5 IL1A MMP14 IL23A	(+5) TNFRSF18 PDGFA MMP9 FGR CCR7	3.33E-05	0.002233	14
GO:0051272	positive regulation of cellular component movement	BP_FAT	-1.06904	(-9) CXCL8 CXCL1 IGF1 CXCL3 CXCL2 CXCL5 IL1A MMP14 IL23A	(+5) TNFRSF18 PDGFA MMP9 FGR CCR7	4.38E-05	0.002648	14
GO:0040017	positive regulation of locomotion	BP_FAT	-1.06904	(-9) CXCL8 CXCL1 IGF1 CXCL3 CXCL2 CXCL5 IL1A MMP14 IL23A	(+5) TNFRSF18 PDGFA MMP9 FGR CCR7	4.59E-05	0.002709	14
GO:0001568	blood vessel development	BP_FAT	-1.06904	(-9) CXCL8 APOLD1 LOXL2 GREM1 IL1A MMP14 LOX IL1B CYP1B1	(+5) TMPRSS6 ITGB2 PDGFA FGF9 CHI3L1	9.41E-04	0.023812	14
GO:0030155	regulation of cell adhesion	BP_FAT	1.04257	(-9) CXCL8 TNC IGF1 GREM1 IFT74 MMP14 IL23A IL1B CYP1B1	(+14) PRR5 PRNP PTPRR TNFRSF18 EBI3 CHRD SOX13 IGF2 ABAT ARHGDIB CTLA4 MAP3K8 CCR7 SKAP1	1.34E-08	1.02E-05	23
GO:0071495	cellular response to endogenous stimulus	BP_FAT	1.09109	(-8) ERRFI1 CXCL8 TNC HMGA2 FSTL1 GREM1 IL1B PDE4B	(+13) CDKN1C HCN4 TMPRSS6 ITGB2 CAMK2A CHRD IGF2 LDLRAD4 BAIAP2 FBXO32 FGF9 ADAMTSL2 ZYX	0.001661	0.035013	21
GO:0042327	positive regulation of phosphorylation	BP_FAT	1.14708	(-7) CSF3 CSF2 IGF1 GREM1 IL1A IL23A IL1B	(+12) PRR5 TNFRSF18 IGF2 PDGFA MMP9 FGR GRM4 FGF9 CHI3L1 MAP3K8 CCR7 MDFI	6.35E-04	0.01945	19
GO:0010562	positive regulation of phosphorus metabolic process	BP_FAT	1.14708	(-7) CSF3 CSF2 IGF1 GREM1 IL1A IL23A IL1B	(+12) PRR5 TNFRSF18 IGF2 PDGFA MMP9 FGR GRM4 FGF9 CHI3L1 MAP3K8 CCR7 MDFI	0.002401	0.044629	19
GO:0045937	positive regulation of phosphate metabolic process	BP_FAT	1.14708	(-7) CSF3 CSF2 IGF1 GREM1 IL1A IL23A IL1B	(+12) PRR5 TNFRSF18 IGF2 PDGFA MMP9 FGR GRM4 FGF9 CHI3L1 MAP3K8 CCR7 MDFI	0.002401	0.044629	19
GO:0051249	regulation of lymphocyte activation	BP_FAT	1.1547	(-4) MMP14 IL23A IL1B IGF1	(+8) PRR5 PRNP EBI3 IGF2 SOX13 CTLA4 CCR7 MAP3K8	5.94E-04	0.01945	12
GO:0042110	T cell activation	BP_FAT	1.1547	(-4) IL23A IL1B IGF1 ITGAL	(+8) PRR5 PRNP EBI3 IGF2 SOX13 CTLA4 CCR7 MAP3K8	0.001156	0.027216	12
GO:0070489	T cell aggregation	BP_FAT	1.1547	(-4) IL23A IL1B IGF1 ITGAL	(+8) PRR5 PRNP EBI3 IGF2 SOX13 CTLA4 CCR7 MAP3K8	0.001156	0.027216	12
GO:0071593	lymphocyte aggregation	BP_FAT	1.1547	(-4) IL23A IL1B IGF1 ITGAL	(+8) PRR5 PRNP EBI3 IGF2 SOX13 CTLA4 CCR7 MAP3K8	0.001177	0.027216	12
GO:0070486	leukocyte aggregation	BP_FAT	1.1547	(-4) IL23A IL1B IGF1 ITGAL	(+8) PRR5 PRNP EBI3 IGF2 SOX13 CTLA4 CCR7 MAP3K8	0.001333	0.0296	12
GO:0016337	single organismal cell-cell adhesion	BP_FAT	1.21268	(-6) SLC7A11 IGF1 ITGAL IL23A IL1B CYP1B1	(+11) PRR5 PRNP EBI3 ITGB2 SOX13 IGF2 ABAT ITGAD CTLA4 MAP3K8 CCR7	3.08E-04	0.011769	17
GO:0098602	single organism cell adhesion	BP_FAT	1.21268	(-6) SLC7A11 IGF1 ITGAL IL23A IL1B CYP1B1	(+11) PRR5 PRNP EBI3 ITGB2 SOX13 IGF2 ABAT ITGAD CTLA4 MAP3K8 CCR7	6.75E-04	0.020027	17
GO:0044093	positive regulation of molecular function	BP_FAT	1.25724	(-12) ARHGAP9 ERRFI1 CSF3 CSF2 BEX1 CXCL1 HMGA2 IGF1 GREM1 MMP14 IL23A IL1B	(+19) RGS13 ITGB2 CAMK2A PDGFA ARHGEF10L MEFV GRM4 FGF9 ARHGDIB CCR7 MAP3K8 EGLN3 IGF2 MMP9 FGR FCER2 IL3RA CHI3L1 MDFI	1.79E-04	0.007902	31
GO:0030029	actin filament-based process	BP_FAT	1.29099	(-5) FHOD3 CSF3 CXCL1 PDE4B PFN4	(+10) HCN4 KRT8 PDGFA ARHGEF10L BAIAP2 MOBP ARHGDIB ZYX CCR7 PACSIN1	0.001292	0.029062	15
GO:0061045	negative regulation of wound healing	BP_FAT	1.34164	(-1) SERPINB2	(+4) TMPRSS6 PDGFA WFDC1 ABAT	0.001497	0.03254	5
GO:0046903	secretion	BP_FAT	1.34164	(-7) LGALS3BP CSF2 HMGA2 IGF1 IL1A IL1B SCG5	(+13) SERPINA1 CAMK2A IGF2 PDGFA ABAT SYT7 FGR GRM4 KCNMB4 CHI3L1 CCR7 IL13RA2 TSPOAP1	0.001644	0.03499	20
GO:1903035	negative regulation of response to wounding	BP_FAT	1.34164	(-1) SERPINB2	(+4) TMPRSS6 PDGFA WFDC1 ABAT	0.002377	0.044629	5
GO:0031399	regulation of protein modification process	BP_FAT	1.34715	(-10) ERRFI1 CSF3 CSF2 UCHL1 IGF1 GREM1 IL1A IL23A IL1B JDP2	(+17) CDKN1C PRR5 PTPRR ITGB2 PDGFA LDLRAD4 GRM4 FGF9 CCR7 MAP3K8 PRNP TNFRSF18 IGF2 MMP9 FGR CHI3L1 MDFI	9.93E-04	0.024521	27

GO:0065009	regulation of molecular function	BP_FAT	1.37249	(-17) ARHGAP9 ERRFI1 CSF3 CSF2 BEX1 CXCL1 UCHL1 PDE4B CYP1B1 SERPINB2 HMGA2 IGF1 GREM1 MMP14 IL23A IL1B SCG5	(+26) CDKN1C SERPINA1 RGS13 ITGB2 CAMK2A WFDC1 PDGFA ARHGEF10L ELFN2 MEFV CACNG8 GRM4 FGF9 ARHGDIB CCR7 MAP3K8 PRNP EGLN3 IGF2 MMP9 FGR FCER2 PPP2R2C IL3RA CHI3L1 MDFI	7.36E-05	0.003786	43
GO:0045785	positive regulation of cell adhesion	BP_FAT	1.38675	(-4) IGF1 IFT74 IL23A IL1B	(+9) PRR5 TNFRSF18 EBI3 CHRD IGF2 CTLA4 MAP3K8 CCR7 SKAP1	8.15E-05	0.004055	13
GO:0007159	leukocyte cell-cell adhesion	BP_FAT	1.38675	(-4) IGF1 ITGAL IL23A IL1B	(+9) PRR5 PRNP EBI3 ITGB2 SOX13 IGF2 CTLA4 MAP3K8 CCR7	7.48E-04	0.020576	13
GO:0009967	positive regulation of signal transduction	BP_FAT	1.4	(-9) CSF3 CSF2 CYP1B1 FZD9 IGF1 GREM1 IL1A IL23A IL1B	(+16) CDKN1C PRR5 WNT2B PDGFA ABAT GRM4 FGF9 CCR7 MAP3K8 TNFRSF18 IGF2 MMP9 FGR CHI3L1 MDFI SKAP1	5.80E-04	0.01945	25
GO:0016310	phosphorylation	BP_FAT	1.41421	(-12) ERRFI1 CSF3 CSF2 PAPSS2 UCHL1 MEF2B HMGA2 IGF1 GREM1 IL1A IL23A IL1B	(+20) CDKN1C PRR5 PTPRR ITGB2 CAMK2A PDGFA LDLRAD4 GRM4 FGF9 SPEG CCR7 MAP3K8 PRNP TNFRSF18 IGF2 MMP9 FGR IL3RA CHI3L1 MDFI	0.002065	0.040843	32
GO:0009790	embryo development	BP_FAT	1.41421	(-6) CXCL8 CSF2 HMGA2 IGF1 GREM1 MMP14	(+12) CDKN1C PTPRR WNT2B ITGB2 CHRD KRT8 PDGFA MMP9 FGF9 APLNR PDZD7 MDFI	0.002151	0.041494	18
GO:0050863	regulation of T cell activation	BP_FAT	1.50756	(-3) IL23A IL1B IGF1	(+8) PRR5 PRNP EBI3 IGF2 SOX13 CTLA4 CCR7 MAP3K8	1.85E-04	0.007944	11
GO:1903037	regulation of leukocyte cell-cell adhesion	BP_FAT	1.50756	(-3) IL23A IL1B IGF1	(+8) PRR5 PRNP EBI3 IGF2 SOX13 CTLA4 CCR7 MAP3K8	2.67E-04	0.01069	11
GO:0007155	cell adhesion	BP_FAT	1.5667	(-12) LGALS3BP TNC SLC7A11 ITGAL LOXL2 IFT74 CYP1B1 IGF1 GREM1 MMP14 IL23A IL1B	(+21) PRR5 PTPRR EBI3 ITGB2 CHRD ABAT ARHGDIB CTLA4 CCR7 MAP3K8 PRNP CADM2 TNFRSF18 IGF2 SOX13 BAIAP2 ITGAD COL5A3 ZYX CD22 SKAP1	5.79E-06	5.77E-04	33
GO:0022610	biological adhesion	BP_FAT	1.5667	(-12) LGALS3BP TNC SLC7A11 ITGAL LOXL2 IFT74 CYP1B1 IGF1 GREM1 MMP14 IL23A IL1B	(+21) PRR5 PTPRR EBI3 ITGB2 CHRD ABAT ARHGDIB CTLA4 CCR7 MAP3K8 PRNP CADM2 TNFRSF18 IGF2 SOX13 BAIAP2 ITGAD COL5A3 ZYX CD22 SKAP1	6.24E-06	6.02E-04	33
GO:0001932	regulation of protein phosphorylation	BP_FAT	1.56893	(-9) ERRFI1 CSF3 CSF2 UCHL1 IGF1 GREM1 IL1A IL23A IL1B	(+17) CDKN1C PRR5 PTPRR ITGB2 PDGFA LDLRAD4 GRM4 FGF9 CCR7 MAP3K8 PRNP TNFRSF18 IGF2 MMP9 FGR CHI3L1 MDFI	5.34E-05	0.002945	26
GO:0042325	regulation of phosphorylation	BP_FAT	1.56893	(-9) ERRFI1 CSF3 CSF2 UCHL1 IGF1 GREM1 IL1A IL23A IL1B	(+17) CDKN1C PRR5 PTPRR ITGB2 PDGFA LDLRAD4 GRM4 FGF9 CCR7 MAP3K8 PRNP TNFRSF18 IGF2 MMP9 FGR CHI3L1 MDFI	1.61E-04	0.007197	26
GO:0010647	positive regulation of cell communication	BP_FAT	1.56893	(-9) CSF3 CSF2 CYP1B1 FZD9 IGF1 GREM1 IL1A IL23A IL1B	(+17) CDKN1C PRR5 WNT2B PDGFA ABAT SLC8A2 GRM4 FGF9 CCR7 MAP3K8 TNFRSF18 IGF2 MMP9 FGR CHI3L1 MDFI SKAP1	8.40E-04	0.022532	26
GO:0043085	positive regulation of catalytic activity	BP_FAT	1.56893	(-9) ARHGAP9 ERRFI1 CSF2 CXCL1 IGF1 GREM1 MMP14 IL23A IL1B	(+17) RGS13 CAMK2A PDGFA ARHGEF10L MEFV GRM4 FGF9 ARHGDIB CCR7 MAP3K8 EGLN3 IGF2 FGR FCER2 IL3RA CHI3L1 MDFI	8.71E-04	0.022981	26
GO:0023056	positive regulation of signaling	BP_FAT	1.56893	(-9) CSF3 CSF2 CYP1B1 FZD9 IGF1 GREM1 IL1A IL23A IL1B	(+17) CDKN1C PRR5 WNT2B PDGFA ABAT SLC8A2 GRM4 FGF9 CCR7 MAP3K8 TNFRSF18 IGF2 MMP9 FGR CHI3L1 MDFI SKAP1	9.04E-04	0.023442	26
GO:0002694	regulation of leukocyte activation	BP_FAT	1.60357	(-4) IGF1 MMP14 IL23A IL1B	(+10) PRR5 PRNP EBI3 SOX13 IGF2 FGR CTLA4 MAP3K8 CCR7 IL13RA2	1.30E-04	0.006186	14
GO:0032940	secretion by cell	BP_FAT	1.60591	(-6) LGALS3BP HMGA2 IGF1 IL1A IL1B SCG5	(+13) SERPINA1 CAMK2A IGF2 PDGFA ABAT SYT7 FGR GRM4 KCNMB4 CHI3L1 CCR7 IL13RA2 TSPOAP1	9.61E-04	0.0241	19
GO:0006468	protein phosphorylation	BP_FAT	1.61645	(-11) ERRFI1 CSF3 CSF2 UCHL1 MEF2B HMGA2 IGF1 GREM1 IL1A IL23A IL1B	(+20) CDKN1C PRR5 PTPRR ITGB2 CAMK2A PDGFA LDLRAD4 GRM4 FGF9 SPEG CCR7 MAP3K8 PRNP TNFRSF18 IGF2 MMP9 FGR IL3RA CHI3L1 MDFI	2.01E-04	0.00827	31
GO:0007166	cell surface receptor signaling pathway	BP_FAT	1.6641	(-20) ERRFI1 CSF3 CSF2 CXCL8 GRIK4 CXCL1 ITGAL CXCL3 CXCL2 CXCL5 PDE4B GREM1 IL1A MMP14 IL1B FSTL1 IFT74 FZD9 HMGA2 IGF1	(+32) CDKN1C PTPRR WNT2B ITGB2 ABAT LDLRAD4 GRM4 FGF9 ADAMTSL2 CTLA4 CCR7 IL13RA2 TNFRSF18 KRT8 MMP9 FGR FCER2 ITGAD IL3RA SKAP1 MDFI TMPRSS6 EBI3 CAMK2A CHRD PDGFA CACNG8 PRNP IGF2 BAIAP2 TSPAN15 ZYX	1.36E-09	4.18E-06	52
GO:0090287	regulation of cellular response to growth factor stimulus	BP_FAT	1.66667	(-2) GREM1 IL1B	(+7) CDKN1C FBN3 FGF9 TMPRSS6 ADAMTSL2 CHRD LDLRAD4	7.33E-04	0.020576	9

GO:0009966	regulation of signal transduction	BP_FAT	1.67748	(-16) ARHGAP9 ERRFI1 CSF3 CSF2 CXCL8 UCHL1 CYP1B1 FZD9 HMGA2 IGF1 GREM1 IL1A MMP14 IL23A IL1B MGLL	(+27) CDKN1C PRR5 PTPRR WNT2B TMPRSS6 RGS13 CHRD PDGFA ABAT ARHGEF10L LDLRAD4 CACNG8 GRM4 FGF9 ARHGDIB ADAMTSL2 CCR7 MAP3K8 PRNP TNFRSF18 IGF2 MMP9 FGR TSPAN15 CHI3L1 MDFI SKAP1	2.31E-05	0.001626	43
GO:0032268	regulation of cellular protein metabolic process	BP_FAT	1.71499	(-12) ERRFI1 CSF3 CSF2 UCHL1 SERPINB2 IGF1 GREM1 IL1A MMP14 IL23A IL1B JDP2	(+22) CDKN1C PRR5 PTPRR SERPINA1 ITGB2 WFDC1 PDGFA LDLRAD4 MEFV GRM4 FGF9 CCR7 MAP3K8 PRNP EGLN3 TNFRSF18 IGF2 MMP9 DAZL FGR CHI3L1 MDFI	0.001179	0.027216	34
GO:0022407	regulation of cell-cell adhesion	BP_FAT	1.73205	(-3) IL23A IL1B IGF1	(+9) PRR5 PRNP EBI3 IGF2 SOX13 CTLA4 ABAT CCR7 MAP3K8	3.51E-04	0.012748	12
GO:0019220	regulation of phosphate metabolic process	BP_FAT	1.73205	(-9) ERRFI1 CSF3 CSF2 UCHL1 IGF1 GREM1 IL1A IL23A IL1B	(+18) CDKN1C PRR5 PTPRR ITGB2 PDGFA LDLRAD4 ELFN2 GRM4 FGF9 CCR7 MAP3K8 PRNP TNFRSF18 IGF2 MMP9 FGR CHI3L1 MDFI	6.08E-04	0.01945	27
GO:0051174	regulation of phosphorus metabolic process	BP_FAT	1.73205	(-9) ERRFI1 CSF3 CSF2 UCHL1 IGF1 GREM1 IL1A IL23A IL1B	(+18) CDKN1C PRR5 PTPRR ITGB2 PDGFA LDLRAD4 ELFN2 GRM4 FGF9 CCR7 MAP3K8 PRNP TNFRSF18 IGF2 MMP9 FGR CHI3L1 MDFI	6.14E-04	0.01945	27
GO:0050790	regulation of catalytic activity	BP_FAT	1.85934	(-12) ARHGAP9 ERRFI1 CSF2 CXCL1 UCHL1 SERPINB2 IGF1 GREM1 MMP14 IL23A IL1B SCG5	(+23) CDKN1C SERPINA1 RGS13 CAMK2A WFDC1 PDGFA ARHGEF10L ELFN2 MEFV GRM4 FGF9 ARHGDIB CCR7 MAP3K8 EGLN3 IGF2 MMP9 FGR FCER2 PPP2R2C IL3RA CHI3L1 MDFI	6.19E-04	0.01945	35
GO:0051246	regulation of protein metabolic process	BP_FAT	1.85934	(-12) ERRFI1 CSF3 CSF2 UCHL1 SERPINB2 IGF1 GREM1 IL1A MMP14 IL23A IL1B JDP2	(+23) CDKN1C PRR5 PTPRR SERPINA1 EBI3 ITGB2 WFDC1 PDGFA LDLRAD4 MEFV GRM4 FGF9 CCR7 MAP3K8 PRNP EGLN3 TNFRSF18 IGF2 MMP9 DAZL FGR CHI3L1 MDFI	0.001897	0.038774	35
GO:0007167	enzyme linked receptor protein signaling pathway	BP_FAT	1.88562	(-5) ERRFI1 IGF1 FSTL1 GREM1 IL1B	(+13) CDKN1C PTPRR TMPRSS6 CHRD IGF2 PDGFA LDLRAD4 BAIAP2 MMP9 FGR FGF9 ADAMTSL2 ZYX	0.002151	0.041494	18
GO:0050865	regulation of cell activation	BP_FAT	2	(-4) IGF1 MMP14 IL23A IL1B	(+12) PRR5 PRNP EBI3 SOX13 IGF2 PDGFA ABAT FGR CTLA4 MAP3K8 CCR7 IL13RA2	1.63E-05	0.00132	16
GO:0010646	regulation of cell communication	BP_FAT	2.26274	(-17) ARHGAP9 ERRFI1 CSF3 CSF2 CXCL8 UCHL1 CYP1B1 GREM1 IL1A MMP14 IL23A IL1B SCG5 MGLL FZD9 HMGA2 IGF1	(+33) CDKN1C PRR5 PTPRR WNT2B ABAT ARHGEF10L LDLRAD4 SLC8A2 GRM4 FGF9 ARHGDIB ADAMTSL2 MAP3K8 CCR7 LZTS1 TNFRSF18 MMP9 FGR CHI3L1 SKAP1 MDFI TMPRSS6 RGS13 CAMK2A CHRD PDGFA CACNG8 KCNMB4 PRNP IGF2 BAIAP2 SYT7 TSPAN15	6.73E-07	1.48E-04	50
GO:0023051	regulation of signaling	BP_FAT	2.26274	(-17) ARHGAP9 ERRFI1 CSF3 CSF2 CXCL8 UCHL1 CYP1B1 GREM1 IL1A MMP14 IL23A IL1B SCG5 MGLL FZD9 HMGA2 IGF1	(+33) CDKN1C PRR5 PTPRR WNT2B ABAT ARHGEF10L LDLRAD4 SLC8A2 GRM4 FGF9 ARHGDIB ADAMTSL2 MAP3K8 CCR7 LZTS1 TNFRSF18 MMP9 FGR CHI3L1 SKAP1 MDFI TMPRSS6 RGS13 CAMK2A CHRD PDGFA CACNG8 KCNMB4 PRNP IGF2 BAIAP2 SYT7 TSPAN15	1.11E-06	1.90E-04	50

PUBLICATIONS

In Preparation

Peat TJ, Gaikwad SM, Dubois W, Gorjifard S, Phyo Z, Andres M, Gyabaah-Kessie N, Girvin AT, Taylor A, Miller MA, Zhang J, Zhang Y, Kazandijian D, Michalowski AM, Simmons JK, Thomas CJ, Mock BA. High-throughput drug screen identifies therapeutic combinations targeting oncogenes and tumor suppressors in multiple myeloma. *Sci Transl Med*. 2021.

Peat TJ, Gaikwad SM, Dubois W, Andres M, Gyabaah-Kessie N, Zhang Y, Kazandijian D, Michalowski AM, Mock BA. Efficacy and cooperative targets of combined CDK/HDAC inhibition in preclinical models of multiple myeloma. *Sci Transl Med*. 2021.

Published

Yan H, Malik N, Kim YI, He Y, Li M, Dubois W, Liu H, **Peat TJ**, Nguyen JT, Tseng YC, Ayaz, G, Alzamzami W, Chan K, Andresson T, Tessarollo L, Mock BA, Lee MP, Huang J. Fatty acid oxidation is required for embryonic stem cell survival during metabolic stress. *EMBO Reports*. 2021 Jun 4;22(6):e52122.

Wei BR, Hoover SB, Peer CJ, Dwyer JE, Adissu HA, Shankarappa P, Yang H, Lee M, **Peat TJ**, Figg WD, Simpson RM. Efficacy, tolerabilility and pharmacokinetics of combined targeted MEK and dual mTORC1/2 inhibition in a preclinical model of mucosal melanoma. *Molecular Cancer Therapeutics*. 2020 Nov;19(11)2308-2318.

Zhang S, Dubois W, Zhang K, Simmons JK, Gorjifard S, Gaikwad S, **Peat TJ**, Mock BA. Mouse tumor susceptibility genes identify drug combinations for multiple myeloma. *Journal of Cancer Metastasis and Treatment*. 2020;6:21.

Chen J, Zhang S, Feng X, Wu Z, Dubois W, Thovarai V, Ahluwalia S, Gao S, Chen J, **Peat TJ**, Sen SK, Trinchieri G, Young NS, Mock BA. Conventional co-housing modulates murine gut microbiota and hematopoietic gene expression. *International Journal of Molecular Science*. 2020 Aug 26;21(17):e6143.

Gary J, Simmons JK, Xu J, Zhang S, **Peat TJ**, Watson N, Gamache BJ, Zhang K, Kovalchuk AL, Michalowski AM, Chen J, Thaiwong T, Kiupel M, Gaikwad S, Etienne M, Simpson RM, Dubois W, Testa JR (in press). Hypomorphic mTOR downregulates CDK6 and delays thymic Pre-T LBL tumorigenesis. *Molecular Cancer Therapeutics*. 2020 Aug 3;0671.2019.

Zhang S, Dubois W, Zhang K, Simmons JK, Gorjifard S, **Peat TJ**, Mock BA (in press). Tumor susceptibility genes identify drug combinations for multiple myeloma. *Journal of Cancer Metastasis and Treatment*. 2020;6:21.

Li J, Dubois W, Thovariai V, Wu Z, Feng X, **Peat TJ**, Zhang S, Sen S, Trinchieri G, Chen J, Mock BA, Young NS. Attenuation of immune mediated bone marrow damage in conventionally-housed mice. *Molecular Carcinogenesis*. 2020 Feb;59(2):237-245.

Malik N, Yan H, Moshkovich N, Yang H, Sanchez V, Cai Z, **Peat TJ**, Jiang S, Liu C, Lee M, Mock BM, Wakefield L, Yuspa S, Huang J. The transcription factor CBFB suppresses breast cancer through orchestrating translation and transcription. *Nature Communications*. 2019 May 6;10(1):2071.

Peat TJ, Miller MA. Pathology in Practice: Mulberry heart disease in a two-month-old crossbred gilt. *Journal of the American Veterinary Medical Association*. 2018 Sept 15;253(6):719-721.

D'Hue CA, Dhawan D, **Peat TJ**, Ramos-Vara J, Jarmusch A, Knapp DW, Cooks RG. Fatty acid patterns detected by ambient ionization mass spectrometry in canine invasive urothelial carcinoma from dogs of different breeds. *Bladder Cancer*. 2018 Jul 30;4(3):283-291.

Peat TJ, Edmondson E, Miller MA, DuSold D, Ramos-Vara JA. PAX8, Napsin-A and CD10 as immunohistochemical markers of canine renal cell carcinoma. *Veterinary Pathology*. 2017 Jul;54(4):588-594.

Jarmusch AK, Kerian KS, Pirro V, **Peat TJ**, Thompson CA, Ramos-Vara JA, Childress MO, Cooks RG. Characteristic lipid profiles of canine non-Hodgkin's lymphoma from surgical biopsy tissue sections and fine needle aspirate smears by desorption electrospray ionization – mass spectrometry. *The Analyst (RSC)*. 2015 Sep 21;140(18):6321-9.